AN NMR STUDY OF MOLECULAR DYNAMICS IN ORGANIC CRYSTALLINE COMPOUNDS

Martin Rogerson

A Thesis Submitted for the Degree of PhD
at the
University of St Andrews

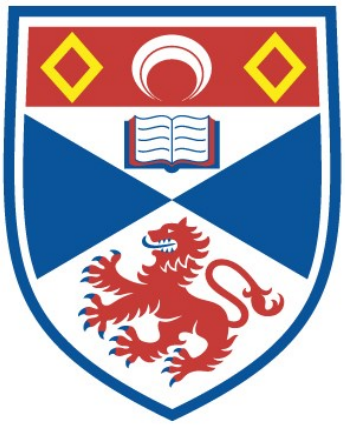

1995

An NMR Study of Molecular Dynamics in Organic Crystalline Compounds

Being a thesis by

Martin Rogerson

Submitted for the degree of
Doctor of Philosophy
in the Faculty of Science of the
University of St Andrews.

January 1995.

United College of St Salvators
and St Leonards College.

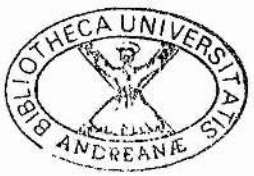

Declaration

I, Martin Rogerson, hereby certify that this thesis has been composed by myself, that it is a record of my own work and that it has not been accepted in partial or complete fulfilment of any other degree or professional qualification.

I was admitted to the Faculty of Science of the University of St Andrews under Ordinance General No. 12 in October 1991 and as a Candidate for the degree of PhD. in October 1992.

Signed. January 1995.

Certification

I hereby certify that the candidate has fulfilled the conditions of the Resolution and Regulations appropriate to the degree of PhD.

Signed. January 1995.

Copyright

Acknowledgements

No work of this sort is possible without the technical assistance and back-up of many skilled people all of whom I would like to thank. Therefore, many thanks go to Mrs S Smith for the elemental analyses, Mrs M Parker for her help (and transport), Mr C Smith for equipment and Mr R Cathcart for maintenance work.

I am grateful, too, for the kind hospitality and help given to me by Prof F Fulop during my Six weeks working in his laboratory at the Pharmaceutical Institute in Szeged, Hungary.

I would also like to thank Mrs Melanja Smith for her assistance with the NMR work and both she and Mr John Smith for moral support over the past three years.

I very much appreciate the opportunity that the EPSRC has given me in funding this project and the British council and Hungarian Committee for Technological Development for the above trip.

Finally, special thanks must go to Dr Frank Riddell without whose help, enthusiasm and, what is more important, faith, this project would not have been possible.

Dedication

I dedicate this thesis to the memory of my Mum and Dad, whose sacrifices in life have given me the opportunity to better my own.

Publications

F. G. Riddell, S. Arumugam, K. D. M. Harris, M. Rogerson and J. H. Strange (1993), A ^{13}C CP/MAS NMR Study of a Double *tert*-Butyl Group Rotation in the Solid State Using $T_1\rho$ and Line Shape Measurements. *J. Am. Chem. Soc*, **115**, 1881-1885.

F. G. Riddell, P. G. Bruce, P Lightfoot and M. Rogerson (1994), Probing Molecular Motion by Solid State NMR and High Resolution Powder X-Ray Diffraction. *J. Chem. Soc., Chem. Commun.*, 209.

Abstract

Using a combination of solid–state NMR techniques including $T_1\rho$ measurements, dynamic line shape analyses and 2D EXSY data, a variety of intramolecular motions including rotations of methyl, *t*-butyl, *t*-amyl, phenyl, trimethylammonium and trimethylphosphonium groups in a series of quaternary ammonium and phosphonium salts have been investigated. Where possible, activation parameters E_a, $\Delta G^{\ddagger}$, $\Delta H^{\ddagger}$ and $\Delta S^{\ddagger}$ have been derived. A range of values was recorded, especially for $\Delta S^{\ddagger}$ which ranged from +75 $JK^{-1}mol^{-1}$ for a phenyl group to -57 JK^{-1} mol^{-1} for a *t*-butyl group. It was shown that ^{13}C and ^{31}P $T_1\rho$ measurements from CP/MAS spectra can give quantitative information on the kinetics of intramolecular motions that agree with line shape analysis.

Recent work using X-ray crystallography has suggested that some derivatives of bicyclo[3.3.1]nonane show evidence of conformational equilibria in the solid state. Using ^{13}C CP/MAS NMR, 22 derivatives of bicyclo[3.3.1]nonane were studied, some at variable temperature. No evidence of conformational equilibria was observed in the chosen compounds.

Solid–state NMR has been used to follow the kinetics of ring–chain tautomerism in a bicyclic tetrahydro-1,3-oxazine derivative. This was found to form initially the metastable chain on crystallisation, which then cyclises. The kinetics of the cyclisation were followed and the activation energy for the solid–state reaction was derived. In contrast to this, a related pyrimidine derivative has been found to form initially the metastable ring on cyclisation which quickly ring opens to the chain.

Contents

Chapter One

Introduction

1. Nuclear magnetic Resonance Spectroscopy

Nuclear magnetic resonance (NMR) spectroscopy has been, for many years now, the principle spectroscopic tool of analysis used by organic chemists. Indeed, a well equipped chemistry laboratory is not without the services of an NMR spectrometer. With modern machines, solution NMR spectroscopy can be quickly performed as a matter of routine and the ease of solid-state NMR is becoming increasingly likewise. It is the non-invasive nature of NMR which makes it ideal for kinetic studies and this thesis explores some of the applications of NMR spectroscopy to the investigation of solid-state molecular dynamics.

1.1 The Principles of NMR Spectroscopy[1-3].

In this section the basic principles of NMR spectroscopy are outlined. It is important to have a fundamental understanding of these concepts to accredit some observations in the later chapters.

1.1.1. The Spin Quantum Number.

The spin quantum number, I, has allowed values of zero, integer or half-integer. The simple rules governing this are

I = 0 if the nucleus has an even number of both protons and neutrons, (e.g. ^{14}C and ^{16}O).

I = half-integer if the sum of the protons and neutrons is an odd number, (e.g. ^{1}H, ^{13}C, ^{15}N and ^{17}O).

I = integer if the nucleus has an odd number of both protons and neutrons, (e.g. ^{2}H and ^{14}N).

There are two approaches to nuclear magnetic resonance, each with its own merits and limitations.

The first approach relies on the nuclei of many elements being magnetic. This is due to the fact that they have both electric charge and spin. Being magnetic they behave like bar magnets in an applied field, $\mathbf{B_o}$, but, unlike bar magnets which always align with the applied field, nuclei with I = 1/2 can adopt two positions; either aligned with or against the magnetic field, the latter being of higher energy.

1.1.2. Nuclei with Spin Quantum Number = $\frac{1}{2}$

Nuclei with spin quantum number equal to $\frac{1}{2}$ have only two allowed orientations in a magnetic field represented by $I = \pm\frac{1}{2}$. The angular momentum, P, given by

$$\mathbf{P = \frac{h}{2\pi}\sqrt{I(I+1)}} \quad \text{.....(Eq. 1.1)}$$

is calculated to be 0.866 units ($h/2\pi$) for $I = \frac{1}{2}$. More nuclei will be in the lower energy state and if all the orientations are added together then we have a net magnetisation aligned with the field along the z-axis. It is convenient to show this magnetisation in the form of a vector arrow, M_o. The size of M_o will differ from isotope to isotope.

The number in the higher and lower energy levels (N_β and N_α respectively) is given by the Boltzman distribution:

$$\frac{N_\beta}{N_\alpha} = \mathbf{exp(-\Delta E / kT)} \quad \text{.....(Eq. 1.2)}$$

The most important nuclei with $I=\frac{1}{2}$ for organic chemists are ^1H and ^{13}C. In the presence of an applied field, B_o, they will align themselves in both the higher and lower energy orientation, with the energy difference, ΔE, given by:

$$\mathbf{\Delta E = h\gamma B_o / 2\pi} \quad \text{.....(Eq. 1.3)}$$

Where h is Planck's constant and γ is the magnetogyric ratio (a proportionality constant, differing for each nucleus). ΔE varies in direct proportion to the applied field. Therefore, the larger the magnetic field, the larger ΔE is. Transitions between the two energy levels are possible when the incoming radiofrequency (RF) exactly matches the energy difference. The two are said to be in resonance. So if a sample containing ^1H nuclei is subject to an applied field and irradiated by a radiofrequency such that $\Delta E = h\nu$, then some of the nuclei will absorb this energy and move from the lower energy state to the higher (figure 1.1). At the same time some will emit energy and move from the higher to the lower energy state with the consequent promotion of another nucleus to the higher level.

Figure 1.1: Nuclear Transitions between the Lower and Higher Energy States.

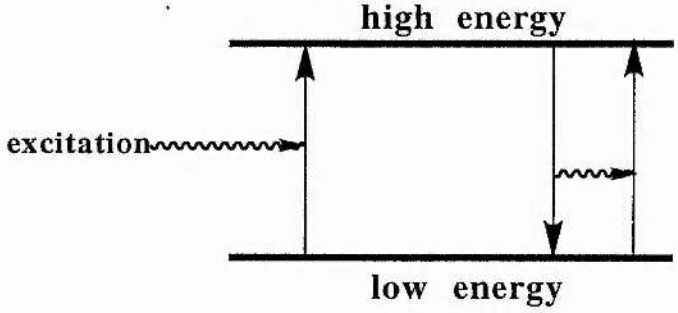

Since there are more nuclei in the lower energy state, the effect of both these processes results in a net absorption of energy and the NMR spectrometer registers this absorption plotting it as a peak in the spectrum.

The second approach is to compare the spinning nucleus to a gyroscope. Because it is spinning and gravity exerts a downward pull on it the axis of the gyroscope moves around a conical path. This motion is termed **precession**. A charged spinning body subject to an applied magnetic field will behave analogously. This precession is known as Larmor precession and the frequency of the precession is given by the Larmor equation (substitution of $\Delta E = h\nu$ into eq. 1.3 gives eq. 1.4):

$$\nu = \frac{\gamma B_o}{2\pi} \quad \text{.....(Eq. 1.4)}$$

Again there are two energy levels for $I = \frac{1}{2}$ nuclei (figure 1.2).

Figure 1.2: The Lower and Higher Energy Levels of a Precessing Nucleus.

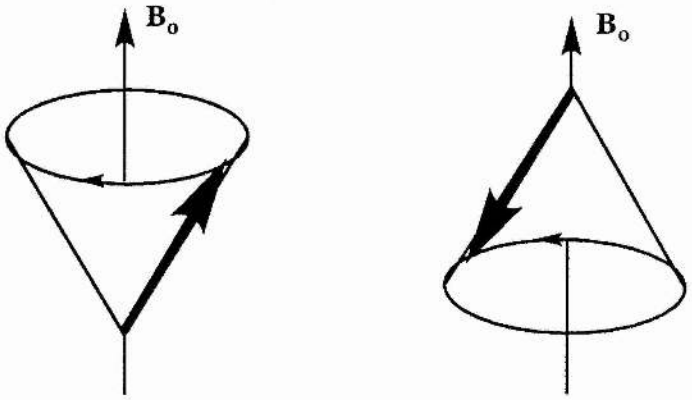

A precessing proton can absorb radiofrequency energy and move between the high and low energy states, provided the frequency of precession is exactly equal to the radiofrequency; i.e. they are in resonance. There is a vector sum, M, of the magnetisation. The Larmor equation applies to this vector sum. If a magnetic field is applied along the x axis nothing happens. But if a magnetic field is applied rotating at the Larmor frequency then M is tipped towards the y axis. Thus, if we define rotating frame axes of z, x', and y' in which x' and y' rotate about z at the Larmor frequency, a radio frequency, ν, applied along x' is equivalent to a magnetic field along x'.

In this way, electromagnetic radiation at the Larmor frequency tips M around x'. According to the length of the application of ν (pulse width) M can be turned through any number of degrees.

1.1.3. Relaxation Phenomena

Conventional NMR works by measuring the absorption of radiofrequency by the sample as the nuclei are excited from the low energy state to the higher. Net

absorption of radiofrequency by the sample only arises because there is an excess of nuclei in the lower energy state at thermal equilibrium. Irradiation at the resonance frequency stimulates upward and downward transitions. Energy is only absorbed during an upward transition and once the populations of lower and higher states are equal, no more energy is absorbed. The system is said to be saturated and absorption can only continue if the nuclei relax back from the higher level to the lower.

Relaxation implies the loss of energy from the system. Most is lost by radiationless transfer to the surroundings of the nuclei within the sample. The random tumbling of molecules and the vibrations of bonds and electrons set up many fluctuating electric dipoles and a proportion of these will be of appropriate frequency to interact with the higher energy nucleus and absorb its excess energy. This transfer of energy to the surrounding lattice is called **spin-lattice relaxation** and the time constant for it is defined as $\mathbf{T_1}$.

Nuclei can spend time in both the high and low energy states. Each of these states has a particular lifetime. The process of spin-lattice relaxation shortens the lifetime of the spin states leading to a net loss of energy from the system. However the process where nuclei swap orientations in figure 1.1 also shortens the spin state lifetimes but with no net loss of energy from the system. This spin-spin exchange leading to randomising of the spin states in the xy plane is part of the process of **spin-spin relaxation** and the time constant for it is defined as $\mathbf{T_2}$.

In summary,

T_1 is defined as the time constant for relaxation along the field axis (z-axis).

T_2 is defined as the time constant for relaxation in the xy plane.

1.1.4. Chemical Shifts

Not all protons resonate at exactly the same frequency. In a molecule, protons may be bonded to different atoms, e.g. carbon, nitrogen and oxygen, and are therefore

surrounded by a different electron density. This affects the local magnetic field at the nucleus. For example, in a 100 MHz machine, not all protons will resonate at this frequency. Depending on their chemical environment the resonance frequency will be shifted from 100 MHz by a specific amount. The Larmor equation now becomes:

$$\nu = \frac{\gamma B_o (1-\sigma)}{2\pi} \qquad \text{(Eq. 1.5)}$$

Where σ is a shielding constant. This is the chemical shift and it allows us to analyse molecules by their different nuclear environments. The chemical shift is dependent on the degree to which the nucleus is shielded from the applied field B_o by the electron cloud surrounding the nucleus. The more dense the cloud, the more the nucleus is shielded and thus the lower the magnetic field experienced by the nucleus. This leads to a lower precessional frequency and chemical shift. Protons near electronegative nuclei will have higher chemical shifts than those near electropositive ones.

The chemical shift can be quoted in either Hz or parts per million (ppm). However, as the resonance frequency varies with B_o, it is more convenient to use dimensionless units of ppm. If the operating frequency is 100MHz and the chemical shift is 150Hz, this is 1.5 parts per million in 100 million hertz. If the operating frequency is 200MHz then the corresponding shift will be 300Hz but still 1.5 ppm.

The best way of measuring chemical shifts is to reference them to a standard. For ^{1}H and ^{13}C, the most common standard is tetramethylsilane (TMS), the protons of which resonate at the defined working frequency of the spectrometer. Therefore, the TMS signal is set to resonate at 0 ppm and the chemical shifts are expressed in ppm from the TMS signal.

1.1.5. Spin Coupling

Not all spectra consist of single line absorption bands. Most proton spectra contain signals which are split into two or more lines. This is caused by the nucleus interacting with neighbouring $I=\frac{1}{2}$ nuclei and the multiplicity of the splitting is

dependent on the number of neighbouring nuclei plus one (the n+1 rule). If we take two neighbouring nuclei, H_A and H_B which are non-equivalent, the precessional frequency is dependent on the applied field, B_o. Approximately 50% 0f the spins will be aligned with B_o and 50 % opposed. The spins of H_A will interact with those of H_B such that, as far as H_A is concerned, those spins of H_B aligned with B_o will add to the applied field enhancing it, and those spins opposed to B_o will reduce its effect. Thus H_A is experiencing two different applied fields and thus will resonate at two separate frequencies. The difference between the two frequencies is known as the coupling constant, J, and is independent of B_o. Coupling can either be through space or through bonds. In solution the much larger through space coupling is averaged to zero by molecular tumbling and only the scalar J coupling is important.

1.1.6. ^1H Decoupling

^1H spectra can be dramatically simplified by decoupling one nucleus from the other. The same technique is employed for the decoupling of nucleus A from nucleus B whether A and B are the same element or not. In the above, as H_A is split by H_B due to H_A seeing H_B in two magnetic orientations, this splitting will only be seen if the lifetime of H_B in any one spin state is sufficiently long to allow the splitting to be observed. Shortening of the lifetime of the spin states will remove the splitting.

If H_B is irradiated by a separate RF source tuned to its resonance frequency then a single H_A signal will be observed.

1.1.7. The Spectrum

There are two ways of obtaining a spectrum. The first is the simplest and is used with low field strength magnets. This is the continuous wave method. The spectrometer scans through the frequency range from one extreme to the other. When the frequency is in resonance with the nucleus it absorbs the energy and this is picked up by the receiver coil. Alternatively, the radiofrequency is held at the same level and

the applied field is scanned until a signal is generated. The spectrum is plotted directly as it scans.

The other method, and by far the best, is to apply the radiofrequency as a single powerful pulse. The desired range of frequencies are irradiated simultaneously in the pulse which lasts typically a few microseconds. The pulse, which is applied along the x-axis, leads to a signal along the y-axis due to nuclear induction. Once the pulse is complete the nuclei continue to exhibit the effects of the induction and produce the signal along the y-axis. This signal is picked up by the receivers. The signal decays exponentially with time and contains information on all the excited nuclei. This is known as free induction decay (FID). The problem with this is that all the frequencies are recorded at the same time and the resultant interference pattern has to be separated into its individual frequencies. This is done by performing a Fourier transform using a computer. This technique of obtaining a spectrum is known as **pulsed FT NMR**.

The advantages of pulsed FT NMR over continuous wave are many. Continuous wave spectra are very slow to produce whereas collecting the FID and Fourier transform take only a few seconds with modern computers. By leaving a suitable delay between the pulses (so as not to saturate the system) many pulses can be applied and the resultant FIDs added together by computer giving an average FID. This is Fourier transformed to give a spectrum. This averaging cancels out random effects such as noise and greatly enhances the spectrum. The signal-to-noise ratio is increased in proportion to the square root of the number of scans collected and averaged. Where the nucleus being scanned is in low abundance or the sample itself has poor solubility, this is the only means of obtaining a satisfactory spectrum.

1.1.8. Frames of Reference in NMR

There are two frames of reference in NMR.

1.1.8.1. The Laboratory Frame

A proton in a 100 MHz machine is seen by the spectroscopist standing in the laboratory next to the magnet as precessing around a cone at 100MHz. This is the laboratory frame of reference.

1.1.8.2. The Rotating Frame

If the same spectroscopist were to stand upright in the same magnet along the z-axis, and then to spin at 100 MHz he would see the protons lying on the surface of the cones; static not spinning. This is the **rotating frame of reference** and its axes are specified as being x'- and y'-axes. The z axis being the same in both cases. The rotating frame rotates at the Larmor frequency.

1.1.9. ^{13}C Spectra

Next to ^{1}H, the second most studied nucleus by organic chemists is ^{13}C. Unlike ^{1}H the natural abundance of this NMR sensitive nucleus is only 1.1%. The ^{13}C nucleus has a smaller magnetogyric ratio than ^{1}H. NMR sensitivity depends on the 3rd power of the magnetogyric ratio and thus ^{13}C nuclei will give weak signals. Compared to the proton signal, ^{13}C is approximately 64 times weaker. However, worse still, once the low natural abundance is taken into account, the ^{13}C sensitivity is about 6000 times less than ^{1}H. Here, pulsed NMR experiments have become invaluable as described above.

Whereas ^{1}H spectra can furnish the chemist with a great deal of information from the splitting patterns, there is little information to be gained from splitting in ^{13}C spectra and it is therefore more convenient to simplify the spectra by the removal of these patterns using broad band decoupling. This is similar to the single proton decoupled spectra discussed earlier except that all the protons are simultaneously decoupled by a decoupling signal which contains all of the appropriate proton frequencies. A ^{13}C spectrum observed at 25 MHz will have the proton decoupler set at

100MHz and modulated by mixing in other frequencies to create a spread of sidebands around the central 100MHz beam. Again, the lifetimes of the ^{1}H nuclei in the two spin states are so short that splitting doesn't occur and single lines are observed for each ^{13}C environment.

1.1.10. Magnetisation on the y'-Axis

The net magnetisation vector, M_0, represents magnetisation aligned with the z-axis. When this is subject to a RF pulse along the x'-axis the resultant new vector, M_1, is rotated towards the y'-axis. The NMR receiver is tuned to receive signals in the y'-axis and no signal is received until the vector has a y'-axis component.

The amount by which M_0 is rotated by B_1 depends on the duration (pulse width) and power of the pulse. A very short pulse rotates M_0 by a very small amount giving a small y'-axis component and consequently a weak signal. However, it is possible to give a pulse of duration corresponding to a 90° rotation of M_0 directly onto the y'-axis. This is known as the **90° pulse.**

There is a third relaxation time, $T_1\rho$, the spin-lattice relaxation time in the rotating frame. $T_1\rho$ is the time constant for the decay of the magnetisation in the rotating frame and is shown in figure 1.3. A 90° pulse, H_1, is applied along the x'-axis which flips the spins onto the y'-axis. The phase of the pulse is then shifted by 90° so that it is now applied along the y'-axis. This second pulse is called the spin locking pulse and is applied for a time τ. In its absence the y' magnetisation would simply fan out in the xy plane due to T_2 relaxation. The spin locking field prevents this by forcing nuclei that stray off the y'-axis to precess about it. The relaxation of the magnetisation along the y'-axis in the presence of the spin lock is analogous to spin-lattice relaxation T_1. The Larmor equation also applies to this much weaker RF field. If you know H_1 you can predict the frequency by which H_1 forces nuclei to precess about x'. On the other hand, if you know the 360° pulse width, i.e. 1/v, you can get H_1.

Figure 1.3: $T_1\rho$ Relaxation in the Rotating Frame.

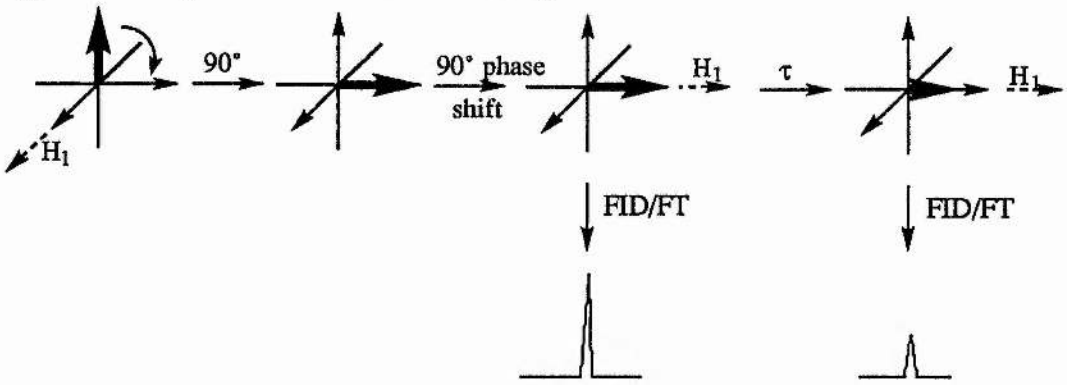

1.2. Solid-state NMR.[4]

Chemistry involves a great deal more than the study of molecules in the solution state. Many of the most exciting advances in modern chemistry involve the chemical and physical properties of solids. It would seem appropriate, therefore, to make NMR studies of such substances in the solid-state. With ordered crystalline solids a study of structure and dynamics is usually undertaken by X-ray diffraction methods but, important materials like polymers, silicates, resins, celluloses, coals and surface-immobilised reagents all containing amorphous structures are very difficult to study by diffraction methods. Solid-state NMR enables the chemist to probe the environment of the atoms in the solid matrix. Instead of being surrounded by a sheath of solvent molecules, the individual molecules of a solid lie side by side in the solid matrix with the orientation of their dipoles fixed in a random pattern. The resultant effect of this can be seen in the chemical shifts and splitting patterns. There are two main interactions:

1.2.1. Dipolar Interactions.

In the solid-state, the proton and carbon nuclei are held close together by the lattice and couple with one another through space. This dipolar coupling is much stronger than the scalar coupling discussed earlier and is a function of molecular orientation. For an isolated pair of $I = \frac{1}{2}$ nuclei there is a through space coupling:

$$J \propto \frac{k}{r^3}(3\cos^2\theta - 1) \quad \text{.....(Eq. 1.6)}$$

Where r is the internuclear distance, k is a constant relating to the two nuclei and θ is the angle between the internuclear vector and B_0. This gives rise to line broadening as each spin in the presence of the local field of the other gives the spectrum of an isolated axially symmetrical molecule. The linewidths are in the order of many Kilohertz.

Figure 1.4: Typical Lineshape for a Pair of Spins.

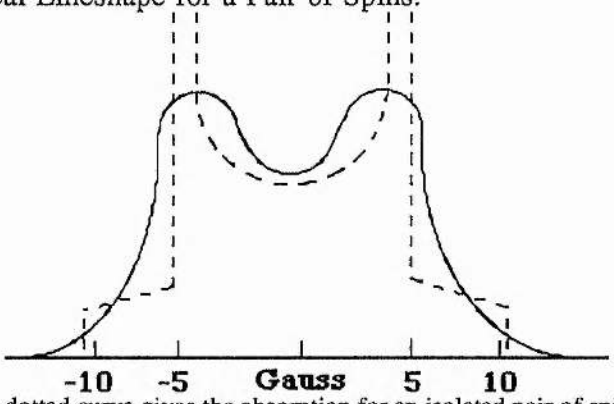

The dotted curve gives the absorption for an isolated pair of spins.
The full curve shows the effect of neighbouring nuclei on the isolated system.

1.2.2. Chemical Shift Anisotropy.

The field experienced by a nucleus depends upon the orientation of the molecule in the magnetic field. This is shown in figure 1.5.

Figure 1.5: Orientations of a Molecule in the Applied Field.

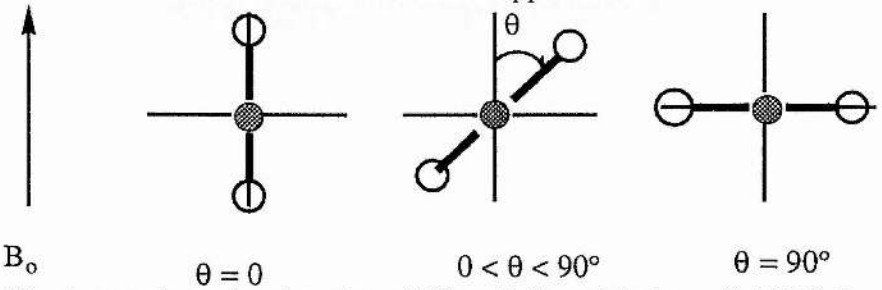

The diagram shows the orientations of CO_2 with C_∞ axis in the applied field, B_o.

The shielding that the central carbon experiences varies with θ. Therefore, a wide chemical shift range is observed (figure 1.6). Since there are more perpendicular arrangements (θ = 90°) than parallel (θ = 0°) this gives a more intense peak.

Figure 1.6: General lineshape due to chemical shift anisotropy.

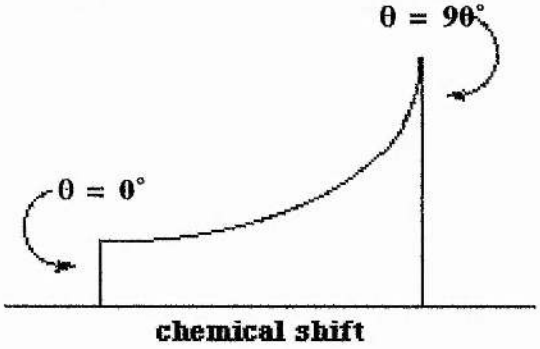

These effects, dipolar coupling and chemical shift anisotropy, are not observable in solution NMR as the rapid molecular tumbling averages the dipolar vectors and the anisotropy to zero. This decouples the magnetic nuclei by the rapid changing of their orientations and leads to a single isotropic chemical shift.

1.2.3. High Resolution Solid-state Spectra

As we have seen above, in the solid-state, chemical shift anisotropy and direct dipolar coupling lead to line broadening in the spectrum and, thus, must be removed if we are to obtain high resolution spectra.

Each of these effects contain the term $(\mathbf{3\cos^2\theta - 1})$. Where θ is the angle determining the orientation of the molecule with respect to B_0. If the nuclei can be "fooled" into believing that $(3\cos^2\theta - 1)$ equals zero, then these interactions become negligible.

For $3\cos^2\theta - 1 = 0$

$3\cos^2\theta = 1$

$\cos^2\theta = 1/\sqrt{3}$

$\theta = \mathbf{54.74°}$

This is the **Magic Angle.**

The magic angle (θ_M) turns out to be the angle between the opposite vertices of a cube. If the nuclei are spun about the magic angle the average interaction is along θ_M. Therefore, anisotropic interactions are greatly reduced (figure 1.7).

Figure 1.7: The Magic Angle.

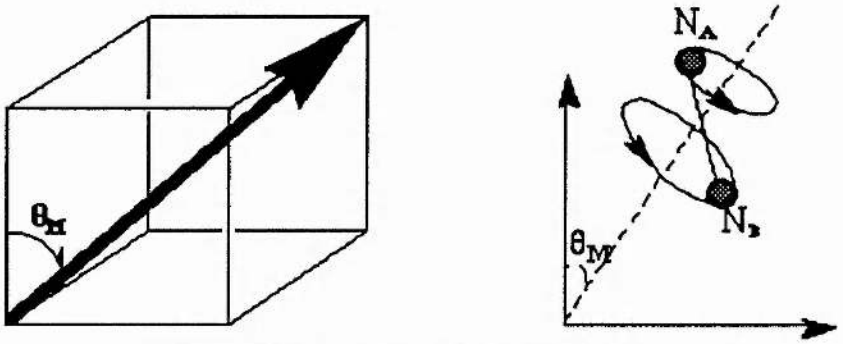

Spinning the sample about θ_M averages the direction of all the N_A/N_B interactions. The average of the vector AB is the magic angle.

The sample is either machined into the shape of a rotor or packed into a ceramic rotor and the rotor is spun by an air turbine around the axis of the magic angle. In addition, double irradiation at the proton frequency decouples the protons from the ^{13}C. This is the same as the scalar decoupling discussed earlier but, it requires much more power to do.

Almost all of the spectra contained in this thesis were obtained using a **cross polarisation sequence.** This effectively enhances the signal/noise ratio and leads to a shortening of the recycle delay between pulses resulting in more pulses in any given time period. The general procedure is outlined below.

1.2.4. Cross Polarisation Sequence

Figure 1.8: The Cross Polarisation Pulse Sequence.

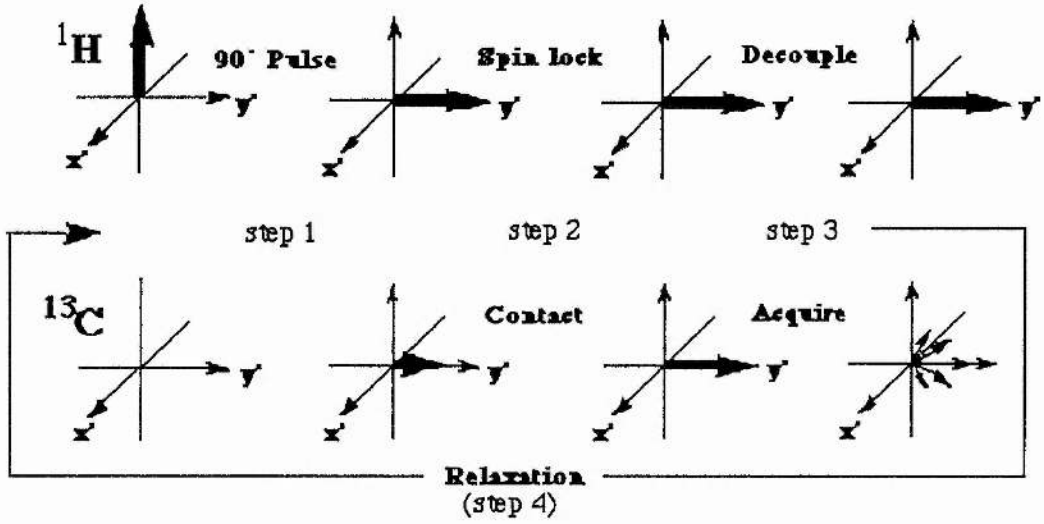

By using cross polarisation it is possible to obtain ^{13}C spectra without using a long relaxation delay. In addition, cross polarisation enhances the signal intensity for ^{13}C. Basically it involves the enhancement of the magnetisation of the rare spins (^{13}C) from that of the abundant spins (^{1}H). In the first step (figure 1.8) the ^{1}H spins are flipped over onto the y'-axis by a 90° pulse along the x'-axis and then spin-locked by a RF pulse along the y'-axis. The ^{1}H spins are kept locked along the y'-axis for a time period t. In this time the ^{13}C spin lock field is applied. Thus both sets of spins are spin-locked onto the y'-axis. By choosing the correct frequency of spin-locking fields H_{1H} and H_{1C}, the net carbon magnetisation may be enhanced by the proton reservoir (step 2). This is the contact period. The magnitudes of the two fields are chosen such that the Hartmann-Hahn condition (Eq. 1.7) is met.

$$\gamma_{1H} H_{1H} = \gamma_{13C} H_{13C} \quad \text{.....(Eq. 1.7)}$$

Since $\gamma_{1H}/\gamma_{13C} = 4/1$, the spin locking field H_{13C} must be four times H_{1H} to satisfy the equality. As a result of this condition both sets of nuclei are forced to

precess about the y'-axis with the same frequency. Therefore, the energy required for spin flips between the two spin energy levels is the same for both nuclei and thus the ^{13}C nuclei will accumulate magnetisation from the proton reservoir. The loss of proton magnetisation during this process is negligible. After the ^{13}C magnetisation has built up during this contact period, the ^{13}C spin locking field is switched off and the carbon FID recorded (step 3). The proton field remains on to decouple the proton-carbon dipolar interactions. There is then a time delay in which the protons and carbons are allowed to relax towards their equilibrium values (step 4). In contrast to the simple pulse-FT experiment, the carbon magnetisation for the FID does not depend on the relaxation of the carbon spins in the delay period, but arises entirely from the contact with the proton spins. This means that the intensity of the carbon spectrum effectively depends on the relaxation of the proton spin system. This is much shorter than the relaxation of the carbon spin system and thus the recycle time for effective accumulation is much shorter than for a conventional ^{13}C pulse-FT experiment.. A further advantage of these spectra is that carbons which are difficult to observe in solution, e.g. carbonyls and quaternary carbons, have intensities comparable to other carbons in the system.

In conclusion the total CP/MAS experiment involves the use of

Cross-polarisation techniques to increase the S/N and to bypass the T_1 relaxation processes of the dilute nuclei being observed.

High power proton decoupling during acquisition to remove the dipolar and scalar interactions.

Continuous magic-angle sample spinning to remove the chemical shift anisotropy and further reduce dipolar interactions.

1.2.5. Spectral Editing in the Solid-State

A very important limitation of the standard CP/MAS experiment in terms of structure elucidation in the solid-state is that it is not easily possible to perform the variety of editing techniques, e.g. DEPT, which may be employed in the measurement

of ^{13}C spectra in solution. This is because the solid-state interactions being removed by decoupling are dipolar in nature and must be completely removed during acquisition. The dipolar interaction between two spins depends dramatically on the internuclear distance and there will thus be a very large difference in the dipolar broadenings of carbon atoms with one or more hydrogens attached compared to those of carbons with no attached hydrogens. It is therefore possible to distinguish between these two types of carbon atoms using a modification of the CP pulse sequence. This is known as **dipolar dephasing.**

1.2.5.1. Dipolar Dephasing

Figure 1.9: The Non-quaternary Suppression (NQS) Pulse Sequence.

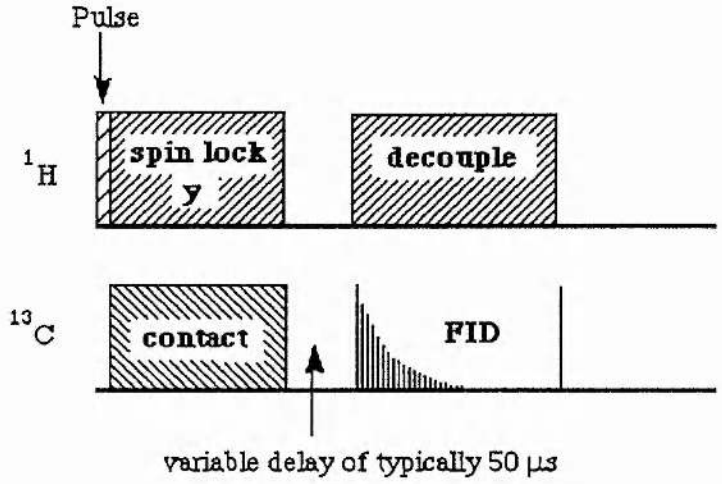

Effectively, this technique is used to suppress resonances due to CH_2 and CH (non-quaternary) carbons leaving only CH_3 and quaternary C peaks. The pulse sequence (figure 1.9) differs from the standard CP sequence by having a small delay, typically 30–100 μsec, between the cross-polarisation step and the acquisition in which the decoupling field is switched off. This dipolar dephasing delay allows the carbon spins to dephase under the influence of the proton dipolar field. The quaternary carbons do not dephase as quickly because they have no directly bound hydrogens to

dephase them. After a short period (typically 50 μs) the decoupling field is reapplied to decouple the dipolar interactions during acquisition of the carbon FID. The spectrum now contains only quaternary and methyl carbons (for methyl carbons, the dominant mechanism for relaxation is by spin rotation).

Thus: Quaternary carbons are least affected,

CH_3 is next least affected,

CH and CH_2 can be edited out if a suitable delay is applied.

1.3. Two-Dimensional NMR Spectroscopy [5]

Figure 1.10: The 2D Pulse Sequence.

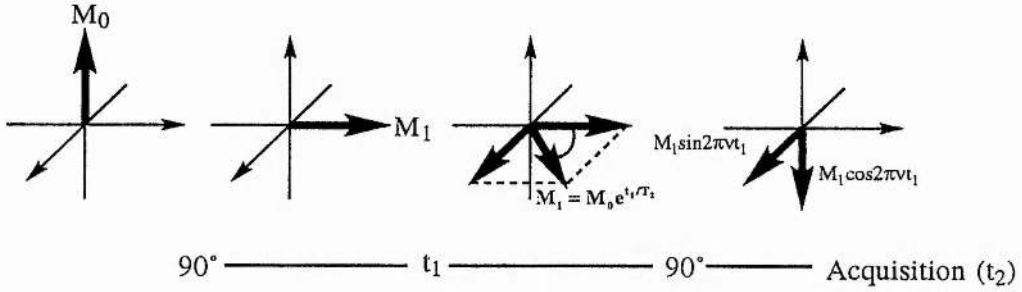

A sample with only one resonance line in its' ^1H spectrum, such a chloroform, will have a chemical shift, ν. After a 90° pulse the spin vector, M_1, precesses in the x'-y' plane. In figure 1.10, M_1 precesses in the x'-y' plane at ν cycles per second for a time t_1. At the end of this interval, t_1, a second 90° pulse is applied along the x'-axis and the NMR signal is measured as a normal FID. The result of this is that the vector has precessed through an angle of $2\pi\nu t_1$ during the interval, so, if its length is M, then the component along the y'-axis is $M\cos 2\pi\nu t_1$ and that along the x'-axis is $M\sin 2\pi\nu t_1$. The value of M is related to the initial magnetisation M_0 by

$$\mathbf{M = M_o e^{-t_1/T_2}} \quad \text{.....(Eq. 1.8)}$$

The second pulse rotates the y'-axis component through another 90° to place it along the z-axis, while leaving the x'-axis component unchanged. Thus the amount of

magnetisation left in the x'-y' plane is $M\sin 2\pi\nu t_1$ and determines the size of the NMR signal. The spectrum obtained is perfectly normal apart from a change in amplitude.

If a series of experiments with different values of t_1, e.g. values from 0 to a few seconds, are performed and the data from each experiment transformed into a spectrum, then a series of peaks is produced with size varying with t_1. The height of the peaks would oscillate sinusoidally with frequency ν as the transverse magnetisation at the end of t_1 is given by $M\sin 2\pi\nu t_1$.

By taking the point from each experiment that corresponds to the top of the peak and plotting these points as a function of t_1, a graph of the signal amplitude is obtained, which is oscillating with frequency ν and decaying exponentially with time constant T_2. The graph is exactly like an FID. A Fourier transform of the graph gives a frequency spectrum with one line, exactly the same as the normal FIDs that made up the spectrum. However, it is normal practise to perform Fourier transforms on every column of points taken from the complete set of FIDs. The two-dimensional Fourier transform converts the data into a two dimensional frequency spectrum which is a function of ν_1 and ν_2. ν_2 is the chemical shift of the peak as is ν_1. Thus we get a square spectrum with both axes representing chemical shifts and a peak appearing in the frequency domain at (ν,ν), i.e. on the diagonal.

This experiment contains no more information than a simple one-dimensional spectrum but contains the basic principles of two-dimensional NMR in which a signal, modulated as a function of t_1, is detected as a function of t_2. **All two-dimensional experiments are performed in this way.**

1.3.1. Two Dimensional Exchange Spectroscopy

In figure 1.10 there is a component of magnetisation which is not detected. This is the part of the transverse magnetisation returned to the z-axis by the second pulse and is also modulated as a function of t_1. If this z-axis component is involved in some physical process then the process can be monitored by returning the component to the x'-y' plane and detecting the resultant signal. One such process in which a

frequency labelled z-axis component is involved is chemical exchange with another nucleus.

If we wait a while after the second pulse, using the pulse sequence:

$$\frac{\pi}{2} - t_1 - \frac{\pi}{2} - \tau_m - \frac{\pi}{2} - t_2$$

then in the presence of exchange a nucleus whose z magnetisation was modulated by one chemical shift during t_1 may have the opportunity to migrate to another site during τ_m, the mixing time. Thus it has a different chemical shift during t_2 and the resulting spectrum will have cross-peaks between the shifts of the exchange sites.

τ_m has to be selected so that the maximum amount of exchange takes place before the final pulse samples the z magnetisation. This requires knowledge of the T_1's of the nuclei involved and of the rate of exchange. However, the purpose of the experiment is to determine these parameters. Chemical exchange can be occurring at any rate but must be in the slow exchange regime to be detected by this method. Therefore an upper limit can be imposed on the rate according to the shift differences involved. For two-site exchange between nuclei with equal populations and shift difference $\Delta\nu$ the coalescence rate k_c is

$$k_c = \frac{\pi\Delta\nu}{\sqrt{2}} \quad \text{.....(Eq. 1.9)}$$

The exchange rate must be less than k_c. At the other extreme, k must not be much less than $1/T_1$ or the z magnetisation will disappear before it has a chance to migrate. The range of useful k values lies between these limits and guesswork must be applied for the value of τ_m to be used.

1.4. Dynamic NMR Spectroscopy

In solution and gas phases molecules are constantly in motion. These motions can take many forms, not in the least, the rapid molecular tumbling responsible for the

simplification of NMR spectra discussed earlier. However, there are a great number of more subtle intramolecular motions and these can, in certain cases, produce effects which are observable in the NMR spectrum.

Much work has been done to determine rates of motion in the gas and, especially, the solution phases. However, until recently, no-one even considered the possibility of molecular motions, aside from vibrations, taking place in the solid as the restricting nature of the crystal lattice should make such processes very difficult indeed. However, the relatively few studies performed in the solid-state show this not to be the case and many molecules in the solid-state are now known to be motionally labile. It is with this in mind that a study of molecules likely to exhibit motion in the solid-state should be undertaken to address the present imbalance.

In general, when the rate of a molecular motion equals or nears the rate of an NMR process then the motion may interact with that process to produce an observable effect in the NMR spectrum. This is the basis of dynamic NMR spectroscopy. Since the rate of the motion is invariably linked to the temperature of the sample, then by measuring or simply observing the change in the spectrum with temperature, it may be possible to calculate the rate and hence, the parameters for the motion, i.e. E_a, $\Delta G^{\ddagger}$, $\Delta H^{\ddagger}$, and $\Delta S^{\ddagger}$.

There are many processes in operation in the acquisition of a spectrum and the frequencies of these processes cover an enormous range. The processes used to measure rates in this thesis are outlined below and are arranged in increasing frequency, beginning with the slowest.

1.4.1. Two Dimensional Exchange Spectroscopy

The details of this experiment are detailed above. This method is appropriate for measurements of rates comparable to spin lattice relaxation rates from **10 to 10^{-3} s^{-1}**.

1.4.2. Chemical Shift Difference

When the rate of motion is less than the chemical shift difference then the shifts of the nuclei in each position are shown in the spectra. As the rate increases towards the chemical shift difference then the corresponding shifts merge together until the rate of motion is greater than the chemical shift difference and an average signal is observed at the mean distance between the peaks. This convergence of shifts is known as coalescence and the temperature at which this occurs is important in the determination of the rate of the motion. The rate of exchange at coalescence is determined using equation 1.9 and the free energy of activation can be calculated using the Eyring equation thus [6],

$$\Delta G_c^{\ddagger} = 19.1T_c(10.32 + \log T_c - \log k_c) \quad \text{.....(Eq. 1.10)}$$

This method of measurement is sensitive to motions in the region 10^2 to 10^4 s^{-1}.

1.4.3. Maximum Dipolar Broadening

Maximum dipolar broadening occurs when the frequency of the incoherent molecular motion is the same as that of the coherent decoupler[6a]. This reduces the decoupling efficiency and so broad lines result. Its maximum is when $k = \omega_1$.

Since $\omega_1 \sim$ 50-100 kHz, this permits a single rate in this range to be measured.

1.4.4. $T_1\rho$ Relaxation

When the rate of motion nears the frequency of the ^{13}C spin lock field, typically 50–100 kHz, it modulates the relaxation in the rotating frame making it more efficient. By measuring the rate of relaxation, i.e. the time constant $T_1\rho$, the rate of motion can be calculated[39]. Measurement of rates in the region of 10^4 to 10^7 s^{-1} can be made.

Using a combination of some or all of these techniques, rates of rotation can be measured from 10^{-3} to 10^7 s^{-1}.

1.5. What is a Conformation?

The term conformation was originally used to denote any one of the infinite number of arrangements of the atoms in space that result from rotation about single bonds. An example of this is the rotation about the C-C bond in ethane. However, this view is too simplistic. The arrangement of the atoms with respect to each other in a molecule of cyclohexane, is not fixed[7]. The individual arrangements are not simply related by bond rotation but are still defined as being conformations of the molecule. For the conformations to interchange, the molecule must not only undergo bond rotations but also bond angle deformations. Therefore, the classical description of a conformation must be expanded to accommodate this. In general, a conformations can be interchanged by rotation about a single bond with any resultant small distortion in bond lengths and angles or by inversion at a three coordinate centre in the molecule.

1.6. Factors Influencing Conformation

Up until the mid 1930's rotation about single bonds was thought to be free in nature. However, theoretical calculations of thermodynamic parameters were in poor agreement with experimental results. Good agreement was not reached until barriers to bond rotations were incorporated into the calculations.[8-9] In ethane, this barrier is the result of the hydrogens becoming alternately eclipsed and staggered as the methyls rotate with respect to each other. The energy differences between the staggered and eclipsed conformations are due to interactions in the electron clouds in the C-H bonds[10].

In the pursuit of conformational information, chemists turn to the classical approach of molecular mechanics.[11] In this approach the conformational energy of the molecule is broken down into the following components;

Torsional forces

Non-bonded interaction

Bond stretching

Bond angle deformation

Electrostatic interaction

Solvent effects

Hydrogen bonding

The quantitative interactions are described below.

1.6.1. Torsional Forces

The general form of the potential function for rotation about a single bond is:-

$$E(\phi) = \frac{1}{2}\sum_{n} E_n(1 + \cos n\phi) \qquad \text{.....(Eq. 1.11)}$$

$E(\phi)$ is the energy when there has been a rotation of ϕ from the eclipsed position. E_n terms are energies associated with each n-fold component of the total function.

The simplest example of rotation about a single C–C bond is that of ethane in which only a three-fold barrier is important[12]; Figure 1.11:

$$E(\phi) = \frac{1}{2}E_3(1+\cos 3\phi) \qquad E_3 = 12.24 \text{ kJmol}^{-1}$$

For n-butane there are two components; a one-fold eclipsing of methyls and a three-fold eclipsing of any group; Figure 1.12.

$$E(\phi) = \frac{1}{2}E_1(1+\cos\phi) + \frac{1}{2}E_3(1+\cos 3\phi)$$

$$E_1 = 8 \text{ kJmol}^{-1} \text{ and } E_3\ 14.5 \text{ kJmol}^{-1}$$

Figure 1.11: The Potential Barrier to the Rotation of Ethane.

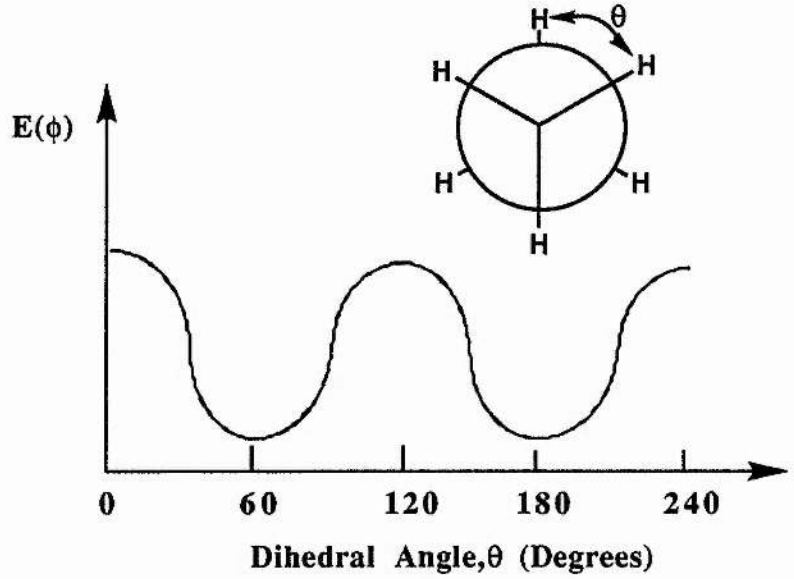

Figure 1.12: Energy Barrier to Rotation for n-Butane.

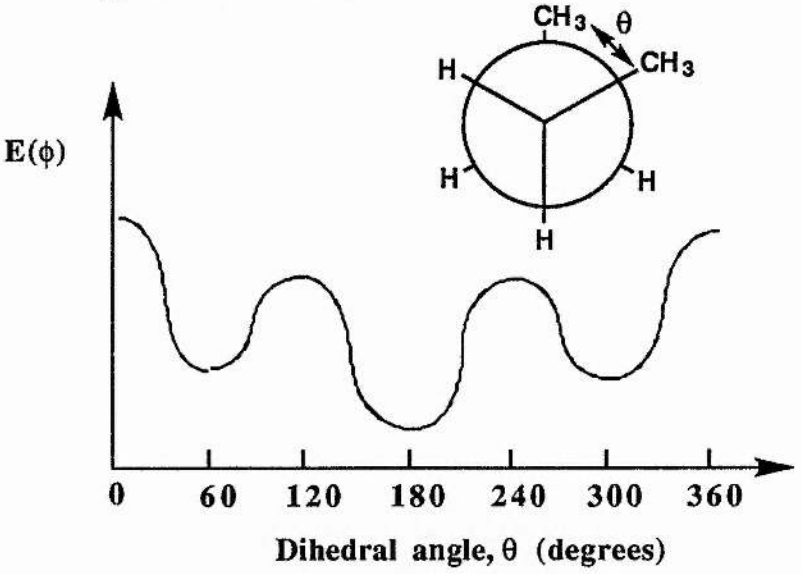

1.6.2. Non-bonded Interactions

Non-bonded interactions comprise of two different terms. One is a due to the weakly attractive forces at long distances. The other concerns repulsive forces of two approaching atoms or groups and operates over short distances.[13] This is expressed in the function:

$$E(r) = Ae^{-Br} - Cr^{-6} \quad \text{(Eq. 1.12)}$$

where E(r) is the interaction energy, r is the distance separating the interacting atoms and A, B and C are constants for the atom pair concerned. The distance at which repulsive and attractive forces between two atoms are equal, i.e. E(r) = 0, is known as the van der Waals distance.

1.6.3. Bond Stretching

Deformation of conformation due to bond stretching is generally small. The expression concerned is an harmonic function:

$$E(l) = A(l-l_0)^2 \quad \text{(Eq. 1.12)}$$

where l is bond length in pm and l_0 is the equilibrium bond length. The typical function for a C-C stretch is thus[11],

$$E(l) = 0.3168(l-152.0)^2 \quad \text{(Eq. 1.13)}$$

1.6.4. Bond Angle Deformation

Bond angle deformations have the following function[13-14]:

$$E(\theta) = K_\theta(\theta - \tau)^2 \quad \text{(Eq. 1.14)}$$

where K_θ is the force constant, θ the new angle and τ the original undeformed angle, corresponding to minimum potential energy. The angle in acyclic hydrocarbons (ca 112.7°) is used, rather than the tetrahedral angle (109.5°), as it gives better agreement. It is easier, proportionally, to bend bond angles than to stretch bonds. For a 1pm stretch in bond length the strain is equal to 1.324 $kJmol^{-1}$ which in turn would give a

deformation in the C-C-C bond angle of 4°. It is easy to see that most of the strain in a molecule will be relieved by deformation of the bond angles.

By careful consideration of all these interactions a picture can be built up of the likely conformation adopted by a specific molecule when free in solution or in the gas phase. Lattice packing forces in solids can lead to molecules crystallising in conformations other than those preferred in solution.

1.7. Conformational Analysis Before NMR

Many measurable physical properties can be used to determine the conformation of a molecule. These properties include dipole moment, electron and X-ray diffraction and spectral properties. Examples of their use in the elucidation of conformation are thus:

1.7.1. Dipole Moment

The *anti* and *gauche* forms of 1,2-dibromoethane differ in dipole moment. In the *anti* form the C-Br bond dipoles are antiparallel and the dipole moment is zero. The actual dipole moment of 1,2-dibromoethane[15] is approximately 1 debye unit and thus the molecule doesn't exist solely in the anti form. The dipole moment also varies with temperature and so the molecule cannot exist solely in the *gauche* form either. Therefore, either the *anti* and *gauche* forms are in equilibrium with each other and this varies with temperature or the molecule exists in either form and librates about the C–C bond without passing into the other form.

1.7.2. X-ray and Electron Diffraction

If the molecule under investigation contains relatively heavy atoms then the position of these atoms can be determined using electron diffraction and thus the conformation will become known. 1,2-dihaloethanes[16] are known to exist in the *anti* conformation in the vapour phase but the precise amounts of each conformer is unclear.

Measurements on n-butane[17] have indicated that 60±15% of the molecules exist in the *anti* conformation at 14°C

X-ray diffraction has been used to determine the conformation of molecules in the solid-state. The X-ray pattern of 1,2-dichloroethane[18] shows that it crystallises exclusively in the *anti* form. It is possible, however, for a molecule to crystallise in more than one conformation. Indeed, 1,1,2,2-tetrabromoethane[19] crystallises in a mixture of the two conformations.

1.7.3. Spectroscopy

This is perhaps the most important method of conformational analysis, especially NMR. Before its advent, many conformational analyses had been performed using infrared, Raman and microwave spectroscopy.

Infrared depends upon vibrations leading to a change in molecular dipole moment. Raman depends upon vibration leading to a change in molecular polarisability.

1.7.3.1. Infrared and Raman Spectra

The maximum number of vibrations and hence infrared and Raman lines, in a non-linear molecule of N atoms is 3N-6. A molecule like 1,2-dibromoethane shows the allowed number of lines in the solid-state spectrum but additional lines are present in the liquid and gas phases. The solid-state spectrum shows that the molecule has a centre of symmetry and thus must crystallise in the *anti* conformer. On liquefaction, some molecules transform to the gauche form.[20] In principle, the position of the equilibrium of the *anti* and *gauche* forms of 1,2-dibromoethane can be calculated from the intensity of the spectral lines using a variation of Beer's Law[21]:

$$\frac{N^t}{N^g} = \left(\frac{E^g}{E^t}\right)\frac{\ln\left(\frac{I_0^t}{I^t}\right)}{\ln\left(\frac{I_0^g}{I^g}\right)} \qquad \text{.....(Eq. 1.15)}$$

where, the superscript t and g refer to *trans* and *gauche* respectively, N is the number of molecules per millilitre, E is the molecular extinction coefficient and I_0 and I are the intensities of the incident and transmitted radiation.

1.7.3.2. Microwave Spectroscopy

Microwave spectra have been used to arrive at estimates of the energy barriers to eclipsed conformations. The height of the barrier can be found from the frequency of the rotational absorption band.[22]

1.8. The Principle of Least Distress

Conformational processes in the gas and solution phases are relatively unhindered by neighbouring molecules. However, in the solid-state, the crystal lattice makes it more difficult for conformational processes to occur and consequently their energies of activation are expected to be higher. In the crystal lattice, the majority of atoms have low amplitude motion and act as a reference frame against which a smaller conformationally mobile group can move. Conformational processes are more likely to occur, and thus be observed by NMR, where there is a small volume change involved during the motion. This idea is termed the principle of least distress[23]. When the conformational process involves the rotation of a group about a single bond, then the more symmetrical the group is, the more easily it will rotate. This principle is demonstrated in figure 1.13.

Figure 1.13: A Rotating Group with Ligands of Differing Size.

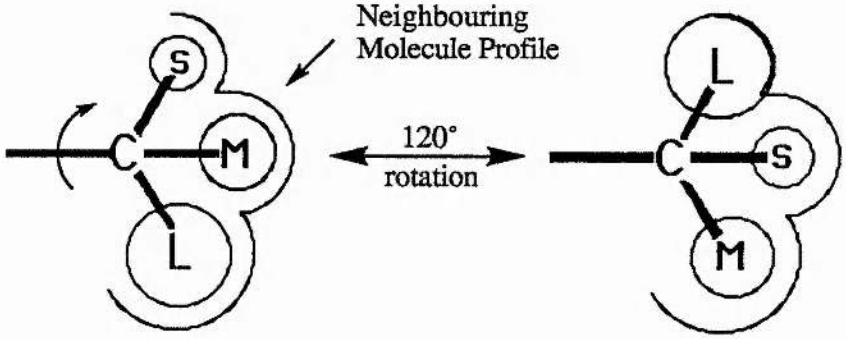

If there is an unsymmetrical group as in figure 1.13, then the distress caused to the lattice as the large group **L** passes through the position occupied by small group **S** will be large. Such a rotational process is, therefore, most likely to be observed when the rotating group approaches conical symmetry.

Chapter Two

Experimental

2.1 Symbols and Abbreviations

mol	moles
h, min	hours, minutes
NMR	nuclear magnetic resonance
ppm	parts per million
Hz	hertz
J	spin-spin coupling constant in Hz
s, d, t, q, m	singlet, doublet, triplet, quartet, multiplet
AB_q	AB quartet
ABX	ABX multiplet
m.p.	melting point
b.p.	boiling point

2.2 Instrumentation

2.2.1 Solution NMR Spectroscopy

All ^1H and ^{13}C solution spectra were obtained on either a Bruker MSL500 spectrometer operating at 500.130 and 125.758 MHz respectively or on a Varian Gemini 200 operating at 200.052 and 50.303 MHz respectively. The quaternary ammonium and phosphonium salts were referenced to methanol (^1H–3.5 ppm and ^{13}C–49.3 ppm) in D_2O and the amines and borane complex to TMS (^1H–0 ppm and ^{13}C–0 ppm) in $CDCl_3$.

2.2.2 Elemental Analysis

Percentage carbon, hydrogen and nitrogen were obtained by Mrs S. Smith using a Carlo-Erba 1106 elemental analyser.

2.2.3 Melting points

All melting points were carried out on an Electrothermal melting point machine. The temperatures are uncorrected.

2.3 Solid–State Spectra

All solid–state NMR spectra were obtained on a Bruker MSL500 spectrometer in either high resolution or high power mode. Solid–state ^{13}C spectra were obtained at 125.758 MHz in the CP/MAS mode using 4 mm o.d. rotors spinning typically at 6–8 kHz. All solid–state spectra including $T_1\rho$ determinations were obtained by the cross polarisation pulse sequence. However, in the case of compound 4 the pulse sequence incorporates a 50 μs dipolar dephasing delay, sufficient to dephase any non-mobile carbons directly bonded to one or two hydrogens. A cross polarisation contact time of 1 ms was used throughout.

Chemical shifts were referenced relative to the CH_2 group in adamantane at 38.56 ppm determined on a separate sample.

The 2D CPEXSY spectra were obtained using a standard pulse sequence including a 1 ms contact time and a mixing time ca. 100–200 ms.

The ^{13}C spin locking frequency during the Hartmann–Hahn condition was determined using single carbon pulses and high power ^1H decoupling on adamantane and was found to be in the region 60–90 kHz. The same radio frequency power was used for the spin lock period in the $T_1\rho$ determinations.

All spinning side bands shown in the spectra are marked thus:

2.4 Calibration of the Variable Temperature Unit [BVT 1000]

The unit was calibrated using the 4 mm MAS probe. Variable temperature spectra were run on compounds with known phase changes[24]. A few samples were chosen, but not all showed a change in the spectrum. Those which did are shown in Table 2.1. The temperature calibration spectra were obtained under conditions as similar as possible to those employed during the measurement of the spectra in this

thesis, thus minimising the effects of heating arising from sample spinning and high power decoupling[25].

Table 2.1: Phase Change Temperature Values for Calibration.

Sample	Phase Change Temperature.	VT Unit Setting	Observations
d-camphor	374	405	Loss of efficiency of CPCYCL but HPDEC works OK.
d,l-camphor	350	380	Doubling of several lines.
pivalic acid	280	271	At high T, t-butyl methyl is a singlet. At low T it is a doublet.
d-camphor	244.5	223	Change in all signals.
adamantane	209	186	Extra broad signals replace 38.56 ppm.

2.5 Line shape Analysis

Line shape analyses for a three site system were calculated using a computer programme kindly supplied by Dr J. E. Anderson. Matching of calculated and observed spectra was done by visual comparison.

Figure 2.1: Compounds Prepared for Study

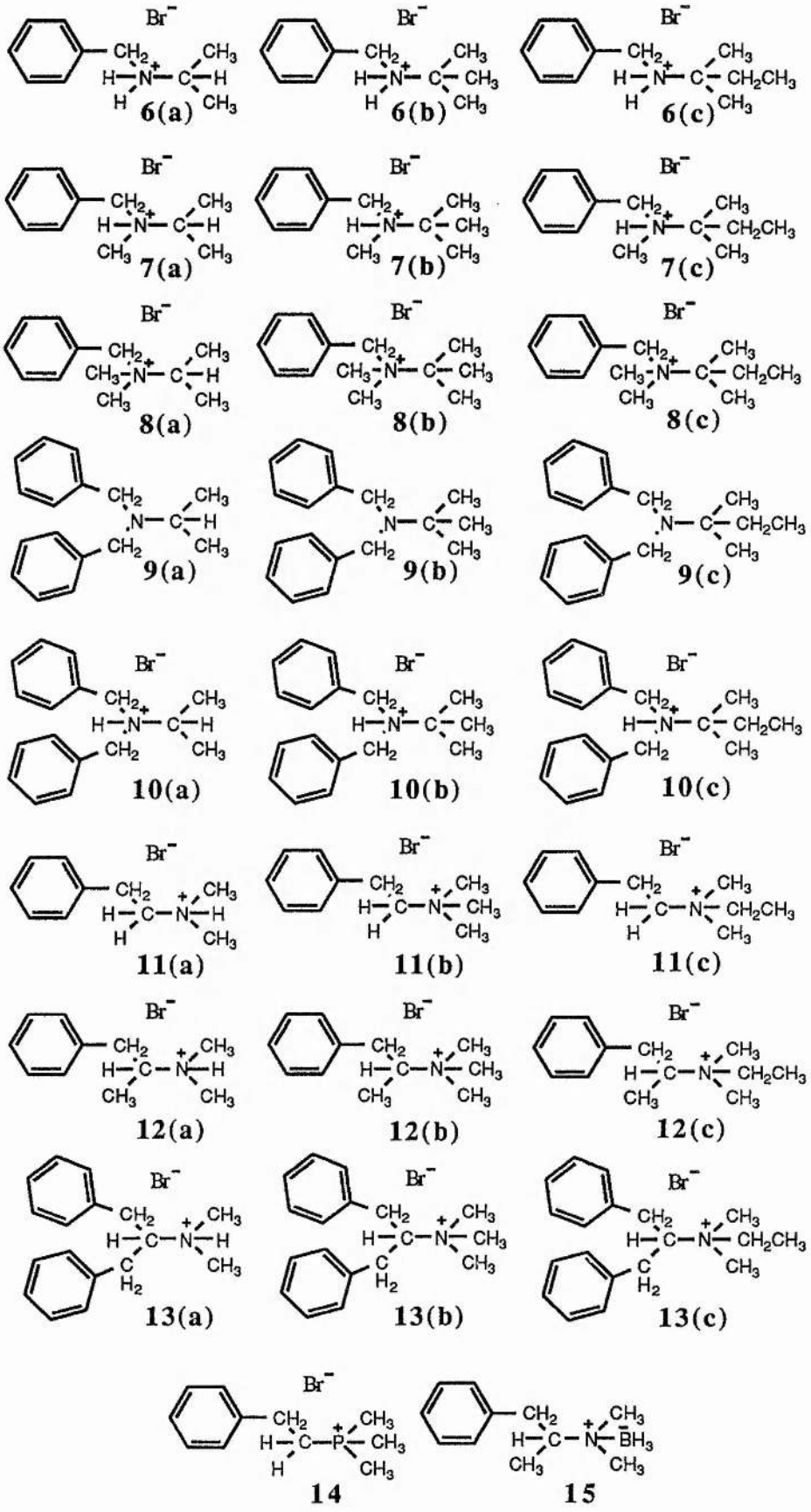

2.6 Synthesis

Elemental Analyses of compounds prepared are given in Table 2.2.

A Preparation of Compounds 6(a), (b) and (c).

A1 Preparation of N-Benzyl-Alkylammonium Bromide

Benzyl bromide [3.42g, 0.02 mol] was added to a large excess of amine [50ml] slowly with cooling, and the resultant precipitate filtered off and recrystallised [ethanol/ether].

A1.1 Preparation of Compound 6(a)

The method of A1 was followed using *i*-propylamine to afford compound 6(a) (4.38g, 95%) as white crystals, m.p. 215–216 °C; ^{1}H NMR (D_2O) 1.5 (6H, d, *J* 6.5, 2 CH_3), 3.7 (1H, m, *J* 6.5, N–CH), 4.4 (2H, s, CH_2) and 7.6 (5H, m, Ph); ^{13}C NMR (D_2O) 18.6 (2 CH_3), 48.6 (CH_2), 60.0 (N–CH), 129.6 (C-2', 6'), 129.8 (C-3', 5'), 130.0 (C-4') and 131.5 (C-1').

A1.2 Preparation of Compound 6(b)

The method of A1 was followed using *t*-butylamine to afford compound 6(b) (3.77g, 78%) as white crystals, m.p. 236–238 °C; ^{1}H NMR (D_2O) 1.6 (9H, s, 3 CH_3), 4.3 (2H, s, CH_2) and 7.6 (5H, m, Ph); ^{13}C NMR (D_2O) 25.3 (3 CH_3), 45.8 (CH_2), 58.3 (4^{ry} C), 129.6 (C-2',6'), 129.7 (C-4'), 129.9 (C-3',5') and 131.8 (C-1')

A1.3 Preparation of Compound 6(c)

The method of A1 was followed using *t*-amylamine to afford compound 6(c) (4.28g, 83%), as white crystals, m.p. 207–208 °C; ^{1}H NMR (D_2O), 1.2 (3H, t, *J* 7.5, Et–CH_3), 1.6 (6H, s, 2 CH_3), 1.9 (2H, q, *J* 7.5, CH_2), 4.4 (2H, s, CH_2) and 7.6 (5H, s, Ph); ^{13}C NMR (D_2O) 7.5 (Et–CH_3), 22.6 (2 CH_3), 30.9 (Et–CH_2), 45.5 (N-CH_2), 61.4 (4^{ry} C), 129.6 (C-2', 6'), 129.8 (C-4'), 130.0 (C-3', 5') and 131.8 (C-1').

B Preparation of Compounds 7(a), (b) and (c).

Methods B1–3 & 6 were used in the preparation of compounds 7(b) and (c). However, this method was not effective for the preparation of compound 7(a) and methods B4–6 were employed instead.

B1 Benzoylation of the Amine

The amine [0.2 mol] was dissolved in NaOH solution [240 ml, 5%] and to this was added benzoyl chloride [30g, 0.21 mol]. The mixture was stirred vigorously for two hours and the resultant precipitate filtered off, recrystallised (ethanol), and dried to give white crystals.

B1.1 Preparation of *t*-Butyl Benzamide.

The general method B1 was followed using *t*-butylamine to afford *t*-butylbenzamide (20.76g, 59%) as a white crystalline solid, m.p. 132–133 °C.[Lit. m.p. = 131–2 °C][25a]

B1.2 Preparation of *t*-Amyl Benzamide.

The general method B1 was followed using *t*-amylamine to afford *t*-amylbenzamide (26.1g, 68%) as a white crystalline solid, m.p. 92–94 °C.[Lit. m.p. = 112–3 °C][25a]

B2 Alkylation of the Amide

NaH [4.4g, 0.11 mol (60% in oil)] was dissolved in dry THF [100ml] and to this was added the amide [0.1 mol] and the mixture heated under reflux for 1 hour. After this time the appropriate alkyl halide [15.6g, 0.11 mol] was added and the heating continued for a further 2 hours. Water [80ml] was then added and the organic layer separated, dried [$MgSO_4$], and the solvent removed to leave a crystalline solid. This was recrystallised from ethanol.

B2.1 Methylation of the *t*-Butyl Amide.

The general method B2 was followed using the *t*-butyl amide and methyl iodide to afford the methylated *t*-butyl amide (13.5g, 71%) as a low melting solid.

B2.2 Methylation of the *t*-Amyl Amide

The general method B2 was followed using the *t*-amyl amide and methyl iodide to afford the methylated *t*-amyl amide (14.8g, 68%) as a low meting solid.

B3 Reduction of the Amide

The amide [0.04 mol] was dissolved in dry THF [20ml] and added dropwise to a solution of $LiAlH_4$ [1.48g, 0.044 mol] in dry THF [50ml]. The mixture was heated under reflux for 1 hour after which NaOH [1.48g, 0.04 mol] in water [1ml] was added to give a white precipitate. The solution was decanted, dried [K_2CO_3], and the solvent removed.

B3.1 Preparation of *N*-Benzyl-*N*-methyl-*t*-butylamine.

The general method B3 was followed using the *t*-butylamide to afford the benzylmethyl amine (6.78g, 96%) as a clear liquid.

B3.2 Preparation of *N*-Benzyl-*N*-methyl-*t*-amylamine.

The general method B3 was followed using the *t*-amylamide to afford the benzylmethyl amine (6.99g, 91%) as a clear liquid.

B4 Benzylation of the Amine

The amine [11.8g, 0.2 mol] was added to NaOH [8g, 0.2 mol] in water [100ml] and to this was added benzyl bromide [34.2g, 0.2 mol] and the solution stirred overnight. The organic layer which separated was found to contain a mixture of mono– and disubstituted amine The mixture was distilled [200°C at 15mm Hg] to afford the benzyl-*i*-propylamine (7.6g, 51%) as a colourless liquid.

B5 Mono-Methylation of the Amine. (The Eschweiller Clark Reaction)

The amine [2.98g, 0.02 mol] was added to 40% aqueous formaldehyde [1.5g, 0.02 mol] in water [12.5ml] with cooling in ice/water. To this was added 98% formic acid [0.94g, 0.02 mol] and the solution heated under reflux for 6 hours. After this time, NaOH pellets [0.8g, 0.02 mol] were added and the resultant mixture extracted with ether, dried[K_2CO_3], and the solvent removed to leave a yellow liquid.

B5.1 Preparation of *N*-Benzyl-*N*-methyl-*i*-propylamine.

The general method B5 was followed using N-benzyl-*i*-propylamine to afford *N*-benzyl-*N*-methyl-*i*-propylamine (2.56g, 79%) as a yellow liquid.

B6 Hydrobromination of the Amine

The amine [0.01 mol] was dissolved in ethanol [20ml] and to this was added 48% hydrobromic acid [1.69g, 0.01 mol]. The solvent was removed leaving a white solid which was recrystallised [ethanol/ether].

B6.1 Preparation of compound 7(a)

The method of B6 was followed using *i*-propylamine to afford compound 7(a) (2.31g, 95%) as white crystals, m.p. 132–134 °C; ^{1}H NMR (D_2O) 1.5 (6H, d, *J* 7, 2 CH_3), 2.8 (3H, s, N-CH_3), 3.8 (1H, m, *J* 7, CH), 4.4 and 4.6 (2H, ABq, *J* 12 N-CH_2) and 7.6 (5H, m, Ph); ^{13}C NMR (D_2O) 16.2 (2 CH_3), 35.4 (N-CH_3), 56.9 (N–CH_2), 57.6 (N–CH), 129.6 (C-2',6'), 130.3 (C-4'), 130.8 (C-1') and 131.0 (C-3',5').

B6.2 Preparation of Compound 7(b)

The method B6 was followed using *t*-butylamine to afford compound 7(b) (2.30g, 89%) as white crystals, m.p. 180–181 °C; ^{1}H NMR (D_2O) 1.7 (9H, s, 3 CH_3), 2.8 (3H, s, N–CH_3), 4.0 and 4.7 (2H, ABq, *J* 12, N-CH_2)and 7.7 (5H, m,

Ph); ^{13}C NMR (D_2O) 24.3 (3 CH_3), 34.0 (N–CH_3), 55.1 (N-CH_2), 64.7 (4^{ry} C), 129.6 (C-2',6'), 130.2 (C-4'), 130.4 (C-1') and 131.2 (C-3',5').

B6.3 Preparation of Compound 7(c)

The method B6 was followed using *t*-amyl amine to afford compound 7(c) (2.27g, 84%) as white crystals, m.p. 156–157 °C; ^1H NMR (D_2O) 1.2 (3H, t, *J* 7.5, Et–CH_3), 1.6 (6H, s, 2 CH_3), 2.1 (2H, q, Et–CH_2), 2.8 (3H, s, N-CH_3), 4.1 and 4.8 (2H, ABq, *J* 12, N-CH_2) and 7.6 (5H, m, Ph); ^{13}C NMR (D_2O) 7.8 (Et–CH_3), 21.2 (2 CH_3), 29.5 (Et–CH_2), 34.0 (N-CH_3), 54.9 (N-CH_2), 68.3 (4^{ry} C), 129.6 (C-2',6'), 130.2 (C-4',1') and 131.3 (C-3',5').

C Preparation of Compounds 8(a), (b) and (c)

C1 Dimethylation of the Amine (The Eschweiller Clark Reaction)

The amine [0.25 mol] was added to 40% aqueous formaldehyde [35g, 0.5 mol] in water [12.5ml] with cooling in ice/water. To this was added 98% formic acid [23.5g, 0.5 mol] and the solution heated under reflux for 6 hours. After this time, NaOH pellets [10g, 0.25 mol] were added and the resultant organic layer separated, dried[K_2CO_3], and distilled.

C1.1 Preparation of *N,N*-Dimethyl-*i*-propylamine.

The general method C1 was followed using *i*-propylamine to afford dimethyl-*i*-propylamine (13.7g, 63%) as a colourless oil.

C1.2 Preparation of *N,N*-Dimethyl-*t*-butylamine.

The general method C1 was followed using *t*-butyl amine to afford dimethyl-*t*-butylamine (14.4g, 57%) as a colourless oil, b.p. 90–91 °C.

C1.3 Preparation of *N,N*-Dimethyl-*t*-amylamine.

The general method C1 was followed using *t*-amylamine to afford dimethyl-*t*-amylamine (19.4g, 67%) as a colourless oil.

C2 Benzylation of the amine

The amine [0.04 mol] was added to a solution of benzyl bromide [6.84g, 0.04 mol] in ethanol [20ml] and the solution heated under reflux for 1 hour. The solvent was removed leaving a white solid which was recrystallised from ethanol/ether.

C2.1 Preparation of Compound 8(a)

The method C2 was followed using *i*-propylamine to afford compound 8(a) (3.09g, 46%) as a white crystalline solid, m.p. 205–206 °C; ^{1}H NMR (D_2O) 1.6 (6H, d, *J* 6.5, 2 CH_3), 3.1 (6H, s, N-CH_3), 3.8 (1H, m, *J* 6.5, N–CH), 4.6 (2H, s, N-CH_2), and 7.7 (5H, m, Ph); ^{13}C NMR (D_2O) 16.3 (2 CH_3), 47.0 (2 N-CH_3), 65.4 (N-CH_2), 66.4 (N–CH), 127.7 (C-4'), 129.4 (C-2',6'), 130.9 (C-1') and 133.2 (C-3',5').

Crystal data: $C_{12}H_{20}NBr$, M_r = 258.2, orthorhombic, Pcab, a = 9.7610(2)Å, b = 29.896(1)Å, c = 10.0389(2)Å, V = 2537.6Å, Z = 8, D_c = 1.17 g cm^{-3}. The structure was solved from X-ray powder diffraction data collected on a Stoe STADI/P transmission system, λ = 1.54056Å ($CuK_{\alpha 1}$). Data was collected over the range $5° < 2\theta < 85°$ in 0.02° steps, the entire run lasting about 15 hours. Data was indexed on the basis of the first 20 observable lines using the program TREOR (M_{20} = 21.6). The pattern decomposition option of the Rietveld program GSAS was used to extract the first 121 integrated intensities from the powder pattern. These were used as input to the direct methods program SIR (12), from which the Br atom was located. The remaining atoms were found via successive difference Fourier / least squares cycles applied to Rietveld refinement of the whole diffraction profile. In the final stages of refinement, chemical constraints were added (C–C (ring) = 140(1)Å, C–C–C (ring) = 120°, C–C (exo) = 155(1)Å, C–N = 157(1)Å). Final agreement indices were R_{wp} = 8.4%, χ^2 = 4.47, for 59 parameters and 4018 observations (919 reflections).

C2.2 Preparation of Compound 8(b)

The method C2 was followed using *t*-butylamine to afford compound 8(b) (3.9g, 36%) as a white crystalline solid, m.p. 196–197 °C; ^{1}H NMR (D_2O) 1.7 (9H, s, 3 CH_3), 3.0 (6H, s, 2 N–CH_3), 4.6 (2H, s, CH_2) and 7.7 (5H, m, Ph); ^{13}C NMR (D_2O) 21.5 (3 CH_3), 42.2 (2 N-CH_3), 59.8 (CH_2), 71.5 (4^{ry} C), 126.0 (C-4'), 127.1 (C-3', 5'), 131.6 (C-2', 6') and 128.6 (C-1').

C2.3 Preparation of Compound 8(c)

The method C2 was followed using *t*-amylamine to afford compound 8(c) (3.48g, 32%) as a white crystalline solid, m.p. 174–175 °C; ^{1}H NMR (D_2O) 1.3 (3H, t, *J* 7, CH_3), 1.8 (6H, s, 2 CH_3), 2.2 (2H, q, *J* 7, CH_2), 3.0 (6H, s, 2 N-CH_3), 4.6 (2H, s, N-CH_2) and 7.7 (5H, m, Ph); ^{13}C NMR (D_2O) 9.7 (Et–CH_3), 19.8 (2 CH_3), 27.9 (Et–CH_2), 44.4 (2 N-CH_3), 62.1 (N-CH_2), 78.5 (4^{ry} C), 128.3 (C-1'), 129.3 (C-2', 6'), 130.8 (C-4'), 133.8 (C-3', 5').

D Preparation of Compounds 9(a), (b) and (c)

D1.1 Preparation of N-Benzoyl-*t*-butylamine.

The general method B1 was followed using *t*-butylamine to afford N-Benzoyl-*t*-butylamine (20.76g, 59%) as white crystals, m.p. 132–133 °C.

D1.2 Preparation of N-Benzoyl-*t*-amylamine.

The general method B1 was followed using *t*-amylamine to afford N-Benzoyl-*t*-amylamine (26.1g, 68%) as white crystals, m.p. 92–94 °C.

D2.1 Alkylation of the *t*-Butyl Amide.

The general method B2 was followed using the *t*-butyl amide and benzyl bromide to afford the benzyl amide (6.56g, 61%) as white crystals, m.p. 104–106 °C

D2.2 Alkylation of the *t*-Amyl Amide.

The general method B2 was followed using the *t*-amyl amide and benzyl bromide to afford the benzyl amide (4.45g, 40%) as white crystals, m.p. 69–72 °C

D3.1 Reduction of the *t*-Butyl Amide to Afford Compound 9(b).

The general method B3 was followed using the *t*-butyl benzyl amide (0.02 mole equivalent) to afford the dibenzyl amine, 9(b), (2.63g, 52%) as white crystals, m.p. 66–68 °C; ^{1}H NMR ($CDCl_3$) 1.2 (9H, s, 3 CH_3), 3.8 (4H, s, 2 CH_2) and 7.3 (10H, m, Ph); ^{13}C NMR ($CDCl_3$) 27.5 (3 CH_3), 54.3 (2 N-CH_2), 55.6 (4^{ry} C), 126.0 (C-4'), 127.0 (C-2', 3', 5', 6') and 142.8 (C-1').

D3.2 Reduction of the *t*-Amyl Amide to Afford Compound 9(c).

The general method B3 was followed using the *t*-amyl benzyl amide (0.02 mole equivalent) to afford the dibenzyl amine, 9(c), (3.45g, 65%) as white crystals, m.p. 41–42 °C; ^{1}H NMR ($CDCl_3$) 1.2 (3H, t, *J* 7.5, Et–CH_3), 1.8 (6H, s, 2 CH_3), 2.2 (2H, q, *J* 7.5, Et–CH_2), 3.6 (4H, s, 2 N–CH_2), 7.2 (4H, d, *J* 7.5, 2, 6), 7.4 (4H, t, *J* 7.5, H–3', 5') and 7.5 (2H, t, *J* 7.5, H-4'); ^{13}C NMR ($CDCl_3$) 8.7 (Et–CH_3), 24.3 (2 CH_3), 32.8 (Et–CH_2), 53.8 (2 N-CH_2), 58.0 (4^{ry} C), 126.0 (C-4'), 127.7 (C-3', 5'), 128.3 (C-2', 6') and 142.7 (C-1').

D4 Preparation of Compound 9(a).

The general method B4 was followed using *i*-propylamine to afford the dibenzyl amine (6.34g, 27%) as white crystals, m.p. 33–34 °C; ^{1}H NMR ($CDCl_3$) 1.0 (6H, d, *J* 7, 2 CH_3), 2.9 (1H, m, CH), 3.5 (4H, s, 2 N-CH_2) and 7.3 (10H, m, Ph); ^{13}C NMR ($CDCl_3$) 18.0 (2 CH_3), 48.6 (2 CH_2), 53.7 (N-CH), 127.1 (C-4'), 128.6 (C-3', 5'), 129.0 (C-2', 6') and 141.4 (C-1').

E Preparation of Compounds 10(a), (b) and (c).

E1.1 Preparation of Compound 10(a)

The general method B6 was followed using compound 9(a) (0.004 mole equivalents) to afford compound 10(a) (1.12g, 88%) as white crystals, m.p. 162–163 °C; ^{1}H NMR (D_2O) 1.6 (6H, d, *J* 6.6, 2 CH_3), 3.8 (1H, m, *J* 6.6, CH), 4.3 and 4.6 (4H, AB_q, *J* 13.4, 2 CH_2), 7.5 (4H, m, H-3', 5') and 7.6 (6H, m, H-'2, 4', 6'); ^{13}C NMR (D_2O) 18.2 (2 CH_3), 56.0 (2 CH_2), 56.8 (N-CH), 132.0 (C-1', 3', 5'), 132.7 (C-4') and 133.8 (C-2', 6').

E1.2 Preparation of Compound 10(b)

The general method B6 was followed using compound 9(b) (0.004 mole equivalents) to afford compound 10(b) (0.96g, 72%) as white crystals, m.p. 190–191 °C; ^{1}H NMR (D_2O) 1.5 (9H, s, 3 CH_3), 4.1 and 4.6 (4H, AB_q, *J* 13.6, 2 CH_2), 6.9 (4H, d, H-2', 6') and 7.2 (6H, m, H-3', 4', 5'); ^{13}C NMR (D_2O) 22.6 (3 CH_3), 52.4 (2 N-CH_2), 65.1 (4^{ry} C), 127.0 (C-3', 5'), 127.4 (C-4'), 128.5 (C-2', 6') and 128.8 (C-1').

E1.3 Preparation of Compound 10(c).

The general method B6 was followed using compound 9(c) (0.004 mole equivalents) to afford compound 10(c) (1.01g, 73%) as white crystals, m.p. 207–208 °C; ^{1}H NMR (D_2O) 1.2 (3H, t, *J* 7.5, Et–CH_3), 1.8 (6H, s, 2 CH_3), 2.2 (2H, q, *J* 7.5, Et–CH_2), 4.4 and 4.9 (4H, AB_q, *J* 13.8, 2 N-CH_2), 7.2 (4H, d, *J* 7.5, H-2', 6'), 7.4 (4H, t, *J* 7.5, H-3', 5') and 7.5 (2H, t, *J* 7.5, H-4'); ^{13}C NMR (D_2O) 8.4 (Et–CH_3), 21.8 (2 CH_3), 29.5 (Et–CH_2), 54.7 (2 N-CH_2), 71.8 (4^{ry} C), 129.4 (C-3', 5'), 129.7 (C-4'), 130.7 (C-2', 6') and 131.2 (C-1').

F Preparation of Compounds 11(a), (b) and (c).

F1 Dimethylation of the Amine

The general method C1 was followed using phenethylamine (0.2 mole equivalents) to afford N,N-Dimethylphenethylamine (25.65g, 43%) as a yellow liquid, b.p. 85°C at 14mm Hg.

F2 Preparation of Compound 11(a)

The general method B6 was followed using N,N-dimethylphenethylamine (0.34 mole equivalents) to afford compound 11(a) (5.18g, 67%) as a white crystalline solid, m.p. 145–146 °C; ^{1}H NMR (D_2O) 3.1 (6H, s, 2 CH_3), 3.2 (2H, t, *J* 7.5, CH_2), 3.5 (2H, t, *J* 7.5, N-CH_2), 7.5 (3H, m, H-2', 4', 6') and 7.6 (2H, m, H-3', 5'); ^{13}C NMR (D_2O) 30.3 (CH_2), 43.3 (2 N-CH_3), 58.8 (N-CH_2), 127.6 (C-4'), 129.0 (C-3', 5'), 129.4 (C-2', 6') and 136.5 (C-1').

F3 Alkylation of the N,N-Dimethylphenethylamine

The amine [2g, 0.013 mol] was dissolved in dichloromethane [2 ml]. The alkyl bromide was then bubbled through the solution and a white precipitate was produced. The product was recrystallised [ethanol/ether].

F3.1 Preparation of Compound 11(b)

The general method F3 was followed using N,N-dimethylphenethylamine and methyl bromide to afford compound 11(b) (2.3g, 70%) as white crystals, m.p. 233–234 °C; ^{1}H NMR (D_2O) 3.1 (9H, s, 3 N–CH_3), 3.2 (2H, t, *J* 7.5, Ph-CH_2), 3.6 (2H, t, *J* 7.5, N-CH_2), 7.5 (3H, m, H-3', 4', 5') and 7.6 (2H, m, H-2', 6'); ^{13}C NMR (D_2O) 30.4 (CH_2), 43.3 (3 N-CH_3), 58.8 (N-CH_2), 127.7 (C-4'), 129.0 (C-3', 5'), 129.4 (C-2', 6') and 136.5 (C-1').

F3.2 Preparation of Compound 11(c)

The general method F3 was followed using N,N-dimethylphenethylamine and ethyl bromide to afford compound 11(c) (2.08g, 62%) as white crystals, m.p. 152–153 °C; ^{1}H NMR (D_2O) 1.3 (3H, t, *J* 7.5, CH_3), 3.0 (6H, s, 2 N-CH_3), 3.1 (2H, t, *J* 7, Ph-CH_2), 3.4 (4H, m, *J* 7.5, 2 CH_2) and 7.3 (5H, m, Ph); ^{13}C NMR (D_2O) 10.3 (CH_3), 31.2 (CH_2), 52.7 (2 N-CH_3), 61.3 (N-CH_2), 62.7 (N-CH_2), 130.2 (C-4'), 131.6 (C-1'), 131.7 (C-3', 5') and 131.8 (C-2', 6').

G Preparation of Compounds 12(a), (b) and (c)

G1 Preparation of Benzylmethyloxime.

Benzylmethyl ketone [13.4g, 0.1 mol] was added to a solution of hydroxylamine sulphate[8.2g, 0.05 mol] and sodium acetate [16.4g, 0.2 mol] in water [50ml]. The solution was shaken vigorously for 10 minutes and the organic layer was separated with ether, dried [$MgSO_4$] and the solvent removed to leave an orange liquid (10.46g, 70%).

G2 Reduction of the Oxime

The oxime [10.46g, 0.07 mol] was dissolved in super dry ethanol [80ml] and the solution brought to the boil. The heat was removed and sodium metal added [16.15g, 0.7 mol] at such a rate as to maintain the vigorous reflux action. Once all the sodium had reacted, the solution was acidified with dilute hydrochloric acid and extracted with ether to remove any unreacted oxime etc. NaOH pellets were then added to the aqueous layer until basic and an oil separated. This was extracted with ether, dried [K_2CO_3] and the solvent removed.

G2.1 Preparation of 1-Phenyl-2-Aminopropane.

The general method G2 was followed using the benzyl methyl oxime to afford 1-phenyl-2-aminopropane (8.51g, 90%) as a yellow liquid.

G3 Preparation of 1-Phenyl-2-(Dimethylamino)propane.

The general method C2 was followed using 1-phenyl-2-amino propane (0.04 mole equivalent) to afford 1-phenyl-2-(dimethylamino)propane (5.94g, 91%) as a yellow liquid.

G4 Preparation of Compound 12(a)

The general method B6 was followed using 1-phenyl-2-(dimethylamino)propane (0.003 mole equivalents) to afford compound 12(a) (0.71g, 97%) as a white crystalline solid, m.p. 154–155 °C; ^{1}H NMR (D_2O) 1.4 (3H, d, *J* 6.5, CH_3), 3.0 and 3.2 (2H, ABX, J_{AX} 6, CH_2), 3.0 (6H, s, 2 CH_3), 3.8 (1H, m, *J* 6.5, CH), 7.4 (3H, m, H-3', 4', 5') and 7.5 (2H, m, H-2', 6'); ^{13}C NMR (D_2O) 12.5 (CH_3), 37.0 (CH_2), 39.5 (2 N-CH_3), 63.7 (N-CH), 127.7 (C-4'), 129.3 (C-3', 5'), 129.5(C-2', 6') and 136.1 (C-1').

G5 Preparation of Compound 12(b)

The general method F3 was followed using 1-phenyl-2-(dimethylamino)propane (0.006 mole equivalents) and methyl bromide to afford Compound 12(b) (1.22, 79%) as a white solid, m.p. 140–141 °C; ^{1}H NMR (D_2O) 1.4 (3H, d, *J* 6.5, CH_3), 3.0 and 3.4 (2H, ABX, J_{AX} 7, Ph-CH_2), 3.3 (9H, s, 3 N–CH_3), 3.9 (1H, m, *J* 6.5, CH), 7.5 (3H, m, H-3', 4', 5') and 7.6 (2H, m, H-2', 6'); ^{13}C NMR (D_2O) 13.0 (CH_3), 36.0 (CH_2), 51.4 (3 N-CH_3), 72.7 (N-CH), 127.6 (C-4'), 129.3 (C-3', 5'), 129.6 (C-2', 4') and 136.5 (C-1').

G7 Preparation of Compound 12(c)

The general method F3 was followed using 1-phenyl-2-(dimethylamino)propane (0.006 mole equivalents) and ethyl bromide to afford compound 12(c) (1.2g, 75%) as a white crystalline solid, m.p. 120–121 °C; ^{1}H NMR (D_2O) 1.4 (3H, d, *J* 7, CH_3), 1.5 (3H, t, *J* 7, CH_3), 3.21 (3H, s, N-CH_3), 3.26 (3H, s, N-CH_3), 2.9 and 3.5 (2H, ABX, J_{AB}7 ,Ph-CH_2), 3.7 (2H, q, *J* 7, N-CH_2), 3.9

(1H, m, *J* 7, N–CH), 7.5 (3H, m, H-3', 4', 5') and 7.6 (2H, m, H-2', 6'); ^{13}C NMR (D_2O) 7.7 (Et–CH_3), 12.6 (CH_3), 35.5 (CH_2), 47.8 (2 N-CH_3), 58.8 (N-CH_2), 69.9 (N-CH), 127.5 (C-4'), 129.2 (C–3', 5'), 129.5 (C–2', 6') and 136.4 (C–1').

H Preparation of Compounds 13(a), (b) and (c).

H1 Preparation of the Dibenzyl Oxime

The general method G1 was followed using dibenzyl ketone to afford the dibenzyl oxime (20.76g, 92%) as a white solid.

H2 Reduction of the Oxime

The general method G2 was followed using dibenzyl oxime (0.044 mole equivalent) to afford 1,3-diphenyl-2-aminopropane (7.57g, 86%) as a yellow liquid.

H3 Preparation of 1,3-Diphenyl-2-(dimethylamino)propane

The general method C1 was followed using 1,3-diphenyl-2-aminopropane (0.033 mole equivalent) to afford 1,3-diphenyl-2-(dimethylamino)propane (5.36g, 86%) as a yellow liquid.

H4 Preparation of Compound 13(a).

The general method B6 was followed using 1,3-diphenyl-2-(dimethylamino)propane (0.002 mole equivalent) to afford compound 13(a) (0.6g, 94%) as a white crystalline solid, m.p. 198–199 °C; ^1H NMR (D_2O) 3.0 (6H, s, 2 N-CH_3), 3.1 and 3.3 (4H, ABX, J_{AX} 7.5, 2 CH_2), 4.1 (1H, m, *J* 7.5, CH), 7.4 (4H, d, *J* 7.5, H-2', 6'), 7.45 (2H, t, *J* 7.5, H-4') and 7.5 (4H, t, *J* 7.5, H-3', 5'); ^{13}C NMR (D_2O) 34.6 (2 CH_2), 40.0 (2 N-CH_3), 69.0 (N-CH), 127.8 (C-4'), 129.4 (C-3', 5'), 129.5 (C-2', 6') and 135.9 (C-1').

H5 Preparation of Compound 13(b)

The general method F3 was followed using 1,3-diphenyl-2-(dimethylamino)propane (0.004 mole equivalent) and methyl bromide to afford compound 13(b) (0.91g, 68%) as a white crystalline solid, m.p. 205–206 °C; ^{1}H NMR (D_2O) 3.1 and 3.3 (4H, ABX, J_{AX} 7.5, 2 CH_2), 3.3 (9H, s, 3 CH_3), 4.2 (1H, m, J 7.5, CH), 7.3 (4H, d, J 7.5, H-2', 6') and 7.4 (6H, m, H-3', 4', 5'); ^{13}C NMR (D_2O) 35.1 (2 CH_2), 52.2 (3 N-CH_3), 77.8 (N-CH), 127.3 (C-4'), 129.2 (C-3', 5'), 129.3 (C-2', 6'), 136.7 (C-1').

H6 Preparation of Compound 13(c)

The general method F3 was followed using 1,3-diphenyl-2-(dimethylamino)propane (0.004 mole equivalent) and ethyl bromide to afford compound 13(c) (0.41g, 32%) as a white crystalline solid, m.p. 209–210 °C; ^{1}H NMR (D_2O) 1.4 (3H, t, J 7.5, CH_3), 3.1 and 3.5 (4H, ABX, J_{AX} 7.5, 2 CH_2), 3.2 (6H, s, 2 N-CH_3), 3.6 (2H, q, J 7.5, N-CH_2), 4.1 (1H, m, N-CH), 7.2 (4H, d, J 7.5, H-2', 6'), 7.4 (6H, m, H-3', 4', 5'); ^{13}C NMR (D_2O) 7.8 (Et–CH_3), 34.9 (2 CH_2), 48.7 (2 N–CH_3), 59.5 (N-CH_2), 75.8 (N-CH), 127.5 (C-4'), 129.3 (C-3', 5'), 129.4 (C-2', 6'), 137.0 (C-1').

J Preparation of Alkyl-Trimethylphosphonium Bromides.

Alkyl bromide [0.005 mol] was placed in a glass tube and to this was added 1M trimethylphosphine in toluene [5ml, 0.005 mol]. The tube was then sealed and placed in an oven at 110°C for 8 hours. A white crystalline solid was produced which was recrystallised [ethanol/ether].

J1 Preparation of Compound 14

The general method J was followed using phenethylbromide to afford compound 14 (1.08g, 84%) as a white crystalline solid, m.p. 168–169 °C; ^{1}H NMR (D_2O) 2.0 (9H, d, J 10.5, 3 P-CH_3), 2.7 (2H, m, P-CH_2), 3.1 (2H, m, CH_2), 7.5

(3H, m, H-3', 4', 5') and 7.6 (2H, m, *J* 7.5, H-2', 6'); ^{13}C NMR (D_2O) 8.0 (3C, d, *J* 55, 3 P-CH_3), 24.7 (1C, d, *J* 55, P-CH_2), 27.0 (CH_2), 127.4 (C-4'), 128.5 (C-3', 5'), 129.4 (C-2', 6') and 139.5 (C-1').

K Preparation of an Amine-Borane Complex.

Borane dimethylsulphide complex (2M in THF), [1.5ml, 0.003 mol] was added to 1-phenyl-2-(dimethylamino)propane [0.5g, 0.003 mol] and the solvent removed to leave a white solid.

K1 Preparation of Compound 15.

The general method K1 was followed using 1-phenyl-2-(dimethylamino)propane to afford compound 15 (0.48g, 90%) as a white solid, m.p. 124–125 °C; ^1H NMR ($CDCl_3$), 1.1 (3H, d, J 7.5, CH_3), 2.6 (3H, s, N-CH_3), 2.5 and 3.7 (2H, AB_q, J_{AB} 7.5, CH_2), 2.7 (3H, s, N-CH_3), 3.1 (1H, m, J 7.5, CH), and 7.3 (5H, m, Ph); ^{13}C NMR ($CDCl_3$), 13.95 (CH_3), 38.5 (CH_2), 47.9 (N-CH_3), 50.8 (N-CH_3), 68.7 (N-CH), 127.0 (C-4'), 129.1 (C-3', 5'), 129.7 (C-2', 6') and 139.4 (C-1').

Table 2.2: Elemental Analysis for the Synthesised compounds

		Carbon		Hydrogen		Nitrogen	
Comp	Formula	Required	Found	Required	Found	Required	Found
6 (a)	$C_{10}H_{16}NBr$	52.19	52.09	7.01	7.06	6.09	6.34
(b)	$C_{11}H_{18}NBr$	54.11	54.38	7.43	7.24	5.74	5.45
(c)	$C_{12}H_{20}NBr$	55.82	55.76	7.81	7.41	5.42	5.68
7 (a)	$C_{11}H_{18}NBr$	54.11	54.10	7.43	7.50	5.74	5.93
(b)	$C_{12}H_{20}NBr$	55.82	55.68	7.81	8.15	5.42	5.47
(c)	$C_{13}H_{22}NBr$	57.36	57.36	8.15	8.41	5.15	5.26
8 (a)	$C_{12}H_{20}NBr$	55.82	56.01	7.81	7.94	5.42	5.42
(b)	$C_{13}H_{22}NBr$	57.36	57.75	8.15	7.78	5.15	5.10
(c)	$C_{14}H_{24}NBr$	58.74	59.14	8.82	9.16	4.89	4.96
9 (a)	$C_{17}H_{21}N$	85.31	85.51	8.84	9.03	5.85	5.85
(b)	$C_{18}H_{23}N$	m.p. 68–70 °C, lit. m.p[23a] 68–70 °C					
(c)	$C_{19}H_{25}N$	85.32	85.73	9.42	9.84	5.24	5.26
10 (a)	$C_{17}H_{22}NBr$	63.75	63.75	6.92	6.91	4.37	4.37
(b)	$C_{18}H_{24}NBr$	64.67	64.91	7.24	7.29	4.19	4.17
(c)	$C_{19}H_{26}NBr$	65.52	65.94	7.52	7.87	4.02	4.04
11 (a)	$C_{10}H_{16}NBr$	52.18	52.41	7.01	7.03	6.09	6.09
(b)	$C_{11}H_{18}NBr$	54.11	54.18	7.43	7.59	5.74	5.72
(c)	$C_{12}H_{20}NBr$	55.82	55.96	7.81	7.97	5.42	5.44
12 (a)	$C_{11}H_{18}NBr$	54.12	54.31	7.43	7.67	5.74	5.74
(b)	$C_{12}H_{20}NBr$	55.82	55.94	7.81	8.01	5.42	5.50
(c)	$C_{13}H_{22}NBr$	57.34	57.77	8.15	8.04	5.14	5.15
13 (a)	$C_{17}H_{22}NBr$	63.75	64.19	6.92	7.08	4.37	4.48
(b)	$C_{18}H_{24}NBr$	64.67	64.88	7.24	7.52	4.19	4.30
(c)	$C_{19}H_{26}NBr$	65.52	65.65	7.52	8.07	4.02	4.06
14	$C_{11}H_{18}PBr$	50.59	50.52	6.95	7.18	—	—
15	$C_{11}H_{20}NB$	74.60	74.36	11.38	10.90	7.91	7.50

2.7 Preparation of Schiff Base for Ring–Chain Tautomerism.

Both the *cis*-2-Aminomethylcyclohexanol and 3-aminopropionamide oxime starting material were kindly supplied by Prof Ferenc Fulop.

2.7.1 Preparation of Compound RC1.

cis-2-Aminomethylcyclohexanol (0.65g, 0.005 mol) was dissolved in ethanol (10 ml) and *p*-nitrobenzaldehyde (0.76g, 0.005 mol) was added. Immediately on dissolution, the solvent was evaporated off at reduced pressure with a maximum water bath temperature of 40 °C. The product was used immediately for kinetic studies.

2.7.2 Preparation of Compound RC2

To a suspension of 3-aminopropionamide oxime (1.03g, 0.01 mol) in ethanol (30 ml) at 20–25 °C, *p*-nitrobenzaldehyde (1.08g, 0.01 mol) was added. After stirring for about 2 min a clear solution resulted to which n-hexane (150 ml) was added with rigorous stirring. An oil precipitated from which the solvent was decanted. With fresh hexane (75 ml) this operation was repeated and finally the product crystallised by trituration with diethyl ether. The product was used immediately on crystallisation.

Chapter Three

Group Rotations

Introduction

Bearing in mind the principle of least distress, the need for highly symmetric groups is apparent if we are to observe rotations about single bonds in the solid-state. The most obvious case for the observation of a rotation is that of the methyl group with C_{3v} symmetry. Each hydrogen as it rotates through 120° moves into a space taken by an identical atom. Thus the barrier to rotation is likely to be very small as such a rotation will cause little distress to the crystal lattice.

Figure 3.1: Compounds (1), (2) and (3) all exhibit intra molecular motion

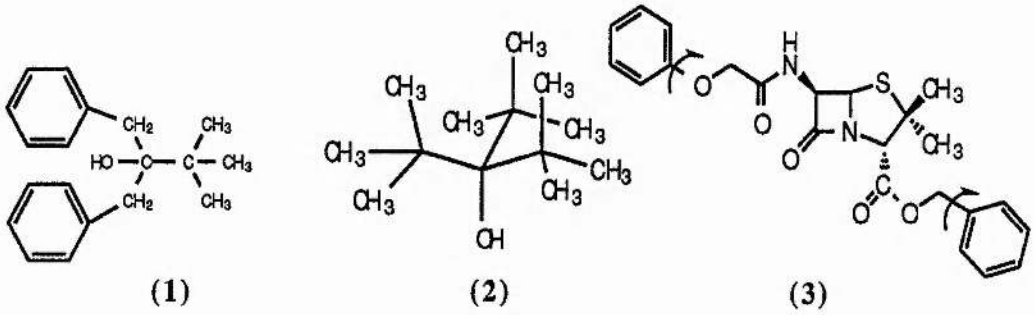

(1) (2) (3)

Similar in its local symmetry, but much larger than the methyl group, is the *t*-butyl group having, predictably, a higher energy barrier to rotation. It too has conical C_{3v} symmetry and is ideal for rotational studies. It is expected that such rotations, however, would be much slower that the methyl group rotation. In solid 1,1-dibenzyl-2,2-dimethylpropan-1-ol[23] (**1**) an average signal is observed for the *t*-butyl methyls above ambient temperature, due to rapid rotation of the group. On cooling this average signal splits into three separate methyl signals as the rotation is frozen out on the NMR time scale. The free energy of activation for this process is calculated as being 54.8 $kJmol^{-1}$ from the coalescence at 293K. The methyl rotation is far too rapid to interact with the NMR processes involved in obtaining the cross-polarised spectra. It is interesting to note that the removal of the constraints of the crystal lattice by measuring

the same process in the solution phase gives a substantially lower activation energy of 38 $kJmol^{-1}$.

Although this group is highly symmetrical, it does not mean to say that the space available to each methyl in a *t*-butyl group is the same in a crystal lattice. The restricted rotation of one methyl in a *t*-butyl group has been observed in solid tri-*tert*-butylmethanol[26] **(2)**. The rotational barrier is anomalously high in energy due to hindrance at one methyl position when the *t*-butyl rotation is frozen out at low temperatures. The free energy of activation has been calculated from the maximum dipolar broadening of the methyl group and is shown to be 31.8 $kJmol^{-1}$.

Many studies on compounds of the form $(CH_3)_3CX$ have been done, where X equals Cl[27], Br[28], I[29], CHO[29], SH[30], NO_2[31] or CN[32-33]. These compounds commonly exist in three or four solid phases. The lowest temperature phases have *t*-butyl and methyl rotations of low enough frequency to be measured by NMR techniques (T_1 and $T_1\rho$ measurements), whereas, in the higher temperature phases whole molecule reorientations are dominant. Table 3.1 shows activation energies for *t*-butyl rotations in these compounds. In most cases the methyl rotation is slower than the *t*-butyl rotation.

Table 3.1: Data for Some Simple *t*-Butyl Derivatives

***t*-Butyl Derivative**	**E_a for *t*-Butyl Rotation**	**Methyl Rotation**
	($kJmol^{-1}$)	(w.r.t. *t*-butyl rot^n)
Cl	15	?
Br	22	slow
I	?	fast
Aldehyde	15	slow
SH	16.2	slow
NO_2	15	fast
CN	16-17	slow

Perhaps even more surprising is the observation of phenyl group rotations in crystalline penicillins[34] (3). One would imagine the barrier to rotation of such a group to be enormous due to the apparently flat ring structure. However, the substantial π density above and below the ring in fact gives the phenyl group a more cylindrical shape and it is thus more susceptible to rotation although in the case of (3) the activation energy is 89 kJmol^{-1} in size.

Of greater interest is the quest for rotating groups with much less symmetry than the *t*-butyl group such as ethyl, *iso*-propyl and *t*-amyl groups. These are likely to have much higher rotational barriers unless the lattice can readily accommodate the rotation of these groups with local C_{2v} symmetry.

Another commonly occurring conformational process of low activation volume, worthy of mention here, is that of pseudorotating cycloalkane rings. A study [35] has been completed on cyclopentane and cyclohexane derivatives in the solid state which gives free energies of activation in the range 38–63.5 kJmol^{-1}. The pseudorotation of cyclopentane rings occurs by the displacement of one CH_2 group out of the ring plane which is then transmitted around the ring. In this way, ring strain is greatly reduced (Figure 3.2).

Figure 3.2: Pseudorotating rings of cyclopentane.

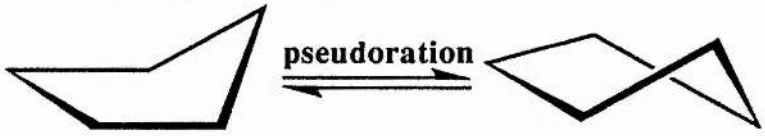

With such interesting and observable processes occurring in the solid-state it seemed appropriate to continue the search for conformationally mobile groups like the methyl, *t*-butyl and phenyl rotations above. Also, a reliable and accurate method of measuring the rates of motion was required.

The quest begins with two double *t*-butyl compounds (4) and (5). The structure of these compounds had been solved by X-ray diffraction[36] and they each contain two *t*-butyl groups. It should be possible, therefore, to relate structure to activation

parameters and to compare the activation parameters for each of the *t*-butyls in the molecule.

3.1 Double *t*-Butyl Group Rotations

Both compounds (4) and (5) were kindly donated by Prof. E Eliel

Figure 3.3: Compounds (4) and (5) containing two *t*-butyl groups

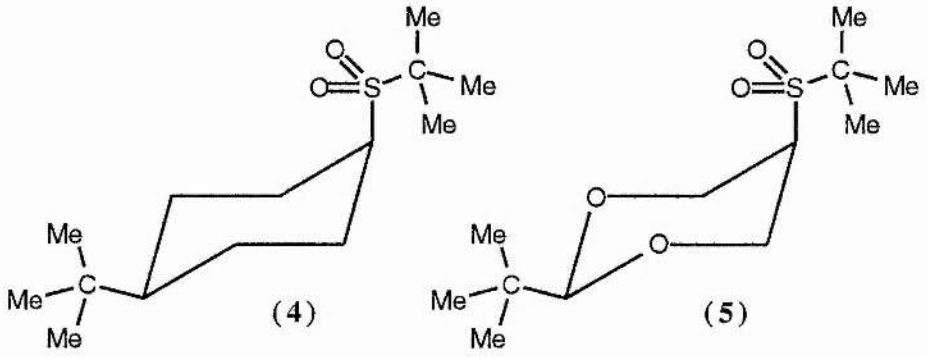

The aim of this experiment was to measure the rate of rotation of both *t*-butyl groups of *cis*-4-*t*-butyl-1-(*t*-butylsulphonyl)cyclohexane, (4), at a number of temperatures using solid state nmr techniques. Hence, the activation parameters for the rotation could be determined. Two methods were applied.

The first involves line shape simulation for a three site system using a computer programme. However this sort of information can only be gained around the point of coalescence where the spectrum changes visibly with temperature.

In observing the coalescence of the *t*-butyl groups in (4) it was observed that at temperatures ca. 50° above coalescence there was a marked reduction in the intensities of the coalescing resonances but not of the other resonances. Furthermore, a crude extrapolation of the coalescence rate data into the region of reduced intensity suggested that the rate of rotation should be about the same as the precessional frequency of the ^{13}C nuclei in the spin lock field for cross polarisation (50–100 kHz). If this were the case a reduction in $T_1\rho$ should ensue, cross polarisation would become much less efficient and the signal intensity would therefore be reduced. We set out to test this

because in principle $T_1\rho$ measurements should considerably extend the temperature range for rate measurements.

3.2 The Theory

Provided that the methyls of the *t*-butyl group are rotating much faster than the *t*-butyl group itself, then for a dipolar interaction between unlike spins[37], i.e. ^{13}C and ^{1}H,

$$\frac{1}{T_1\rho} = \frac{B^2\tau}{(1+\omega_1^2\tau^2)} \quad \text{.....(Eq. 3.1)}$$

Where, B^2 is a measure of the ^{13}C–^{1}H dipolar interaction strength which depends upon molecular geometry, τ is the correlation time for the molecular motion causing the relaxation and ω_1 is the frequency of the ^{13}C nuclei in the spin lock field, which is determined by a single pulse experiment after the Hartmann Hahn condition is established. As the rate and thus τ will vary with temperature, this equation shows the temperature dependence of $T_1\rho$.

$T_1\rho$ has a minimum value at the temperature where,

$$\omega_1\tau = 1 \quad \text{.....(Eq. 3.2)}$$

When this is the case, equation **3.1** may be simplified to equation **3.3**:

$$B^2 = \frac{2}{(T_1\rho)_{min}\tau} \quad \text{.....(Eq. 3.3)}$$

By using the minimum value of $T_1\rho$, the value of B^2 can be determined experimentally and thus, τ values at other temperatures may be calculated by solving the resulting quadratic equation.

The value of τ denotes the correlation time for a 360° reorientation of the *t*-butyl group. This reorientation occurs in a 3-fold potential energy well similar to that discussed in section **1.6**. However, to calculate such terms as enthalpy and entropy of activation for the rotation of a group over this barrier, the rate constant (k) to be used must relate to a 120° rotation only and so,

$$k = \frac{3}{\tau} \quad \text{.....(Eq. 3.4)}$$

Therefore, if the above theory is correct and $T_1\rho$ is temperature dependent, then four predictions can be made and confirmed experimentally:

(a) both the methyl and central carbons of the same group must have their $T_1\rho$ minimum at the same temperature;

(b) if the geometry of the t-butyl groups is consistent (as it should be) then the central and methyl carbons must have a similar minimum value for $T_1\rho$ in each t-butyl group;

(c) the rate constants derived from $T_1\rho$ measurements must lie on the same line of an Eyring plot as the line shape results and

(d) experimentally calculated B^2 values must be comparable to the calculated values using the equation by Abragam[38].

In addition to the rate constants, from the plot of $T_1\rho$ versus Temperature, those values of $T_1\rho$ which lie along the asymptotic slope can be used to derive the activation energy (E_a) for the rotation. This is extremely useful when the accumulated data does not pass through a minimum (usually due to the temperature being outwith the limits of the probe) and as a result an experimentally derived B^2 value cannot be obtained. Looking at equation 3.2, it becomes apparent that:

(a) At higher temperatures $\omega_1\tau << 1$.

(b) At lower temperatures $\omega_1\tau >> 1$ and

Now, using equation 3.1:

$$\text{case (a) gives, } \frac{1}{T_1\rho} = B^2\tau$$

$$\text{and from eq. 3.4, } \tau = \frac{3}{k}$$

$$\text{substituting in k gives, } T_1\rho = \frac{k}{3B^2}$$

$$\therefore T_1\rho \propto k$$

and

$$\text{case (b) gives, } \frac{1}{T_1\rho} = \frac{B^2\tau}{\omega_1^2\tau^2}$$

$$\text{on simplifying, } \frac{1}{T_1\rho} = \frac{B^2}{\omega_1^2} * \frac{1}{\tau}$$

$$\text{substituting in k gives, } \frac{1}{T_1\rho} = \frac{B^2}{\omega_1^2} * \frac{k}{3}$$

$$\therefore T_1\rho \propto k^{-1}$$

As $T_1\rho$ is proportional to the rate, k, a plot of $\ln(T_1\rho)$ versus 1/T gives the activation energy (E_a) for the rotation from the asymptotic slope.

Figure 3.4 shows the room temperature ^{13}C CP/MAS spectrum of compound (4). Unfortunately, the *t*-butyl resonances are partly obscured by the methine and methylene carbons. However, by incorporating a 50μs dipolar dephasing delay into the pulse sequence (NQS) these carbons are edited out leaving the *t*-butyl carbons only. Figure 3.5 represents the temperature dependent ^{13}C nmr spectra of (4) in the solid state. At room temperature the peaks at 61 and 24ppm represent the quaternary and methyl carbons respectively in the S-*t*-butyl group. The remaining peaks at 34 and 29ppm are due to the corresponding carbons in the C-*t*-butyl group. At 163K, the

individual methyl carbons in the S-*t*-butyl group can be seen at 22, 24 and 25ppm (Ratio 1:1:1). The individual methyls in the C-*t*-butyl group are also observable at this temperature but this time as a doublet (ratio 2:1) at 31 and 25ppm (shoulder) respectively. Exchange between these sites was confirmed by observation of cross peaks in a 2D CPEXSY spectrum at 173K using a conventional pulse sequence and a 100ms mixing time. At temperatures above the region where dynamic line shape changes occur, a reduction in the intensities of the *t*-butyl signals is observed due to efficient $T_1\rho$ relaxation.

The rate of relaxation was measured by incorporating a variable delay (typically 0.1–15ms) into the pulse programme before acquisition and noting the relative intensities of the four peaks on transformation. These measurements were performed over the temperature range 209–333K. A plot of ln(intensity) against the variable delay (in msec) gives a straight line graph with slope equal to $-1/T_1\rho$

In this way, $T_1\rho$ values can be calculated for each temperature and the results are shown in Table 3.2. A plot of $T_1\rho$ against temperature gives the expected inverted bell-shaped curve with minimum when the rate of rotation approximates to the frequency of the spin lock field; Figure 3.6.

Looking at the predictions made earlier, it is now clear from Figure 3.6 that the carbons in each t-butyl group have their minimum at the same temperature [prediction (a)]. Both sets of methyls have a minimum value at ca. 2.7ms and the quaternary carbons at ca. 7.5ms [prediction (b)]. Table 3.3 shows the experimental and calculated values for the $^{13}C-^{1}H$ dipolar interaction strength, B^2, which have very good agreement of within a factor of two [prediction (d)]. Many thanks go to Prof. J. H. Strange for this calculation.

This data can be represented in an Eyring plot; Figure 3.7. The data on the left hand side of the line is from the $T_1\rho$ measurements and the line shape analysis is shown on the right hand side.

The graph [Figure 3.7(a)] shows the excellent agreement between the two independent but complementary methods of obtaining data [prediction (c)]. Moreover,

the agreement between the two carbons in the same group is also very good [Figure 3.7(b)].

Table 3.2: $T_1\rho$ Values (msec) for the *t*-Butyl Carbons of (4); [ω_1 = 89 kHz]

T(K)	61ppm	34ppm	29ppm	24ppm
320	16.90			9.39
312	10.89			7.67
305	9.13			4.84
298	7.58			3.70
290	6.22	47.20	16.10	3.15
283	7.84	24.40	9.87	2.59
276	8.11	18.05	6.75	3.50
268	10.76	15.43	6.35	4.46
261	38.16	9.32	2.93	6.26
253	28.65	9.42	3.25	12.80
246		7.37	2.57	14.80
238		8.10	3.16	22.50
232		15.82	4.32	
224		27.25	7.28	

Table 3.3: Calculated and Experimental B^2 Values (s^{-2})

Resonance (ppm)	Experimental value	Calculated value
61	2.0×10^8	1.8×10^8
33	1.5×10^8	1.8×10^8
29	4.1×10^8	7.5×10^8
24	3.9×10^8	7.5×10^8

Figure 3.4: Room Temperature ^{13}C CP/MAS Spectrum of Compound 4

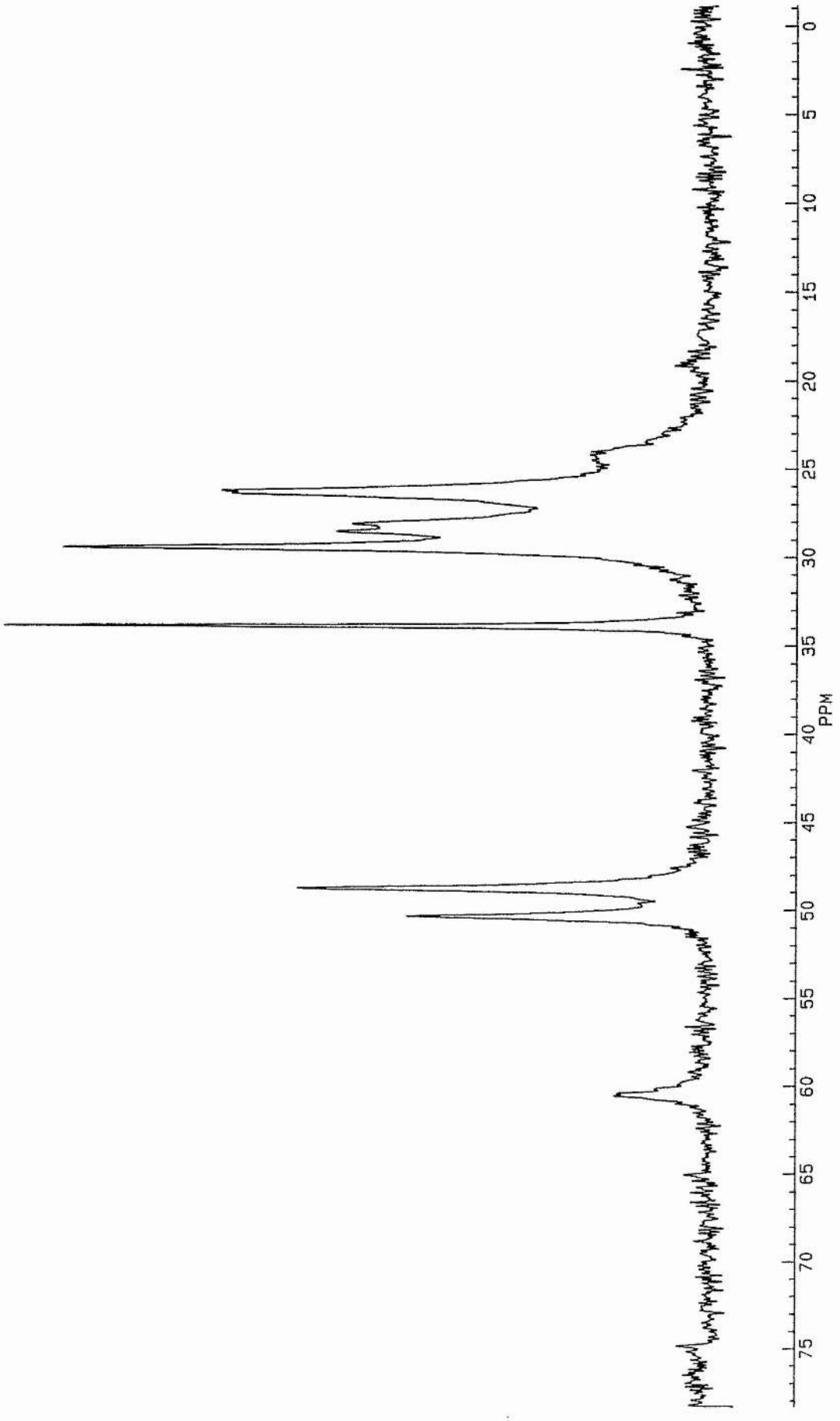

Figure 3.5: Variable temperature ^{13}C CP/MAS Spectra of Compound 4

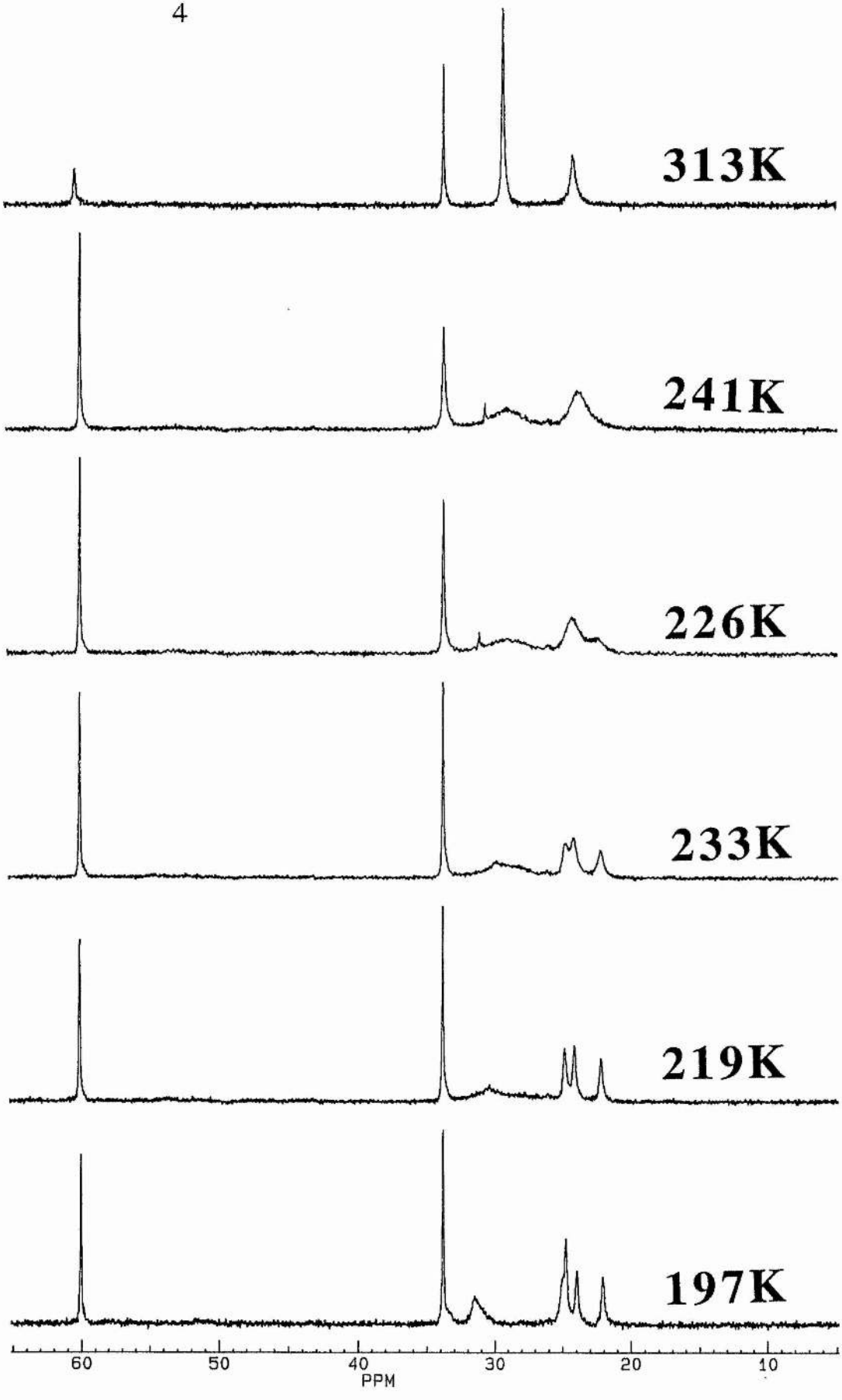

Figure 3.6: $T_1\rho$ versus temperature for the *t*-butyl carbons of (4)

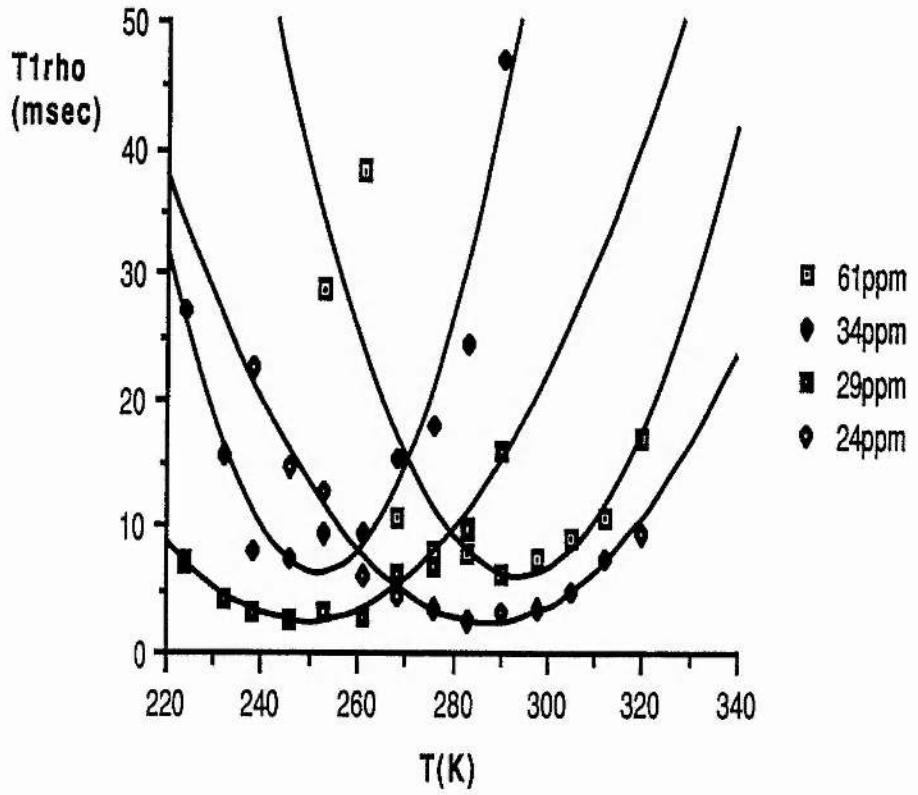

Table 3.4: Rate Constants (s^{-1}) for *t*-Butyl Group Rotations in (4)

T(K)	61ppm	33ppm	29ppm	24ppm
320	1.00×10^7			1.06×10^7
312	6.19×10^6			8.54×10^6
305	5.01×10^6			5.04×10^6
298	3.90×10^6			3.47×10^6
290	2.78×10^6	2.12×10^7	1.95×10^7	2.53×10^6
283	1.68×10^6	1.01×10^7	8.48×10^6	1.68×10^6
276	6.57×10^5	7.82×10^6	7.88×10^6	8.91×10^5
268	4.62×10^5	6.55×10^6	7.37×10^6	6.20×10^5
261	1.22×10^5	3.40×10^6	2.40×10^6	4.12×10^5
253	1.62×10^5	3.46×10^6	3.04×10^6	1.93×10^5
246		1.68×10^6	1.68×10^6	1.60×10^5
238		1.09×10^6	9.78×10^5	1.09×10^5
232		4.17×10^5	6.03×10^5	
224		2.32×10^5	3.29×10^5	
Line Shape Data				
233				3.6×10^4
229				2.8×10^4
225				1.9×10^4
222				1.3×10^4
219				9.0×10^3
215				6.0×10^3
211			1.0×10^5	
209			4.5×10^4	
202			2.0×10^4	

Figure 3.7(a): Eyring plot for the *t*-butyl methyls of (4)

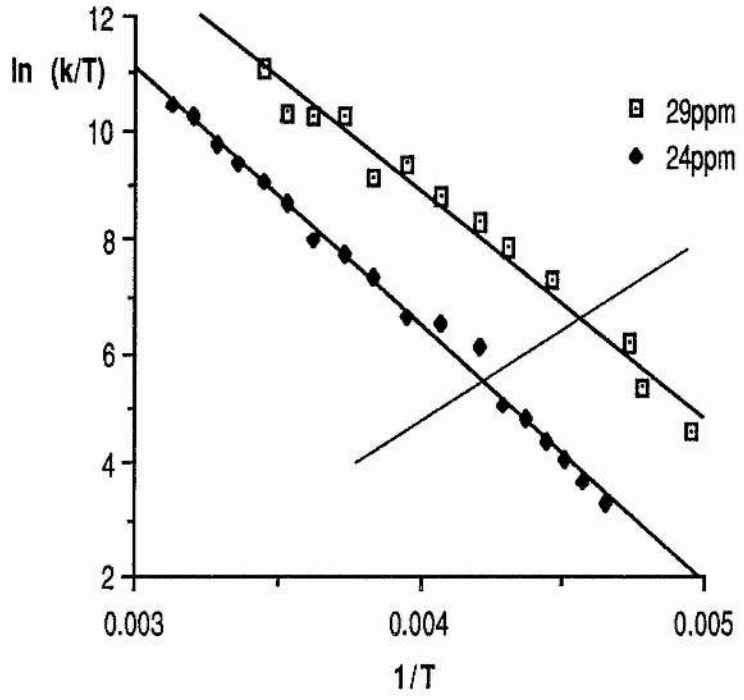

Figure 3.7(b): Eyring plot for all *t*-butyl carbons of (4)

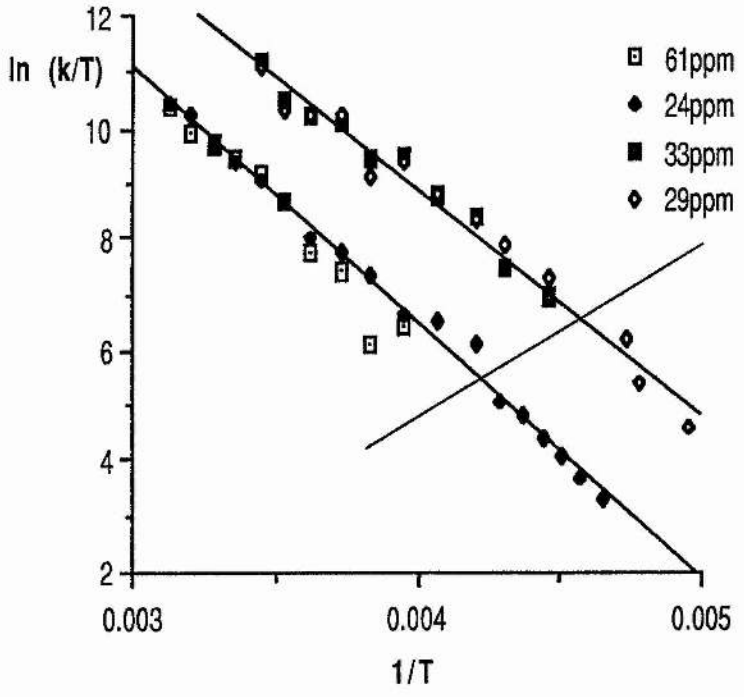

This data can be used to determine the enthalpy and entropy of activation for the rotation of the *t*-butyl groups. The relevant equations are:

$$\Delta H^{\ddagger} = -R(\text{slope}) \quad \text{.....(Eq. 3.5)}$$

$$\Delta S^{\ddagger} = R(\text{int} - \ln(\tfrac{k}{h})) \quad \text{.....(Eq. 3.6)}$$

where R is the Gas constant, int is the intercept of the line on the y axis, k is the Boltzmann constant and h is Planck's constant.

Using these equations the enthalpy and entropy of activation was determined and the values shown in Table 3.5.

Table 3.5: Activation Parameters for Compound (4):

	29/34ppm	24/61ppm
$\Delta H^{\ddagger}$ (kJ mol^{-1})	33.5±3.2	38.2±1.5
$\Delta S^{\ddagger}$ (J K^{-1}mol^{-1})	+10.3±13.5	+9.4±5.9

These values for enthalpy and entropy of activation are fairly accurate as the data spans ~ 150K and was derived by 2 independent but complementary methods. The errors quoted represent 95% confidence limits (taken as 2 times σ).

It can be concluded from this experiment that $T_1\rho$ measurements in ^{13}C CP/MAS NMR spectroscopy can be used to measure rates of internal molecular motions and this together with the line shape data, can be combined to give accurate activation parameters.

When the anisotropic temperature parameters for the methyls are resolved along and perpendicular to the direction of rotation then for each *t*-butyl, two out of three methyl groups show large parameters along the direction of rotation[39]. This is consistent with the *t*-butyl rotation.

Similar to (4) is compound (5), *cis*-2-*t*-butyl-5-(*t*-butylsulphonyl)-1,3-dioxane. The room temperature ^{13}C CP/MAS spectrum is shown in Figure 3.8. Like the previous example this compound also exhibits rapid rotation of its *t*-butyl groups at room temperature as is shown in the variable temperature spectra; Figure 3.9. At ambient temperature the S-*t*-butyl quaternary and methyl carbons can be seen at 62 and 25ppm respectively. The corresponding C-*t*-butyl carbons are located at 36 and 27ppm respectively. The ring C(2) and C(5) are shown at 108 and 50 ppm respectively. The remaining C(4) and C(6) are at 65 and 68 ppm. At the low temperature limit the C-*t*-butyl methyls are at 28.5 and 24ppm in the ratio 2:1. Exchange between these sites is shown in the 2D CPEXSY spectrum at 145K with a 200 ms mixing time. The S-*t*-butyl methyls are as a single peak at 25ppm. Once again, at temperatures above the region where dynamic line shape changes take place, reductions in intensity of the signals from the *t*-butyl groups are observed.

$T_1\rho$ values were measured over the region 335–204K and the values are shown in Table 3.6. The data, expressed graphically (Figure 3.10 and 3.11), again shows inverted bell shaped curves which are consistent with the predictions made earlier. However, due to the unfortunate overlapping of the *t*-butyl methyl signals of both groups at low temperatures it was not possible to perform lineshape analysis on this compound.

Again using equations 3.5 and 3.6 the rate data for compound (5) can be determined and is shown in Table 3.7. Figure 3.12 shows the Eyring plots for the data derived from the two *t*-butyl groups. The data is in very good agreement.

On examination of the corresponding activation parameters (Table 3.8), compound (5) appears to have marginally lower values for both the enthalpy and entropy of activation than compound (4). The decrease in the activation energy may be due to the rotation of the t-butyl groups becoming less hindered in compound (5) as the CH_2s at positions 1 and 3 are replaced by much smaller O atoms.

Figure 3.8: Room Temperature ^{13}C CP/MAS Spectrum of Compound 5

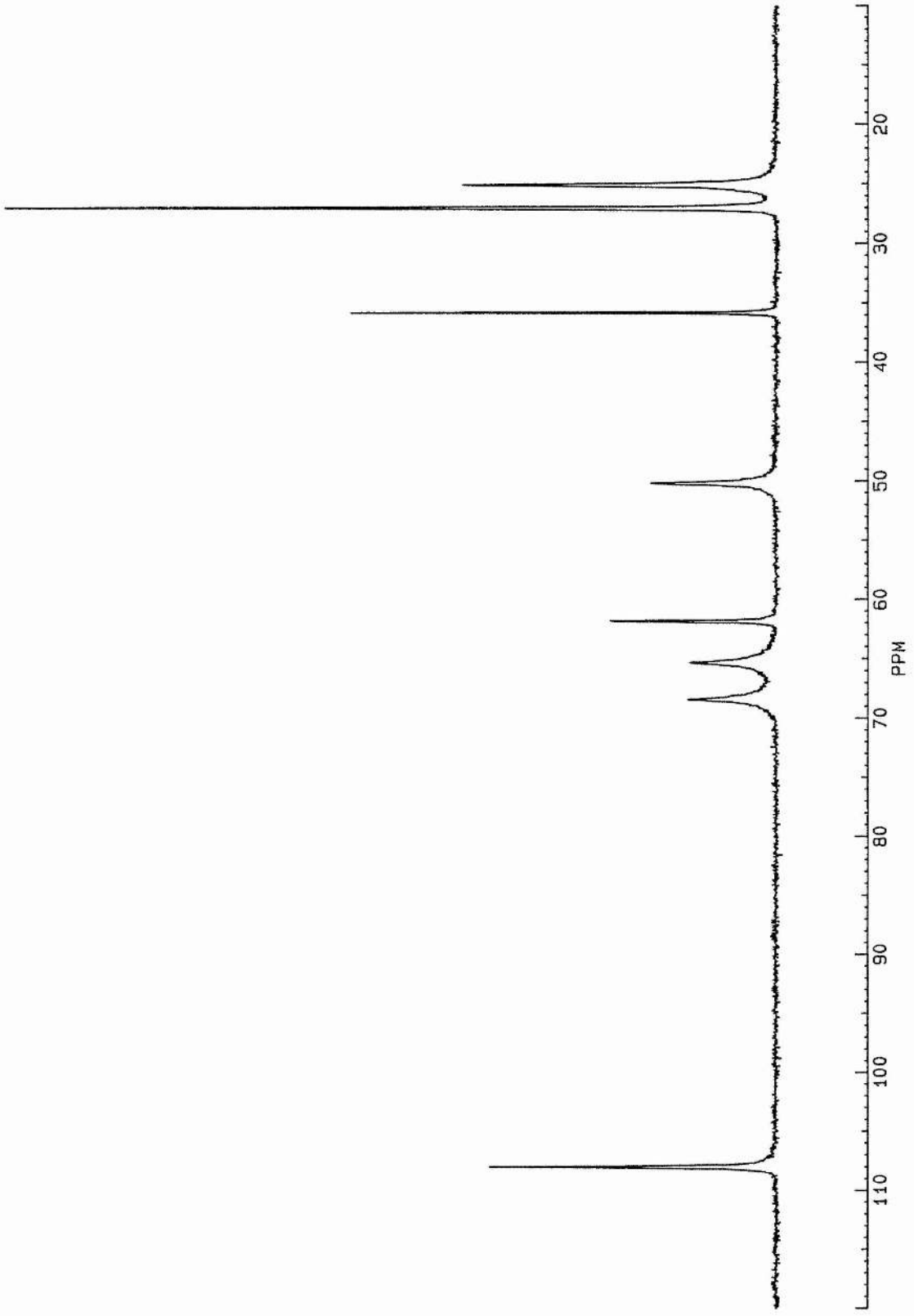

Figure 3.9: Variable Temperature ^{13}C CP/MAS Spectra of Compound 5

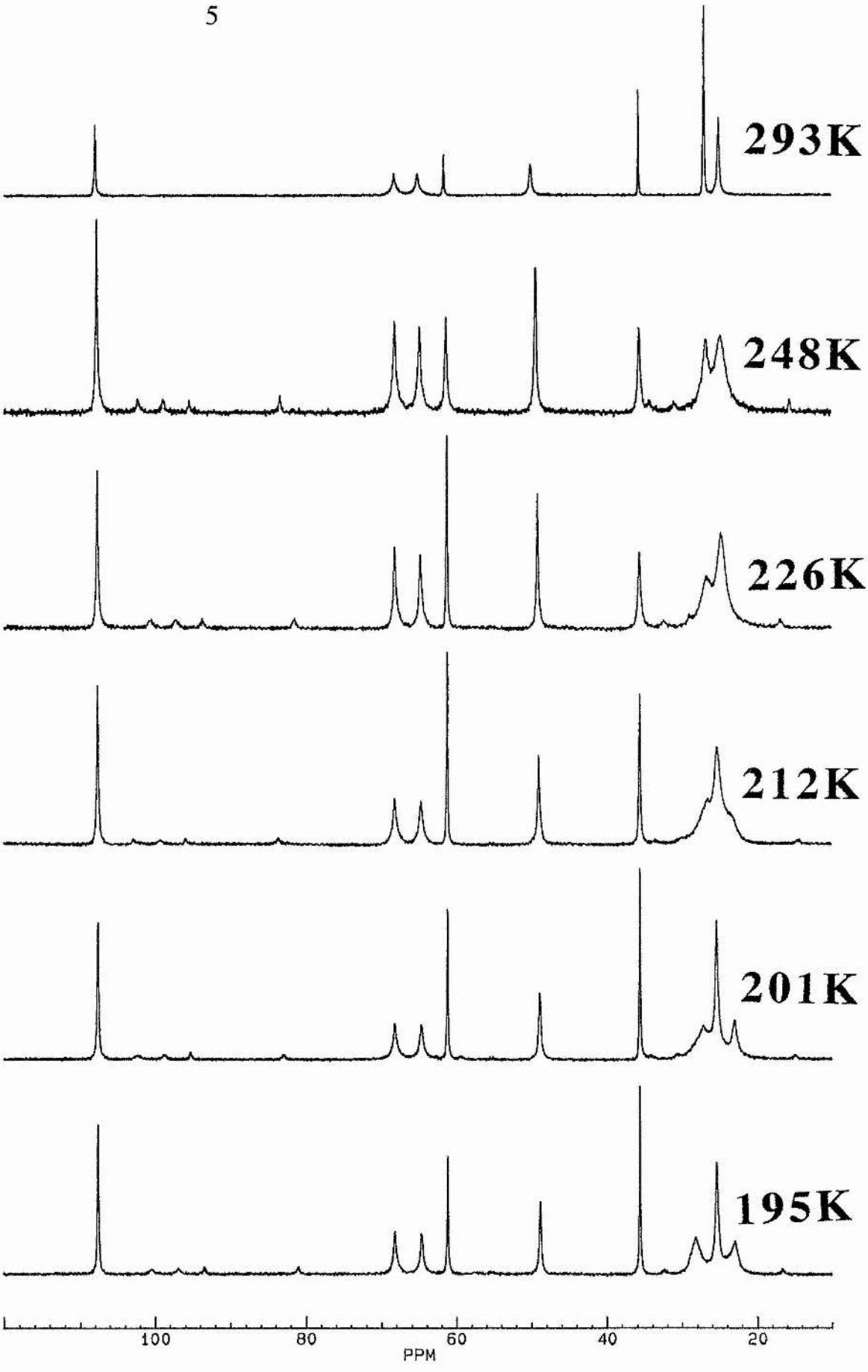

Table 3.6: $T_1\rho$ Values (msec) for the *t*-Butyl Carbons of (5); [ω_1 = 63 kHz]

T(K)	62ppm	36ppm	27ppm	25ppm
328				37.04
321				25.64
313			63.29	23.81
306			50.00	18.52
299	47.62		41.67	14.29
292	31.25		45.46	12.20
284	22.73	47.62	22.22	8.48
277	12.99	22.73	9.43	4.17
270	6.85	52.63	14.49	4.55
262		20.83	8.20	3.79
255	7.04	13.70	5.92	2.38
248	8.26	10.00	4.20	3.02
241	8.85	8.55	2.81	3.95
233	25.64	5.32	3.86	5.75
226	38.46	6.25	4.15	9.17
219		8.20	3.33	11.63
212		9.35	4.07	15.63
204		13.16		18.52

Figure 3.10: T1ρ versus Temperature for the S-*t*-butyl of (5)

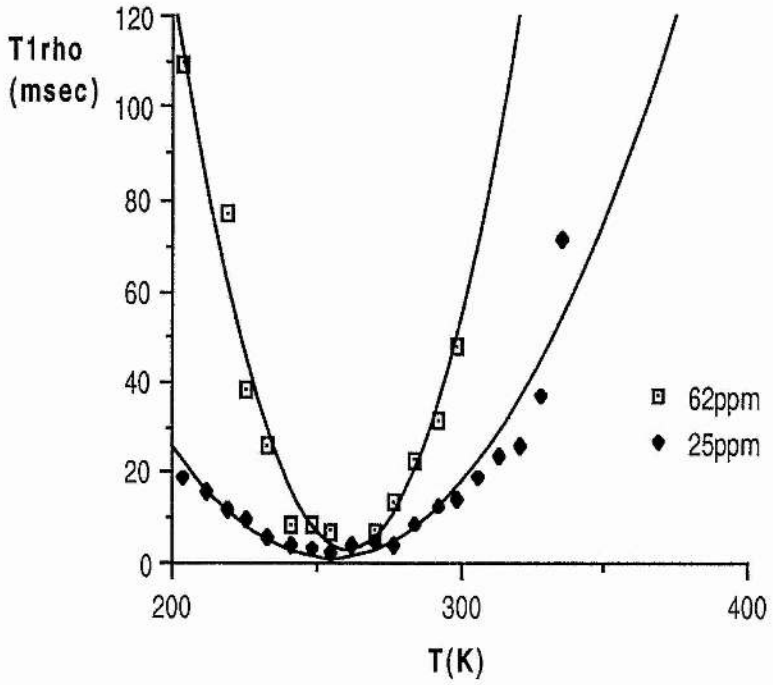

Figure 3.11: T1ρ versus Temperature for the C-*t*-butyl of (5)

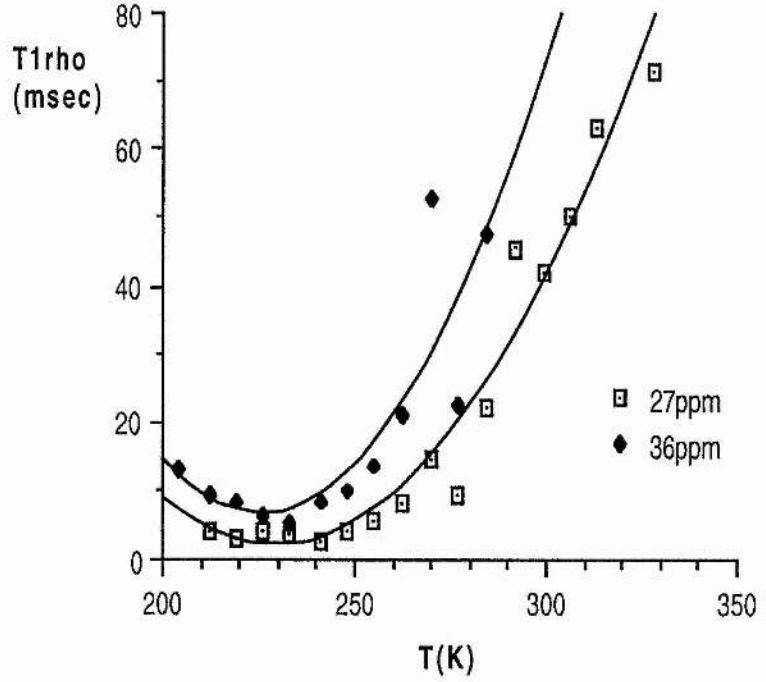

Table 3.7: Rate Constants (s^{-1}) for the *t*-Butyl Group Rotation in (5)

T(K)	62ppm	36ppm	27ppm	25ppm
328				3.7×10^7
321				2.6×10^7
313			5.3×10^7	2.4×10^7
306			4.2×10^7	1.9×10^7
299	1.6×10^7		3.5×10^7	1.4×10^7
292	1.1×10^7		3.8×10^7	1.2×10^7
284	7.7×10^6	2.1×10^7	1.9×10^7	8.3×10^6
277	4.1×10^6	1.0×10^7	7.8×10^6	3.8×10^6
270	1.2×10^6	2.3×10^7	1.2×10^7	4.3×10^6
262		9.1×10^6	6.7×10^6	3.4×10^6
255	9.2×10^5	5.8×10^6	4.7×10^6	1.4×10^6
248	6.2×10^5	4.1×10^6	3.1×10^6	5.6×10^5
241	5.6×10^5	3.4×10^6	1.0×10^6	3.8×10^5
233	1.6×10^5	1.3×10^6	5.0×10^5	2.5×10^5
226	1.1×10^5	6.6×10^5	4.5×10^4	1.5×10^5
219		4.3×10^5	6.3×10^5	1.2×10^5
212		3.7×10^5	4.7×10^5	8.9×10^4
204		2.5×10^5		7.5×10^4

Table 3.8: Activation Parameters for Compound (5)

	27/36ppm	25/62ppm
$\Delta H^{\ddagger}$ (kJ mol^{-1})	26.7±3.6	32.2±2.2
$\Delta S^{\ddagger}$ (J $K^{-1}mol^{-1}$)	-11.3±13.9	-1.3±8.5

Figure 3.12(a): Eyring plot for S-*t*-butyl of (5)

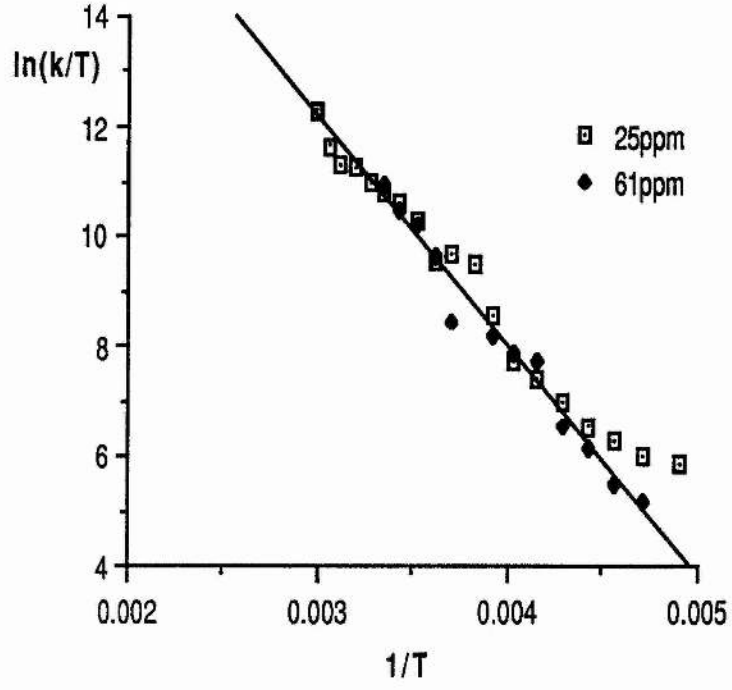

Figure 3.12(b): Eyring plot for C-t-butyl of (5)

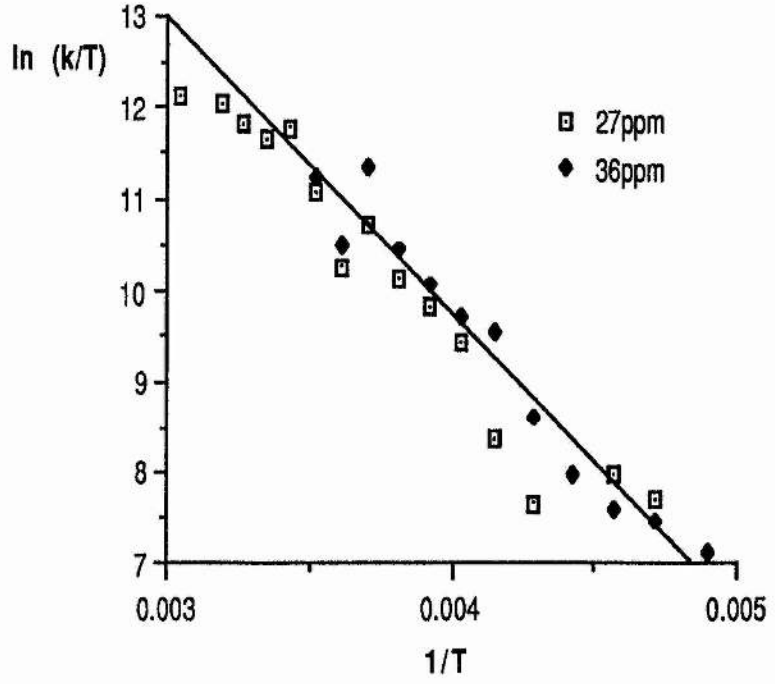

3.3 Group Rotations in Quaternary Ammonium Salts

In view of the success of the $T_1\rho$ method in measuring rates of *t*-butyl group rotations in compounds (4) and (5) it was decided to attempt the method with other groups. Initial experiments were performed on a series of ammonium salts.

Figure 3.13 shows the compounds prepared for study. The first compound to be made was 9(b). The initial idea was that if there were sufficiently large groups present to create a relatively "fixed" lattice framework (e.g. phenyl groups) then a *t*-butyl group could easily rotate relative to this. There could be no doubt that any $T_1\rho$ effects present are only attributable to intramolecular rotations. This was the initial idea. However, this study has produced a multitude of measurable dynamic processes in addition to simple *t*-butyl rotations, principally, slow methyl and phenyl rotations.

Before commencing this study, a few predictions could be made. As previously stated the conical symmetry of the *t*-butyl group allows relatively unhindered rotation in comparison to less symmetrical groups. For this reason, and as a quantitative measure of the principle of least distress, the corresponding *t*-amyl and *i*-propyl derivatives were made and studied. The predictions are as follows:

(1) The bulkier the groups adjacent to the rotating group, the more restricted the rotation should be.

(2) The less symmetrical the group, the greater the barrier to rotation in the solid state should be. There is a greater proportional volume change involved in the rotation of a methyl group into the site normally occupied by a hydrogen, than in rotating an ethyl into the site of a methyl group. Thus, it is expected that *i*-propyl groups will have a higher barrier to rotation than a *t*-amyl group.

Figure 3.13: Compounds Prepared for Study

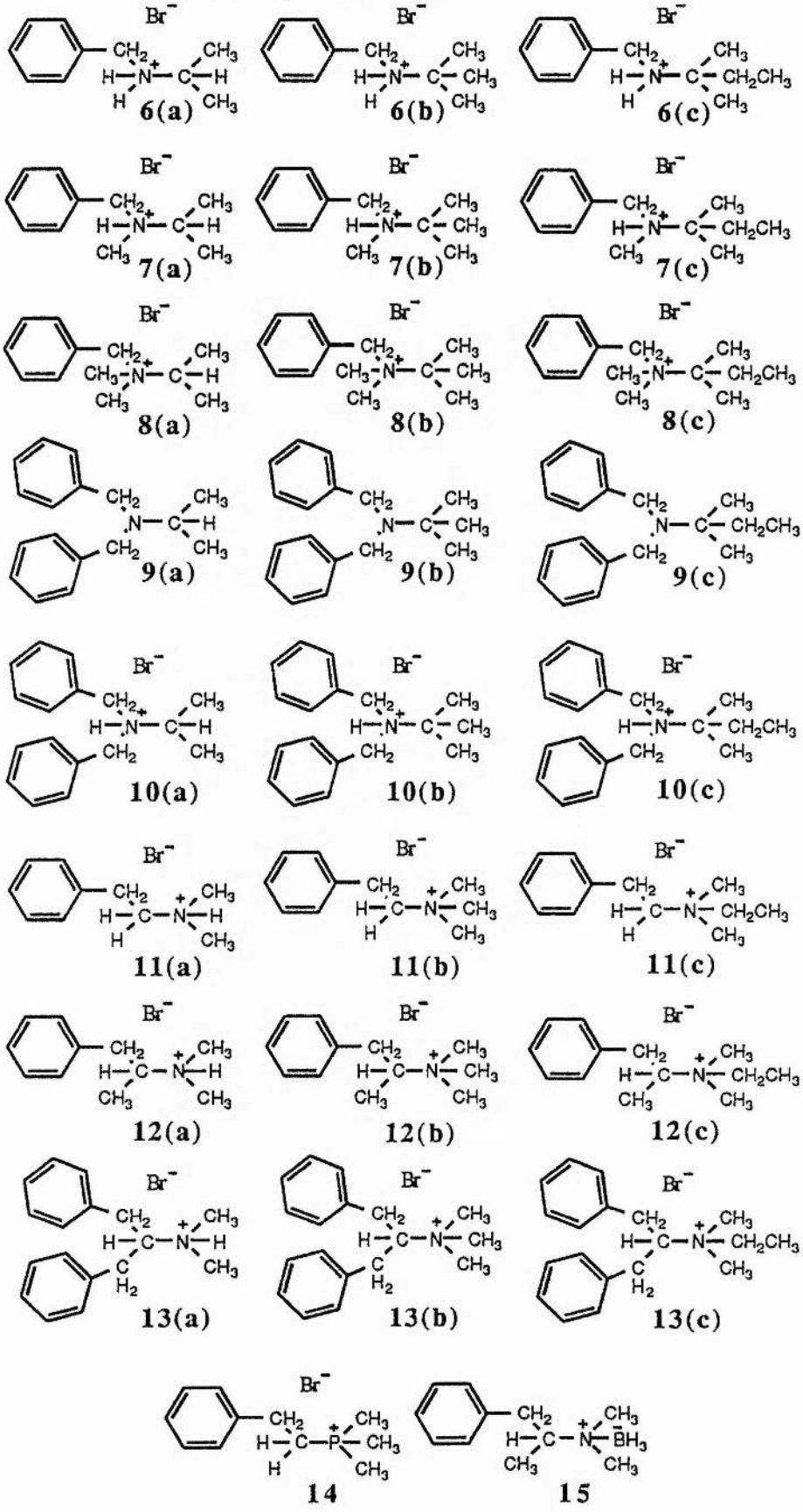

Figure 3.14: Room Temperature ^{13}C CP/MAS Spectra of Compounds 6(a), (b) and (c)

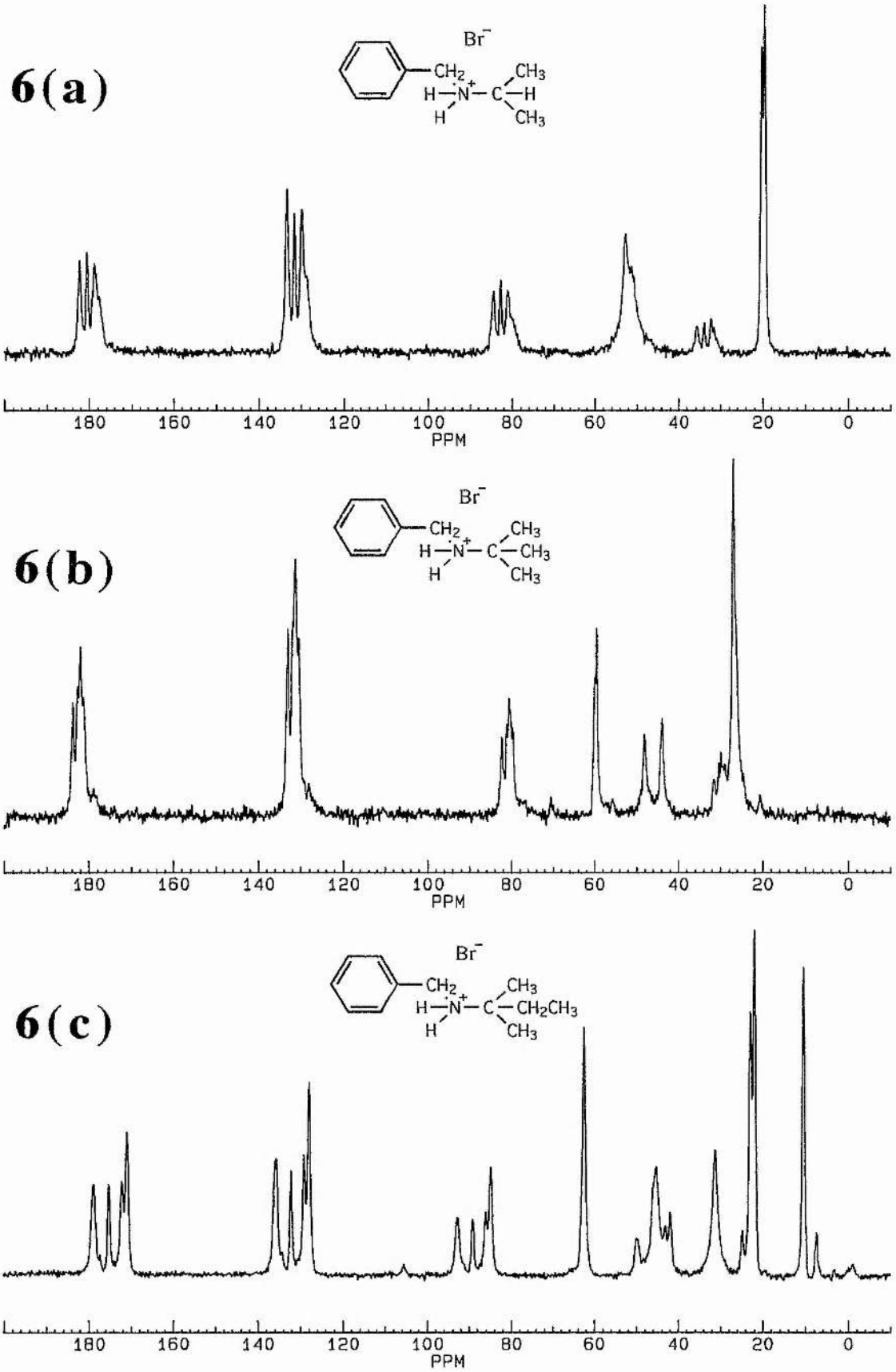

Figure 3.15: Variable Temperature ^{13}C CP/MAS Spectra of the Phenyl carbons of Compound 6(a)

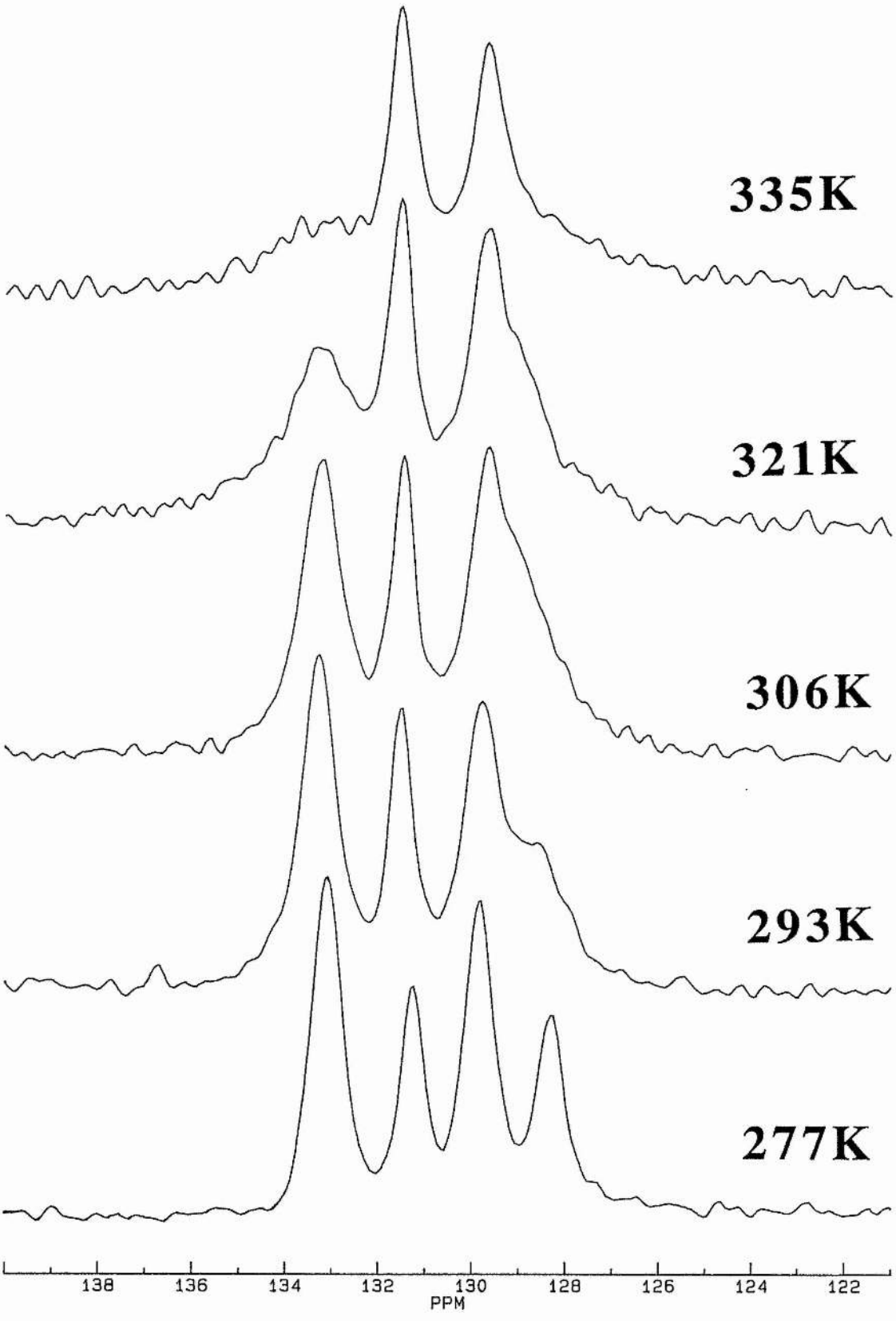

Figure 3.16: Variable Temperature ^{13}C CP/MAS Spectra of Compound 6(b)

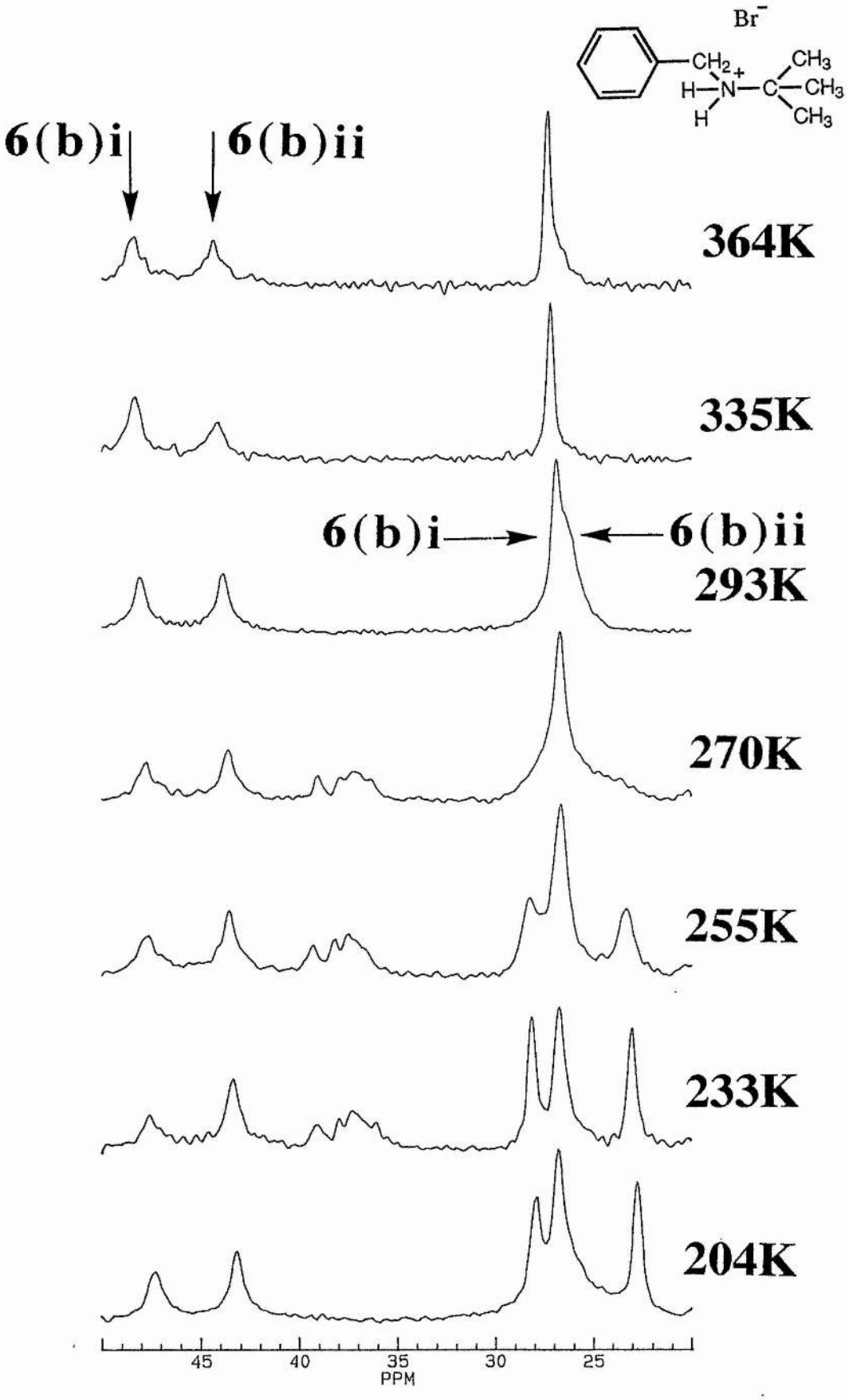

Figure 3.17: Variable Temperature ^{13}C CP/MAS Spectra of the Methyl Group of Molecule 6(b)ii. (The line shapes were obtained by subtracting the spectrum of the $T_1\rho$ reduced signals of 6(b)i at 335K from those spectra where line shape changes were occurring in 6(b)ii.)

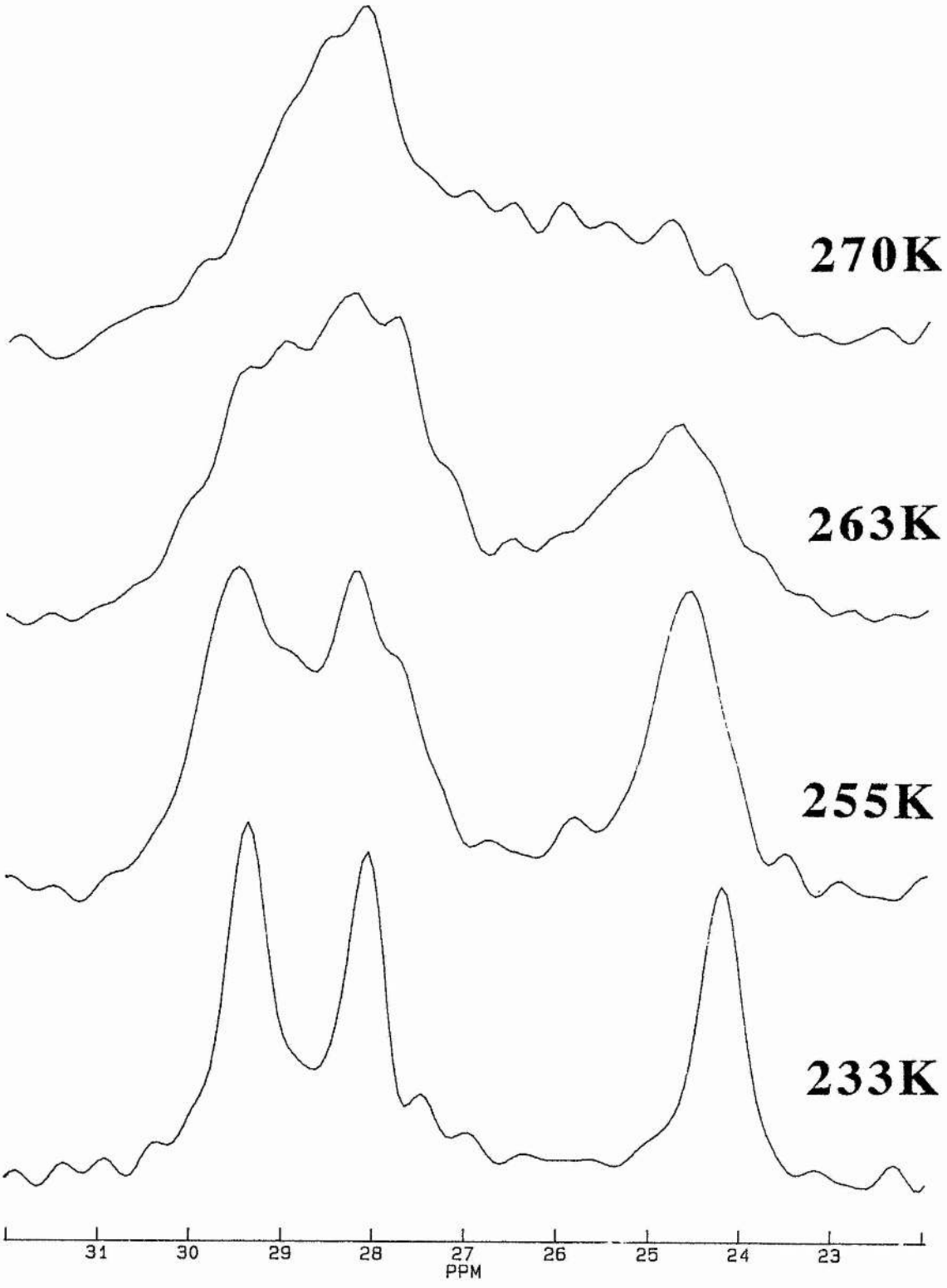

The room temperature spectra of compounds 6(a), (b), & (c) are shown in Figure 3.14.

The spectrum of 6(a) is consistent with one molecule in the asymmetric unit. Unless otherwise stated this is the case for all the compounds of study. The *i*-propyl methyls are located at 19 and 20 ppm. The benzylic CH_2 and N–CH are shown overlapping at 53 ppm with the ring carbons at ca. 130 ppm. Variable temperature spectra show no significant changes in the relative intensities of these lines in the region 350 to 204K. It is therefore assumed that the *i*-propyl group is rotating too slowly to be measured by $T_1\rho$ relaxation.

However, at the lowest temperature there are four lines representing the aromatic ring at 128, 130, 131 and 133 ppm with those at 130 and 133 ppm of double intensity; Figure 3.15. On heating to room temperature and above, the signal at 128ppm, one of the signals at 130ppm and both signals at 133ppm appear to be involved in a coalescence and then diminish in size until at 335K they are seen as a broad hump under the remaining two lines. This phenomenon is representative of a phenyl group rotation, the lines firstly coalescing then reducing in intensity due to $T_1\rho$ relaxation. The two remaining lines are the carbons on the axis of rotation. The apparent doublet coalescence at 293K gives an approximate free energy of activation for the phenyl ring rotation process of 56.2 $kJmol^{-1}$.

The spectrum of compound 6(b) shows two molecules in the asymmetric unit in that all the lines are doubled. The methyl groups of both *t*-butyls are located, overlapping, at 27ppm. The quaternary carbons are overlapped at 60 ppm with the aromatics ca. 130 ppm. The benzylic CH_2s are widely separated at 43 and 47 ppm. The *t*-butyls are rotating rapidly at room temperature as a single average signal is present for each molecule in the unit. However, because they are overlapping, it was not possible to perform $T_1\rho$ measurements on these peaks and instead data on the benzylic CH_2 signals were obtained; Table 3.9. The benzylic carbons should show a reduction in $T_1\rho$ similar to that experienced by the carbons in the rotating group but the $T_1\rho$ values should be longer and the minimum higher. The same theory applies,

however, and rate constants should be accessible from these more remote sensing groups. Variable temperature spectra (Figure 3.16) of this compound allow the separation of the two molecules [6(b)i and 6(b)ii] as the rates of rotation of the two t-butyls are different. The $T_1\rho$ data in conjunction with coalescence data allow sets of spectra to be assigned. Thus the CH_2 at 43 ppm is associated with the slower rotating *t*-butyl. The peaks have their $T_1\rho$ minimum at different temperatures. Additional line shape data was gathered by subtracting the spectrum at 335K (where molecule 6(b)ii is at its $T_1\rho$ minimum) from those spectra where dynamic line shape changes are occurring; Figure 3.17. This allows approximate rates for 6(b)i to be obtained from lineshape changes. The shallower $T_1\rho$ curves only allow a restricted range of rates to be measured (1–1.5 orders of magnitude) compared with the much greater rate range from the rotating group itself.

Table 3.9: $T_1\rho$ (msec) and Rate (s^{-1}) Data for Compound 6(b); [ω_1 = 61 kHz]

43ppm [6(b)ii]			**47ppm [6(b)i]**		
T(K)	**$T_1\rho$**	**k**	**T(K)**	**$T_1\rho$**	**k**
371	25.95	1.2×10^6	255	54.34	1.0×10^7
364	19.69	6.4×10^5	248	34.06	6.1×10^6
357	20.86	8.1×10^5	240	39.68	7.2×10^6
342	19.93	4.6×10^5	233	17.64	1.5×10^6
335	19.76	4.8×10^5	226	20.88	9.1×10^5
321	25.36	2.6×10^5	219	20.84	9.2×10^5
313	28.17	2.2×10^5	212	20.43	6.4×10^5
306	39.93	1.5×10^5	205	28.16	5.9×10^5
Line Shape Data					
270		2.5×10^4			
263		1.0×10^4			
255		4.0×10^3			

The activation parameters were determined for both molecules in the asymmetric unit which appear to differ markedly. For molecule 6(b)i, $\Delta H^{\ddagger}$ = 24.2±8.71 kJmol^{-1} and $\Delta S^{\ddagger}$ = -57.3±38.3 JK^{-1}mol^{-1}. However, 6(b)ii has $\Delta H^{\ddagger}$ = 25.3±3.3 kJmol^{-1} and $\Delta S^{\ddagger}$ = -11.7±9.9 JK^{-1}mol^{-1}

. The spectrum of compound 6(c) shows the *t*-amyl methyl carbons at 22 and 23 ppm with the ethyl CH_2 and methyl at 31 and 10 ppm respectively. The central carbon is shown at 62 ppm. The benzylic CH_2 is at 45 ppm with the aromatics at ca. 130 ppm. The variable temperature spectra of this compound show no change in line shape or relative intensity of the lines with temperature. It is concluded that any rotation taking place is outwith the measurable range of these techniques.

Figure 3.18: Room Temperature ^{13}C CP/MAS Spectra of Compounds 7(a), (b) and (c)

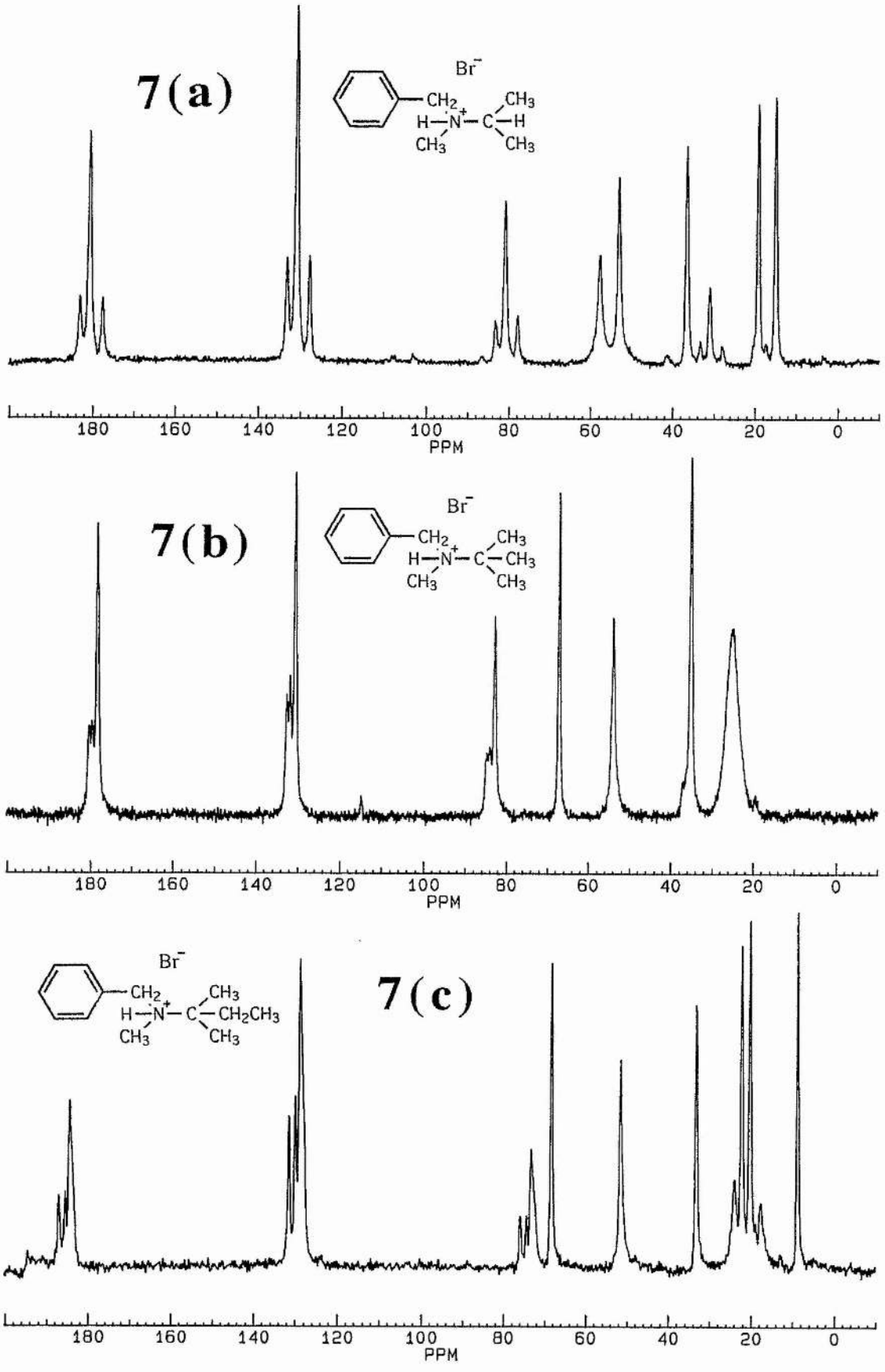

Figure 3.19: Variable Temperature ^{13}C CP/MAS Spectra of the *t*-Butyl Group of 7(b)

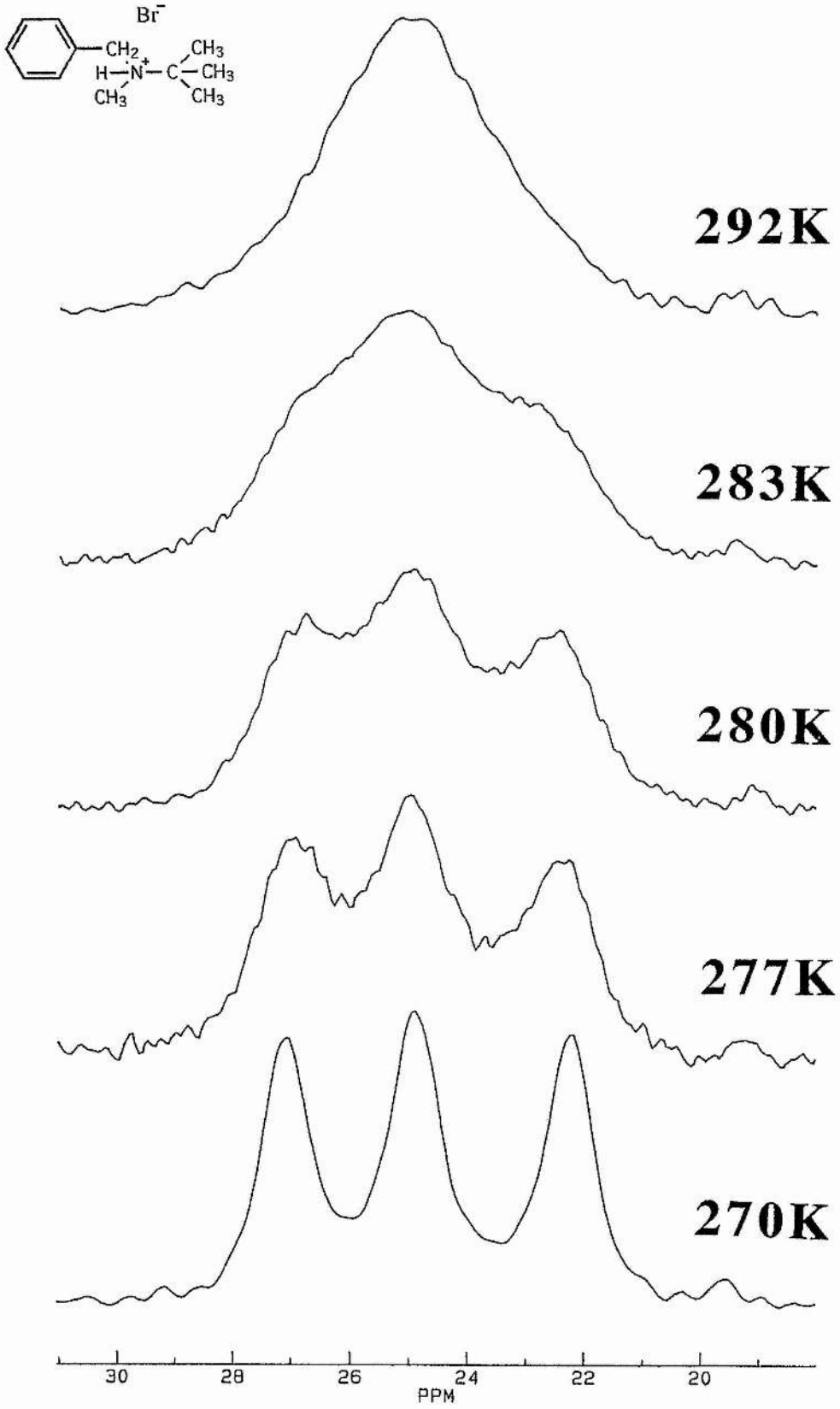

The room temperature spectra of compounds 7(a), (b) and (c) are shown in Figure 3.18.

The spectrum of compound 7(a) shows the *i*-propyl methyls at 15 and 19 ppm. The N–CH and N–methyl are located at 58 and 37 ppm respectively. The benzylic CH_2 is shown at 53 ppm with the aromatics ca. 130 ppm. Variable temperature spectra show no change in the relative intensities of the lines.

The spectrum of compound 7(b) has a broad signal at 25 ppm due to the t-butyl methyl carbons. This signal is dynamically broadened. The central *t*-butyl carbon and N–methyl are located at 67 and 35 ppm respectively. The benzylic CH_2 is shown at 54 ppm with the aromatics at ca. 130 ppm. On cooling from 293 to 263K (Figure 3.19) the *t*-butyl methyl peak splits into three signals (ratio 1:1:1) at 27, 25 and 22ppm. At higher temperatures the single *t*-butyl methyl and quaternary peaks undergo rapid $T_1\rho$ relaxation. This relaxation was measured and the results are shown in Table 3.10. This together with the lineshape data gave the activation parameters, $\Delta H^{\ddagger} = 55.5 \pm 5.7$ $kJmol^{-1}$ and $\Delta S^{\ddagger} = 27.9 \pm 16.6$ $JK^{-1}mol^{-1}$.

The spectrum of compound 7(c) shows the *t*-amyl methyls at 22 and 24 ppm. The ethyl CH_2 and methyl are located at 26 and 11 ppm respectively. The N–methyl and central t-amyl carbon are at 35 and 68 ppm respectively. The benzylic CH_2 is shown at 53 ppm with the aromatics at ca. 130 ppm. On heating the *t*-amyl methyl and quaternary carbons undergo rapid $T_1\rho$ relaxation and the results are shown in Table 3.11(a) and (b). The activation parameters derived from the methyl data are $\Delta H^{\ddagger} = 54.9 \pm 7.8$ $kJmol^{-1}$ and $\Delta S^{\ddagger} = 17.8 \pm 22.9$ $JK^{-1}mol^{-1}$.

The rates derived from the two methyl groups at 22 and 24 ppm are in good agreement with each other. The central carbon at 68 ppm and the methyl on the ethyl group at 11 ppm are also consistent with these methyl rates. This consistency can only mean that the whole t-amyl group must be rotating rapidly in this temperature range. This is the first example of the measurement of rotation of a *t*-amyl group in the solid.

Compound 7(c) has no line shape data as the *t*-amyl methyls are diastereotopic and hence, cannot coalesce.

Table 3.10: $T_1\rho$ (msec) and Rate (s^{-1}) Data for Compound 7(b); [ω_1 = 61 kHz]

	25 ppm		67 ppm	
T(K)	$T_1\rho$	k	$T_1\rho$	k
371	4.67	6.4×10^6	6.21	1.4×10^6
364	4.46	3.8×10^6	6.14	1.2×10^6
357	3.21	2.0×10^6	7.63	5.8×10^5
350	2.76	1.0×10^6	7.35	6.2×10^5
342	4.79	3.7×10^5	11.14	3.5×10^5
335	6.21	2.7×10^5	16.26	2.3×10^5
328	8.48	1.9×10^5	23.69	1.5×10^5
320	12.32	1.3×10^5	39.20	9.0×10^4
Line Shape Data				
293		3.5×10^4		
283		1.5×10^4		
280		8.0×10^3		
277		4.5×10^3		

Table 3.11 (a): $T_1\rho$ (msec) and Rate (s^{-1}) Data for Compound 7(c); [ω_1 = 62 kHz]

	11ppm		68ppm	
T(K)	$T_1\rho$	k	$T_1\rho$	k
371	8.53	3.2×10^6	9.4	2.9×10^6
364	5.47	1.2×10^6	6.5	1.2×10^6
357	8.37	4.4×10^5	12.2	3.4×10^5
349	12.43	2.7×10^5	21.4	1.8×10^5
342	20.64	1.6×10^5	37.2	1.0×10^5
335	31.79	1.0×10^5	53.3	7.2×10^4
327	46.64	6.9×10^4		

Table 3.11 (b): $T_1\rho$ (msec) and Rate (s^{-1}) Data for Compound 7(c); [ω_1 = 62 kHz]

	22ppm		24ppm	
T(K)	$T_1\rho$	k	$T_1\rho$	k
371	4.13	1.2×10^6	4.27	2.1×10^6
364	4.45	8.2×10^5	3.67	1.2×10^6
357	6.13	4.6×10^5	5.85	4.1×10^5
349	9.27	2.7×10^5	9.03	2.5×10^5
342	13.25	1.9×10^5	12.57	1.8×10^5
335	18.16	1.3×10^5	16.71	1.3×10^5
327	29.13	8.3×10^4	21.07	1.0×10^5
320	39.60	6.2×10^4	31.66	6.8×10^4
313	46.16	5.2×10^4	40.79	5.3×10^4

Figure 3.20: Room Temperature ^{13}C CP/MAS Spectra of Compounds 8(a), (b) and (c)

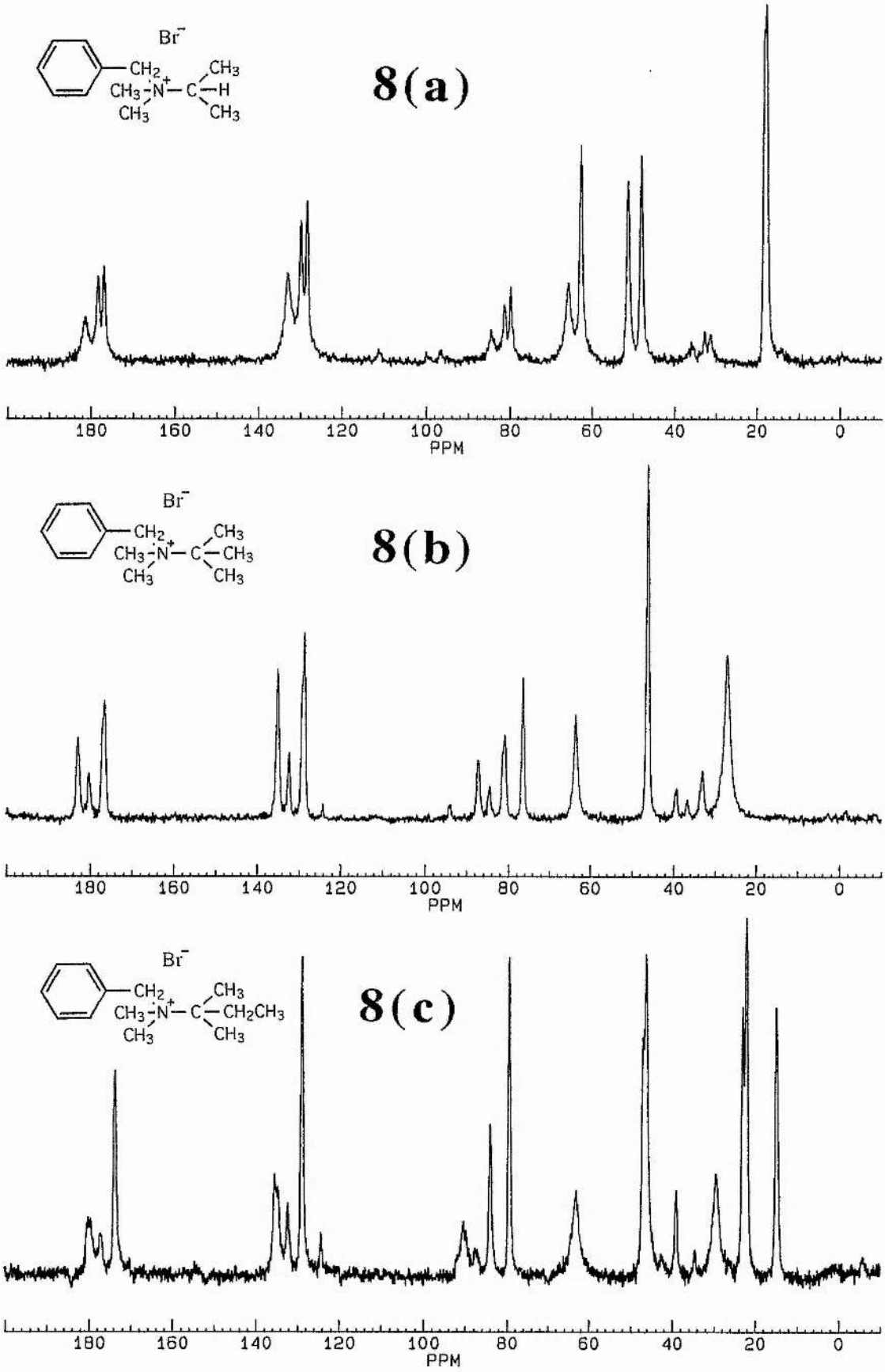

Figure 3.21: Variable Temperature ^{13}C CP/MAS Spectra of the N–Methyls of Compound 8(a)

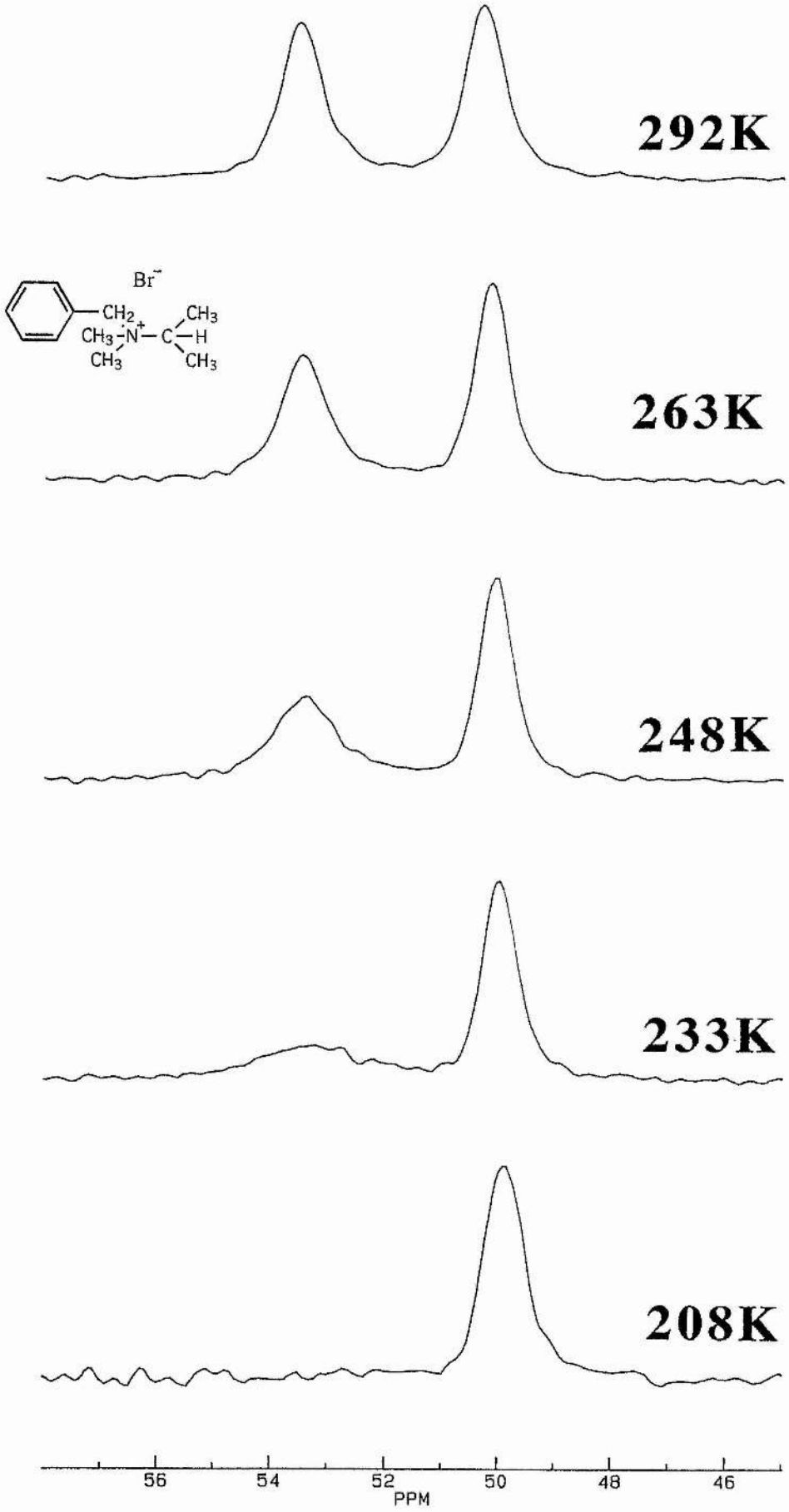

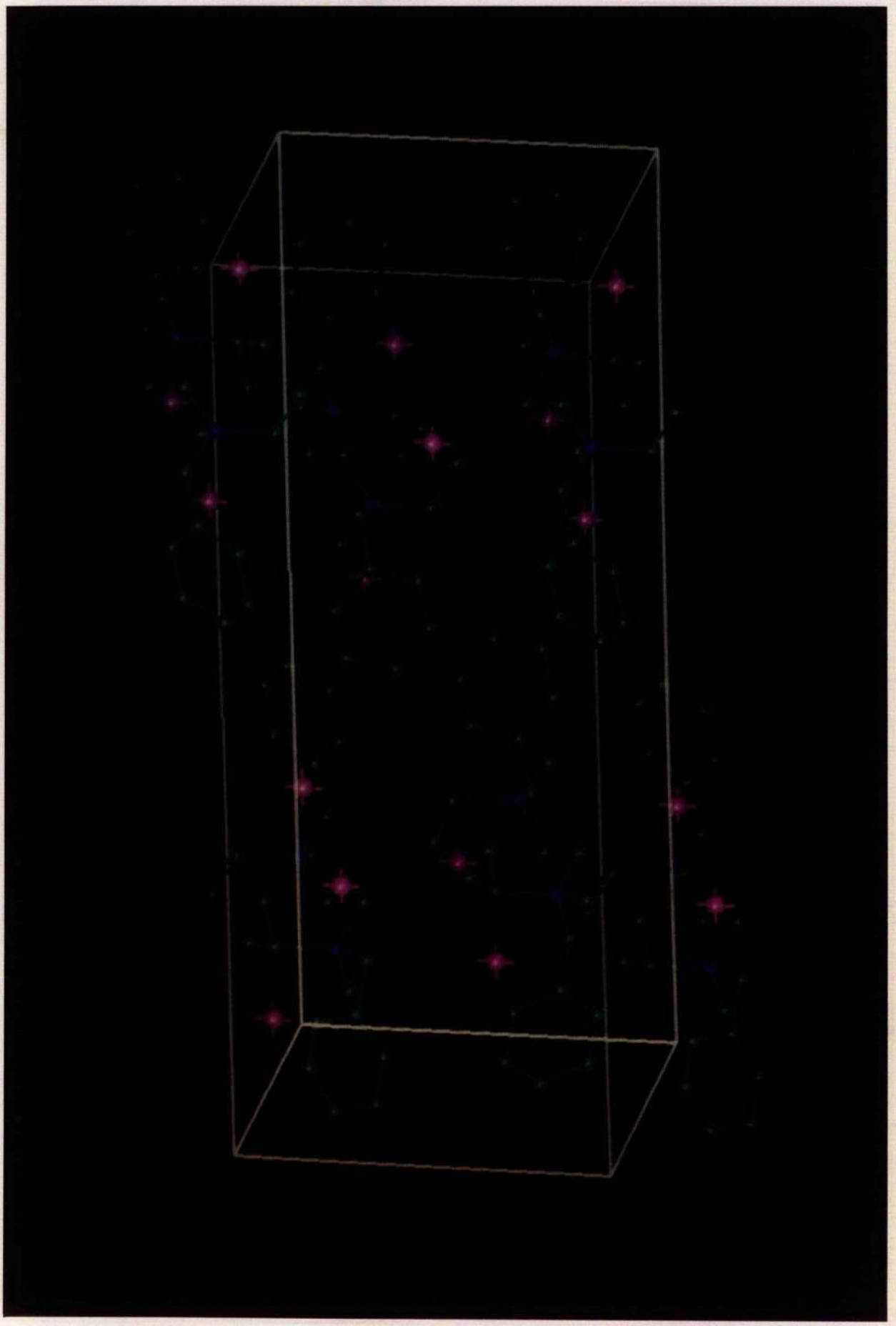

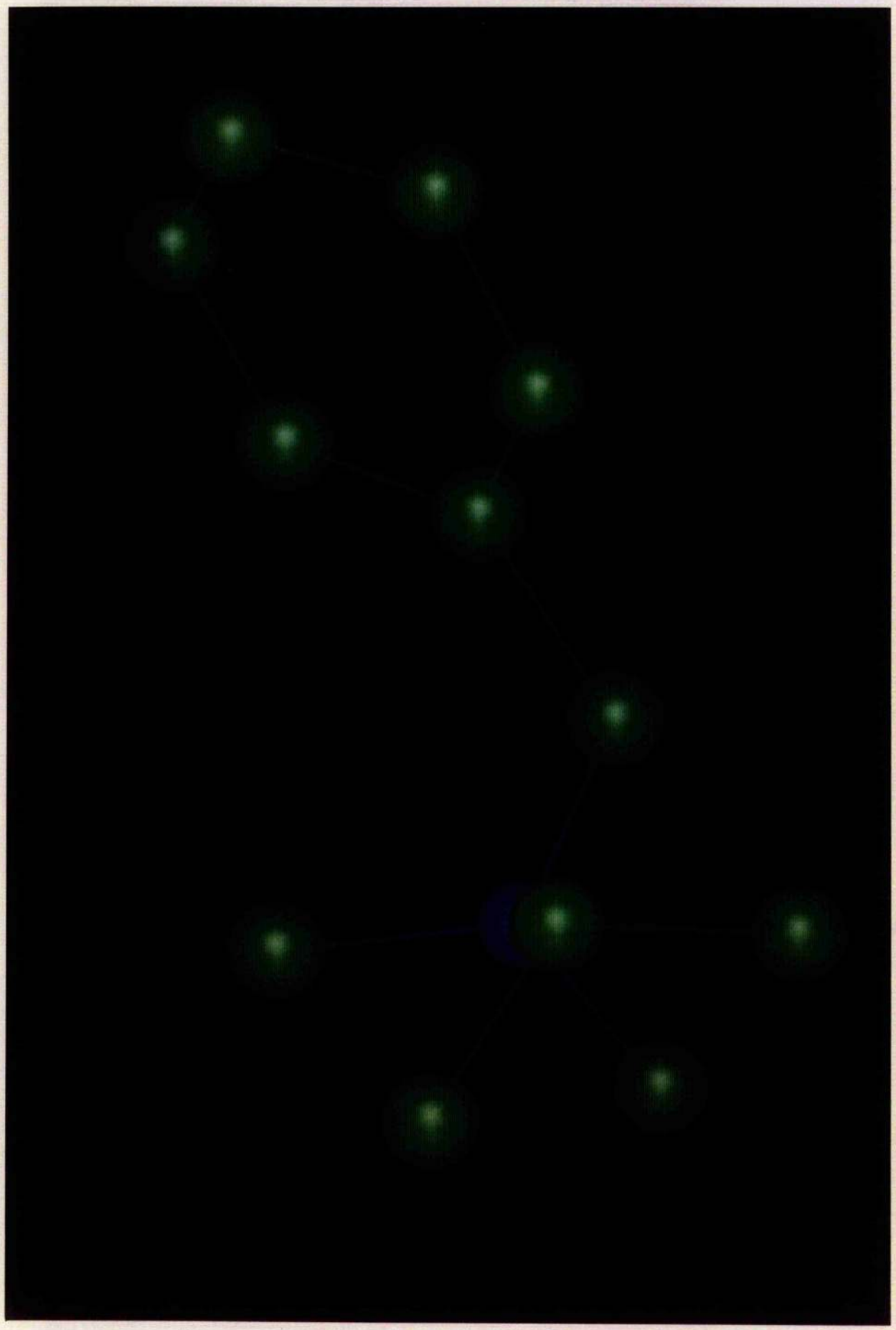

Figure 3.22: Variable Temperature ^{13}C CP/MAS Spectra of the Phenyl Group of Compound 8(a)

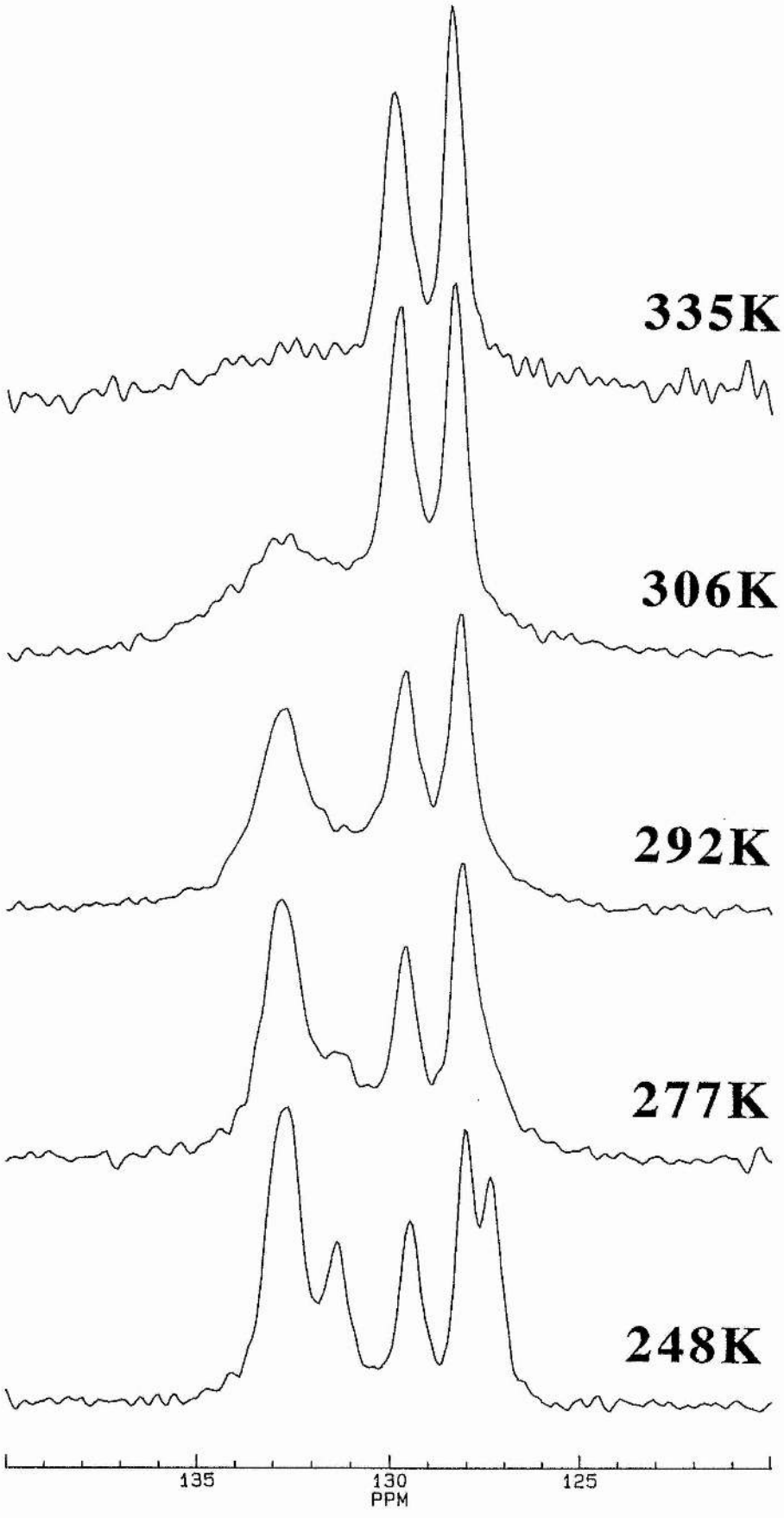

Figure 3.23: Variable Temperature ^{13}C CP/MAS Spectra of the *t*-Butyl Group of Compound 8(b)

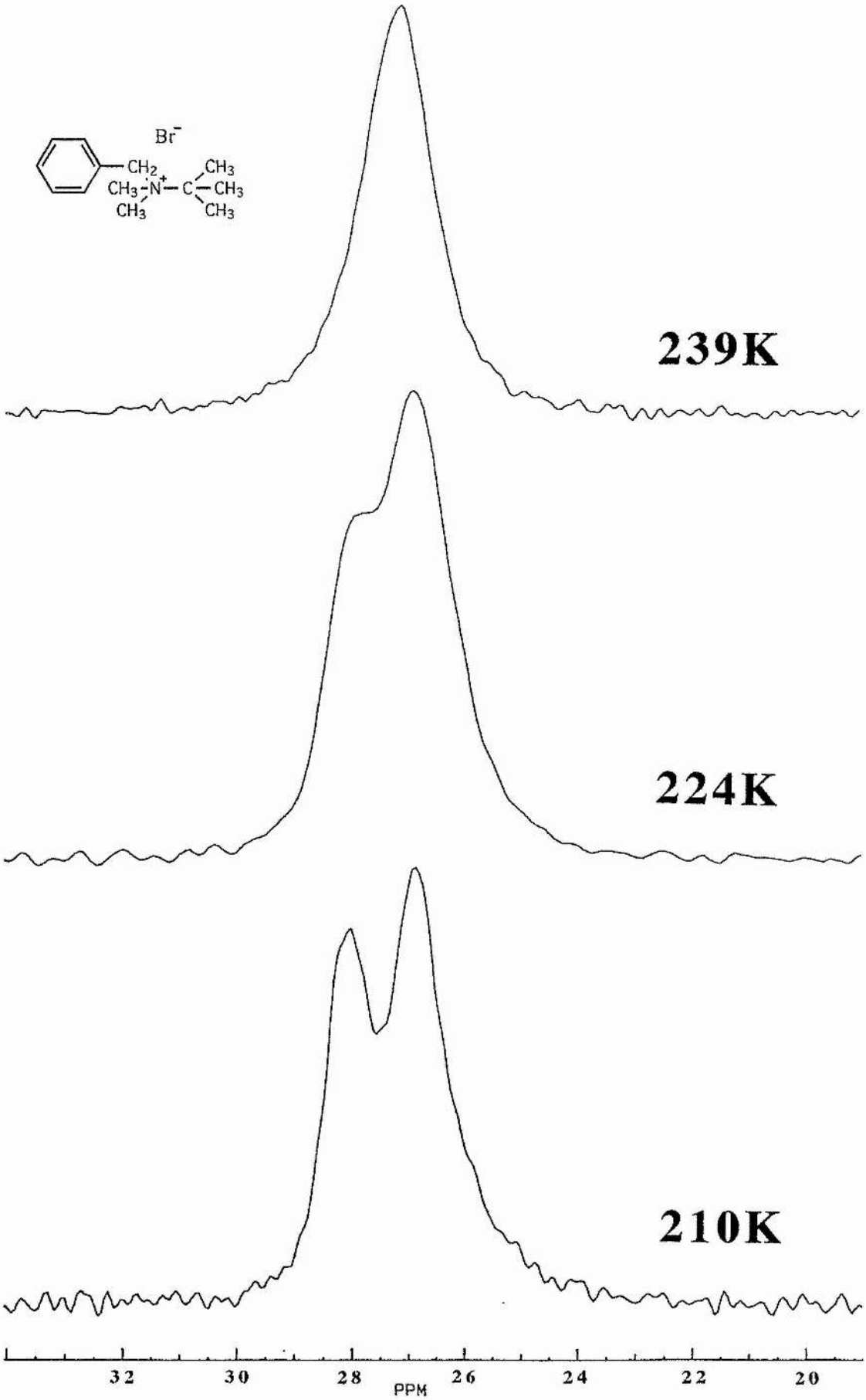

The room temperature spectra of compounds 8(a), (b) and (c) are shown in Figure 3.20.

The spectrum of compound 8(a) shows the *i*-propyl methyls overlapping at 18 ppm. The N–CH and two N–methyls are located at 66, 51 and 48 ppm respectively. The benzylic CH_2 is shown at 63 ppm with the aromatics at ca. 130 ppm. Variable temperature studies show no significant change in relative intensity of the *i*-propyl signals with temperature. However, as the sample is cooled, the peak from one of the N-methyls (51 ppm) broadens slightly and reduces in intensity until it has vanished at 208K (Figure 3.21). The other N-methyl (48 ppm) is unaffected. If the spectra are obtained using single carbon pulses with high power ^1H decoupling the 51ppm peak is still visible but broadened at 208K. Therefore, the loss of signal intensity in the CP spectra of the methyl is associated with a reduction in its ^{13}C $T_1\rho$ value which falls to less than 0.5ms by 208K. The rate of relaxation was measured and is shown in Table 3.12. Because a minimum in the $T_1\rho$ relaxation could not be measured, rate data was not derived. Instead a plot of $\ln(T_1\rho)$ against 1/T was performed which gave a straight line and an activation energy of 26.6± 4.2 $kJmol^{-1}$.

The solid state structure of 8(a) was solved from X-ray powder diffraction data by Dr Philip Lightfoot, here in St Andrews [For crystal data see Experimental Section C2.1]. The packing pattern in the unit cell and the molecular structure of the ammonium ion are shown on pages 93 and 94 respectively.

Two features of this crystal structure are particularly significant in rationalising the NMR data of the N-methyl group discussed above. First, the methyl group has a dihedral angle of 43° along the C–N bond to one of the *i*-propyl methyl groups. This is significantly smaller than the ideal value of 60°. Secondly, this methyl C atom is also significantly closer to the Br^- ion than any other carbon atom, having near neighbour Br^- ions at 368 and 385 pm. The corresponding closest contacts for the other N–methyl carbon are 392 and 394 pm. The extent of the pressure exerted by the bromine upon the methyl is illustrated by the fact that the carbon to bromine vector is in the correct direction to reduce the dihedral angle between the C atom and its *i*-propyl

neighbour from the ideal value of 60° to the observed value of 43°. Hence the powder diffraction data clearly shows that this methyl group is substantially more hindered than the others.

At low temperatures all six aromatic carbons are distinguishable in the spectrum. As the sample is warmed a coalescence phenomenon is observed for four of the phenyl C–H carbons at temperatures around 300K (Figure 3.22) and as the sample is warmed further the coalesced aromatic peaks do not re-emerge up to the upper limit of the measurements. Again, this is probably due to $T_1\rho$ relaxation and the least affected of the peaks, as expected, are those on the axis of rotation which are still visible at high temperatures.

The same X-ray study above shows that the phenyl rings are relatively unencumbered. The closest approach of the carbon atoms between the phenyl rings in adjacent molecules is 396 pm. One adjacent ring is parallel and the other adjacent ring is at an angle of approximately 65°. There is appreciable space in which a phenyl group may rotate.

Table 3.12: $T_1\rho$ Data (msec) for Compound 8(a)

65ppm	
T(K)	$T_1\rho$
262	8.45
255	6.69
247	4.68
240	3.07
232	2.24
225	1.05

The spectrum of compound 8(b) shows the *t*-butyl methyl carbons as a single broad line at 27 ppm with the quaternary carbon at 76 ppm. The two N–methyls are located at 46 ppm. The benzylic CH_2 is shown at 64 ppm with the aromatics ca. 130

ppm. As the sample is cooled the *t*-butyl methyl peak splits into two peaks of equal intensity (Figure 3.23). Three methyl peaks of equal intensity or a 2:1 doublet would be expected not a 1:1 doublet. Plotting chemical shift vs temperature above and below coalescence suggests that one of the methyl resonances is missing or very broad; Figure 3.24. The 210K spectrum suggests that a broadened resonance may be present as a shoulder at ca. 26 ppm. This may be due to the slowing of a methyl rotation such that it undergoes rapid $T_1\rho$ relaxation and is thus severely reduced in intensity.

At higher temperatures the *t*-butyl methyls exhibit the behaviour of a rapidly rotating group. $T_1\rho$ measurements are given in Table 3.13. The rate given at 224K was derived from the coalescence point. The use of $T_1\rho$ data to get rates for *t*-butyl rotation requires that the rotation of the methyls is much more rapid than the *t*-butyl rotation. Where a methyl disappears from the spectrum, this requirement may not be fulfilled. Therefore, caution must be exercised in the interpretation of the data. The data gives activation parameters; $\Delta H^{\ddagger\prime} = 47.7 \pm 6.1$ kJmol^{-1} and $\Delta S^{\ddagger} = 23.5 \pm 20.3$ JK^{-1}mol^{-1}.

Figure 3.24: Chemical Shift Versus Temperature for the *t*-Butyl Methyl Resonances of compound 8(b).

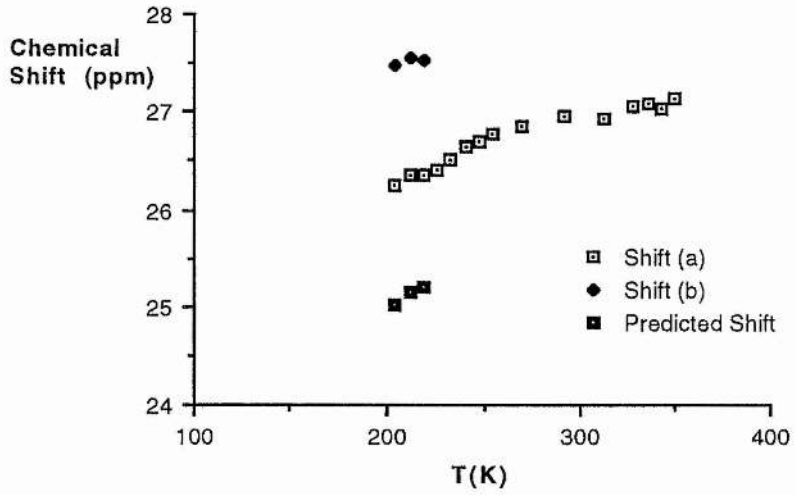

Table 3.13: $T_1\rho$ (msec) and Rate (s^{-1}) Data for Compound 8(b); [$\omega_1 = 61$ kHz]

27ppm		
T(K)	$T_1\rho$	k
349	3.74	5.2×10^6
342	5.25	7.8×10^6
335	2.34	2.1×10^6
327	2.74	3.3×10^6
320	2.23	1.8×10^6
312	3.06	8.1×10^5
305	3.78	6.1×10^5
298	3.53	6.7×10^5
290	4.74	4.6×10^5
283	6.88	3.5×10^5
224		3.3×10^2

The spectrum of compound 8(c) shows the t-amyl methyls at 22 and 23 ppm and the quaternary carbon at 80 ppm. The ethyl CH_2 and methyl are located at 29 and 15 ppm respectively. The N–methyls are at 46 and 47 ppm. The benzylic CH_2 is shown at 63 ppm with the aromatics ca. 130 ppm. Variable temperature spectra show no change in the relative intensity of the peaks. Any rotation must be outside the measurable range of these techniques.

Figure 3.25: Room Temperature ^{13}C CP/MAS Spectra of Compounds 9(a), (b) and (c)

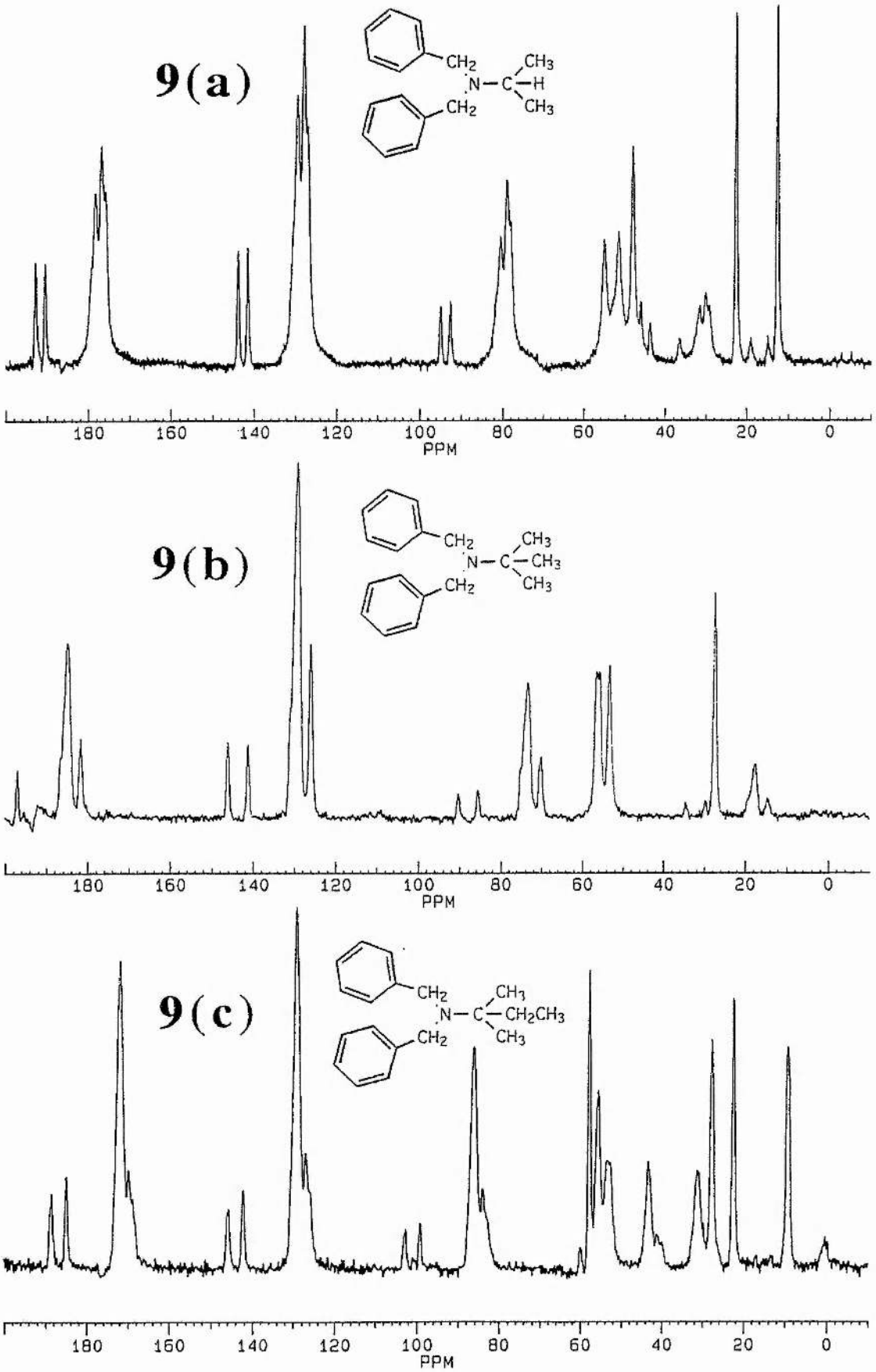

Figure 3.26: Variable Temperature ^{13}C CP/MAS Spectra of the *t*-Butyl Group of Compound 9(b)

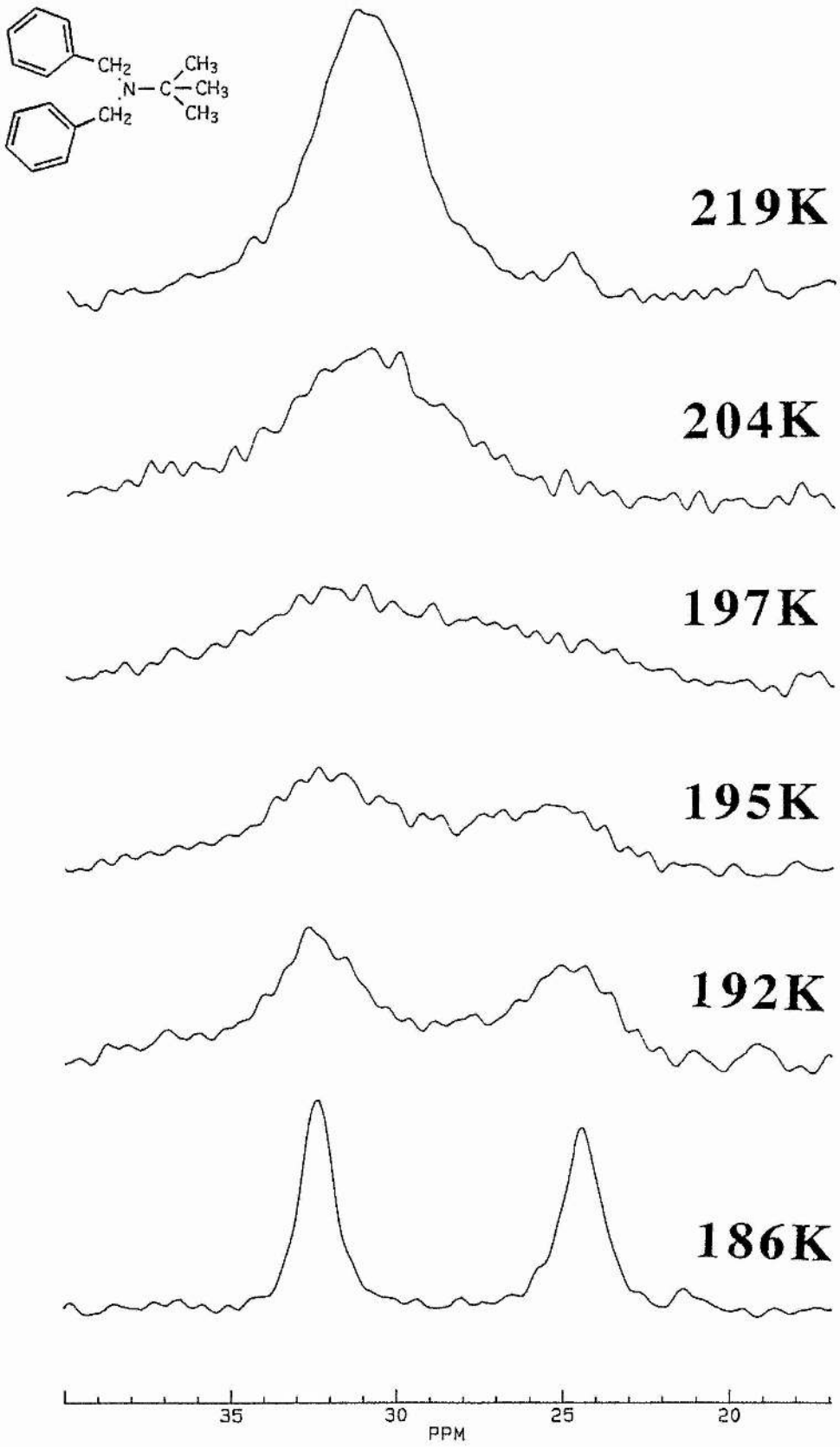

The room temperature spectra of compounds 9(a), (b) and (c) are shown in Figure 3.25.

The spectrum of compound 9(a) shows the *i*-propyl methyls at 13 and 23 ppm. The N–CH is located at 48 ppm. The benzylic CH_2 are shown at 52 and 55 ppm with the aromatics at ca. 130 ppm. There is no change in the relative intensities of the peaks with temperature and thus any rotation is too slow to be measured by these techniques. Interestingly, the benzyls are diastereotopic which is shown by the two CH_2s and two quaternary aromatic carbons at 142 ppm.

Figure 3.27: Chemical Shift Versus Temperature for *t*-Butyl Methyl Resonances of compound 9(b).

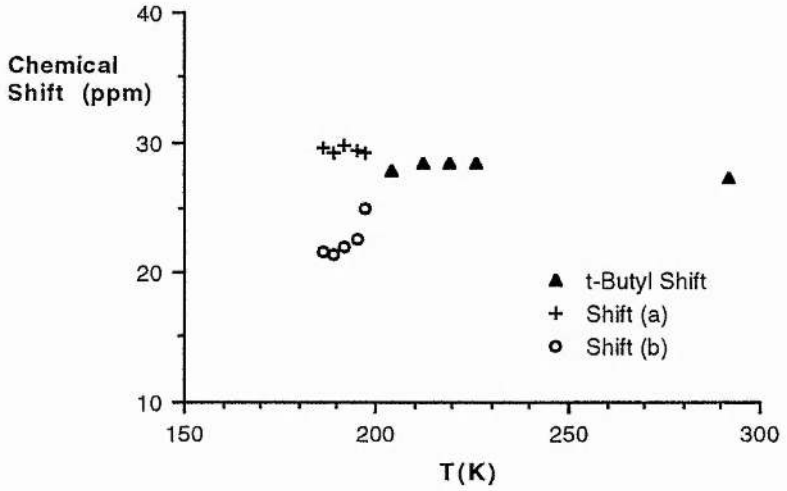

The spectrum of compound 9(b) shows the *t*-butyl methyls as one average signal of reduced intensity at 27 ppm. The central carbon is located at 56 ppm. The benzylic CH_2s are shown at 56 and 53 ppm with the aromatics at ca. 130ppm. Variable temperature spectra show dynamic lineshape changes; Figure 3.26. On cooling to 184K the *t*-butyl methyl peak splits into a doublet (ratio 1:1). Again a plot of chemical shift against temperature shows that there should be another peak, possibly at ca. 30 ppm but this has relaxed away at low temperatures; Figure 3.27.

Above 217K the *t*-butyl methyls exhibit rapid $T_1\rho$ relaxation and the data is shown in Table 3.14. The data gives $\Delta H^{\ddagger} = 33.3 \pm 3.1$ kJmol^{-1} and $\Delta S^{\ddagger} = 13.32 \pm 12.1$

$JK^{-1}mol^{-1}$. Again, caution advised in the interpretation of the results due to the relaxed methyl.

Table 3.14: $T_1\rho$ (msec) and Rate (s^{-1}) Data for Compound 9(b); [ω_1 = 60 kHz]

27ppm		
T(K)	**$T_1\rho$**	**k**
290	19.23	3.2×10^7
283	11.73	1.9×10^7
276	8.43	1.4×10^7
268	4.76	7.4×10^6
265	4.61	7.1×10^6
261	3.98	6.0×10^6
257	3.85	5.8×10^6
253	2.92	3.9×10^6
250	2.97	4.1×10^6
246	2.24	1.8×10^6
243	2.31	1.4×10^6
238	2.43	1.2×10^6
232	3.37	7.0×10^5
224	3.09	7.9×10^5
217	3.41	6.9×10^5

The spectrum of compound 9(c) shows the *t*-amyl methyl peaks at 22 and 28 ppm with the ethyl CH_2 and methyl peaks at 32 and 9 ppm respectively. The quaternary carbon is located at 58 ppm. The benzylic CH_2s are shown at 54 and 56 ppm with the aromatics at ca. 130 ppm. Variable temperature spectra show that there is no change in the relative intensities of the peaks with temperature. There are, therefore, no measurable effects present.

Figure 3.28: Room Temperature ^{13}C CP/MAS Spectra of Compounds 10(a), (b) and (c)

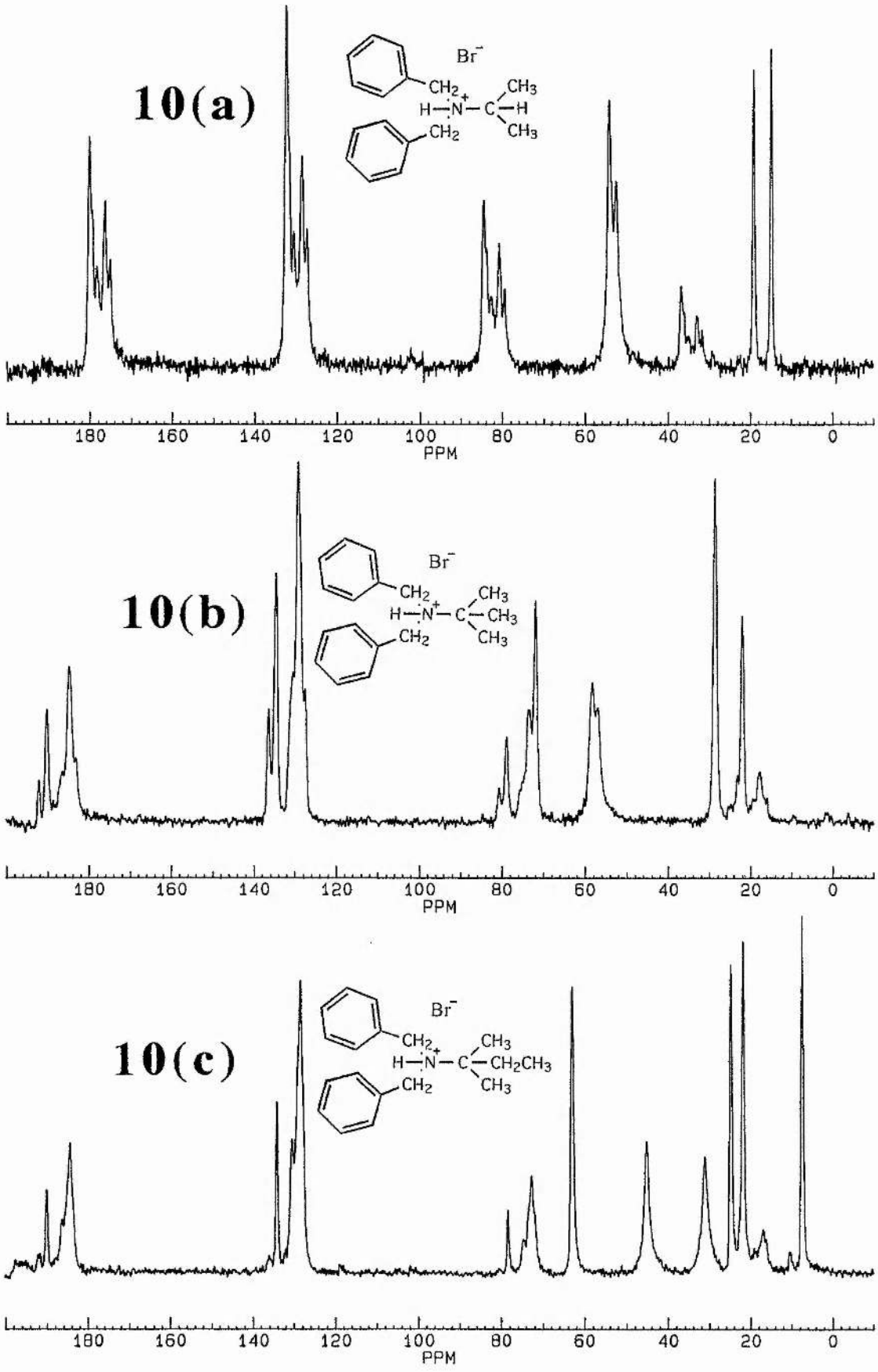

Figure 3.29: Variable Temperature ^{13}C CP/MAS Spectra of the *t*-Butyl Group of Compound 10(b)

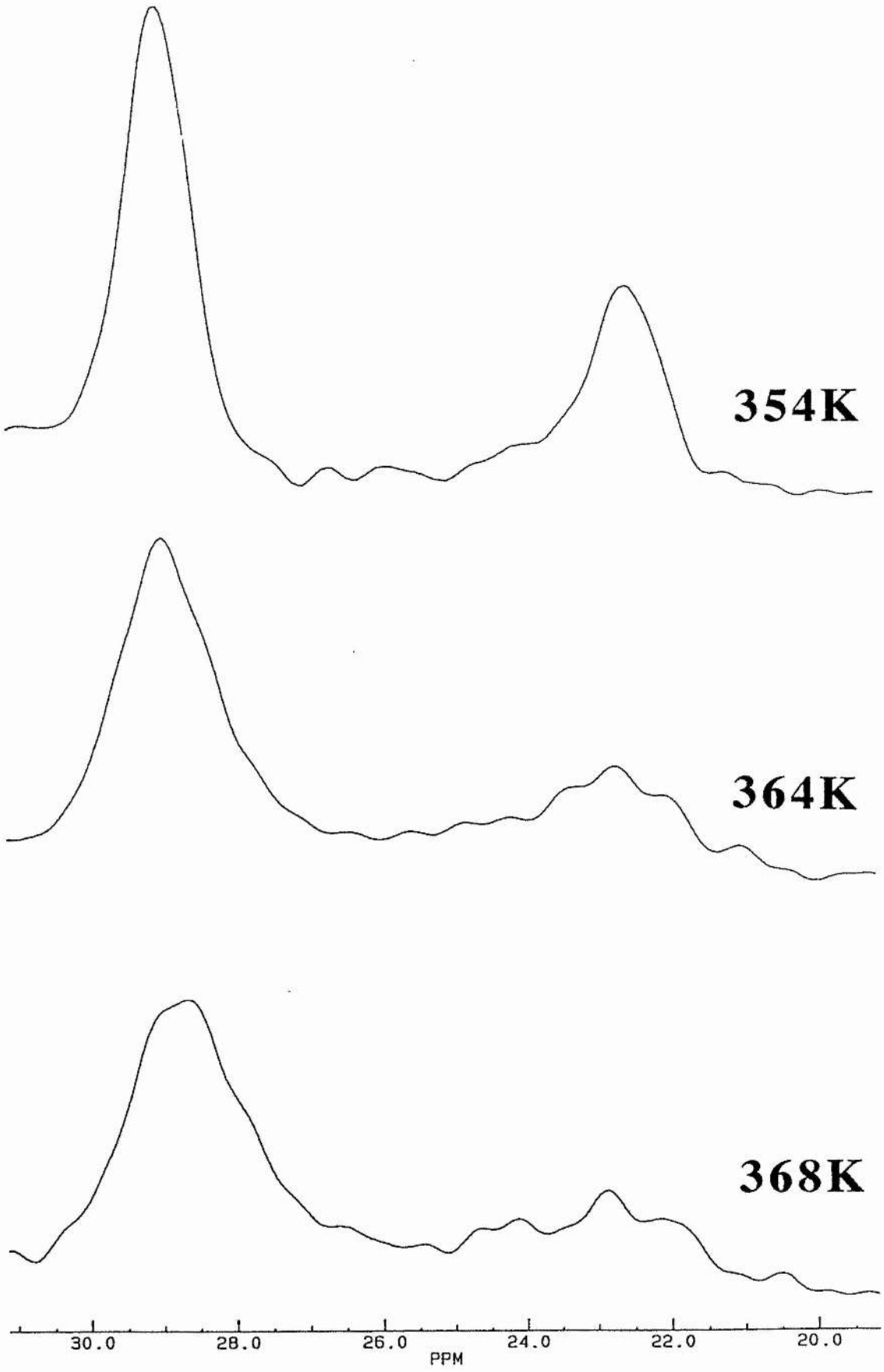

The room temperature spectra of compounds 10(a), (b) and (c) are shown in Figure 3.28.

The spectrum of compound 10(a) shows the *i*-propyl methyls at 15 and 19 ppm. The N–CH is located at 54 ppm. The benzylic CH_2s are shown at 54 and 52 ppm with the aromatics at ca. 130 ppm. Variable temperature studies show no significant changes in the relative intensities of the peaks with temperature.

The spectrum of compound 10(b) shows the *t*-butyl methyls already "frozen out" at room temperature (ratio 2:1). On heating (Figure 3.29), the peaks eventually coalesce at 371K but because the high temperatures involved exceed the upper temperature limit of the probe and so it is not possible to measure the $T_1\rho$ relaxation. Instead, the rate of rotation can be measured using a 2D CPEXSY experiment and the results are given in Table 3.15. The derived activation parameters are: $\Delta H^{\ddagger} = 59.4 \pm 5.2$ $kJmol^{-1}$ and $\Delta S^{\ddagger} = -33.9 \pm 16.4$ $JK^{-1}mol^{-1}$.

Table 3.15: 2D EXSY Rate Data (s^{-1}) for Compound 10(b)

Methyls	
T(K)	k
349	2.0×10^3
342	1.0×10^3
327	5.1×10^2
312	1.3×10^2
298	4.0×10^1
290	2.2×10^1
283	8.9×10^0

The spectrum of compound 10(c) shows the t-amyl methyls at 22 and 25 ppm with the ethyl CH_2 and methyl at 31 and 7 ppm. The quaternary carbon is located at 63 ppm. The benzylic CH_2s are overlapping at 45 ppm with the rings themselves at ca.

130ppm. Variable temperature studies show no significant change in the relative intensities of the peaks. Therefore, no rate data can be derived from the spectra.

Figure 3.30: Room Temperature ^{13}C CP/MAS Spectra of Compounds 11(a), (b) and (c)

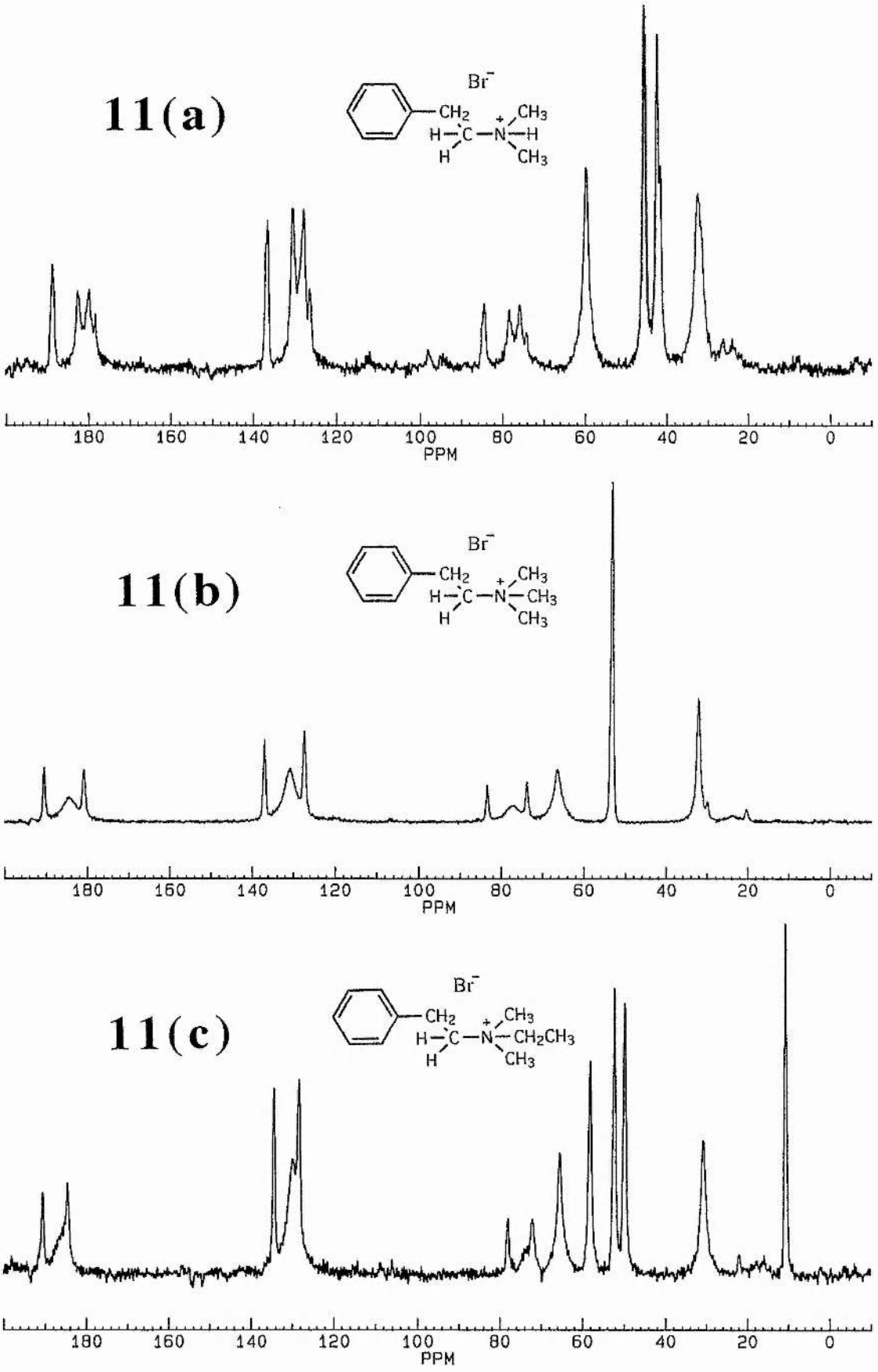

Figure 3.31: Variable Temperature ^{13}C CP/MAS Spectra of the Phenyl Group of Compound 11(a)

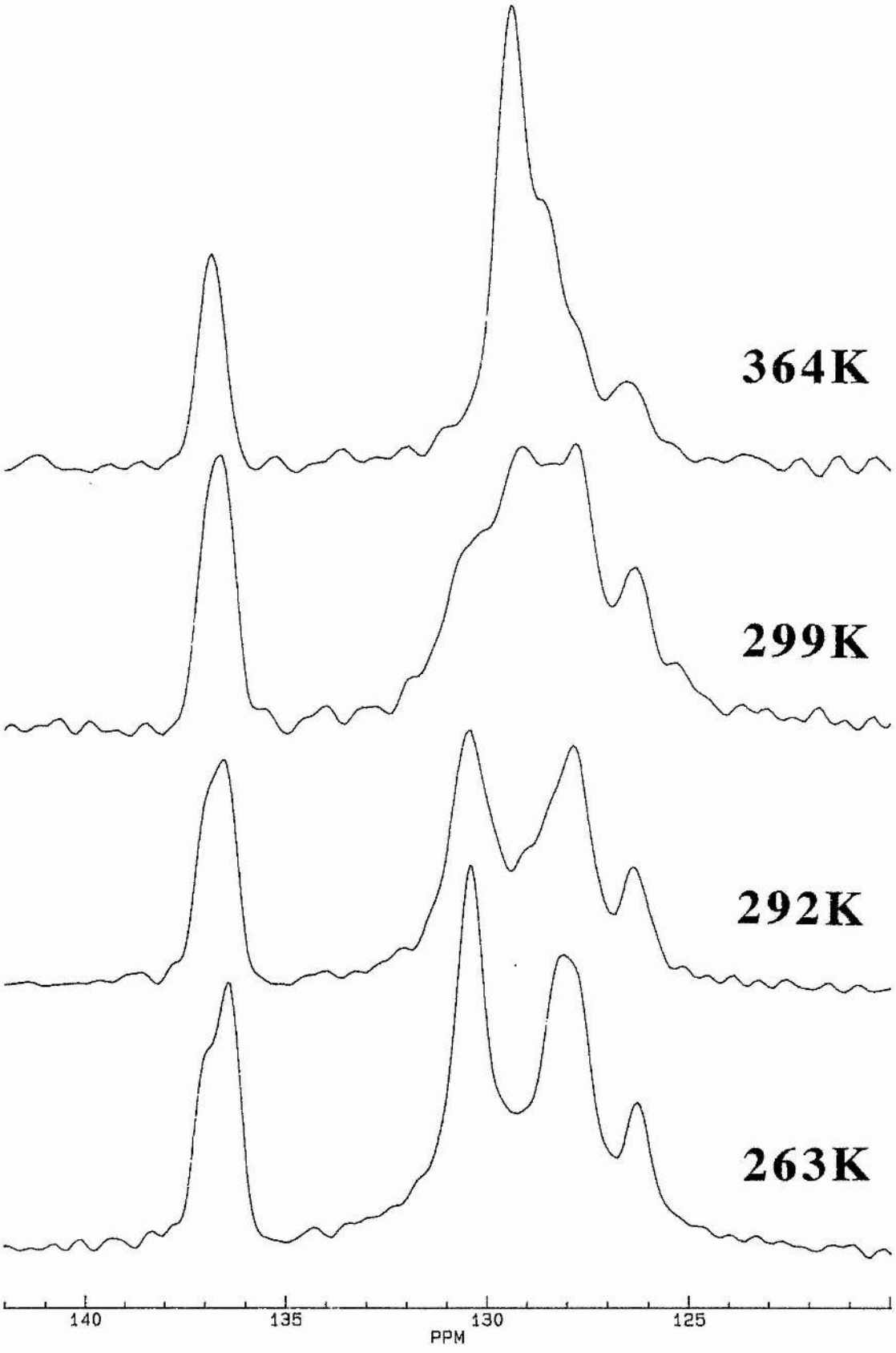

Figure 3.32: Variable Temperature ^{13}C CP/MAS Spectra of the N–Methyls of Compound 11(b)

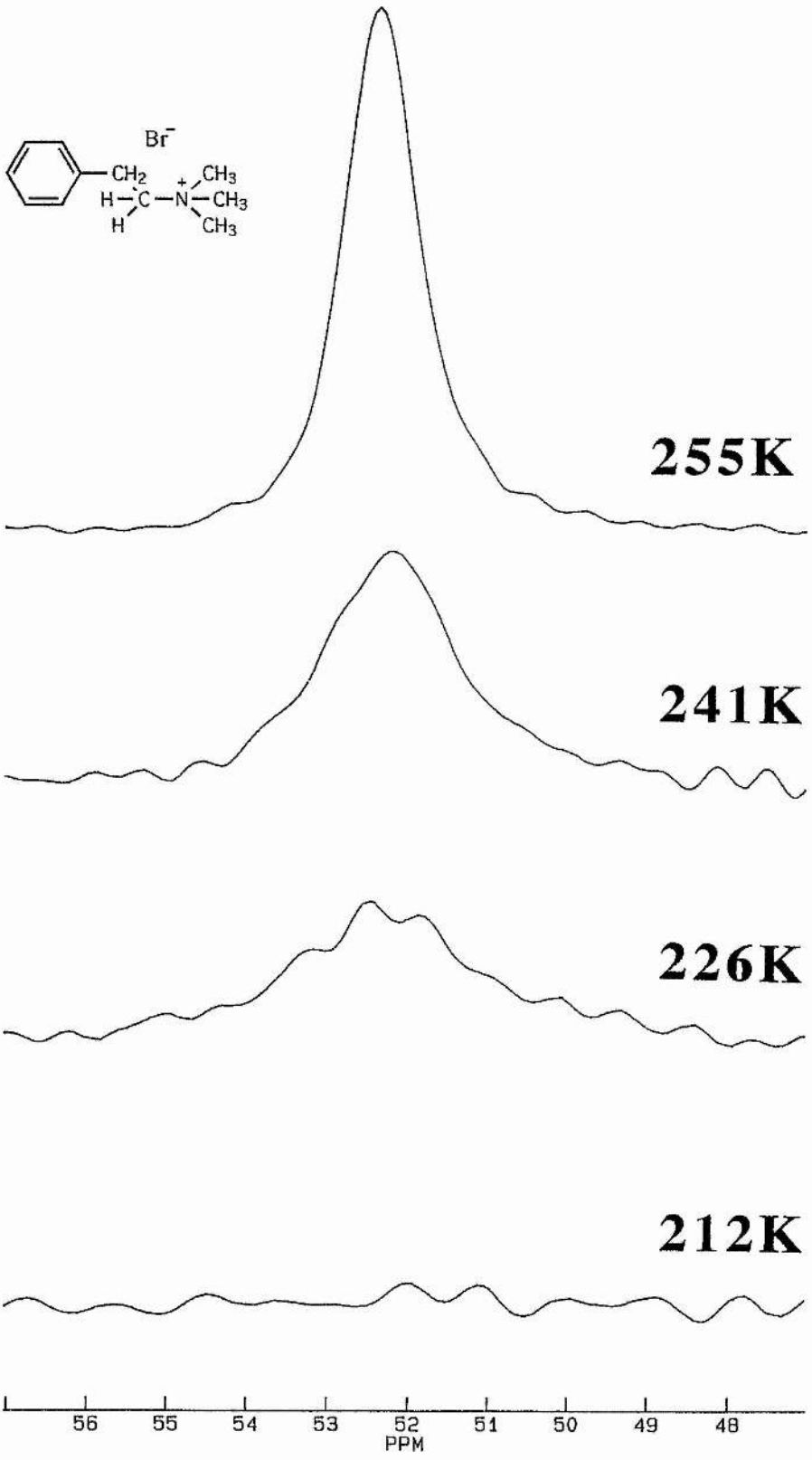

Figure 3.33: Variable Temperature ^{13}C CP/MAS Spectra of the Phenyl Group of Compound 11(b)

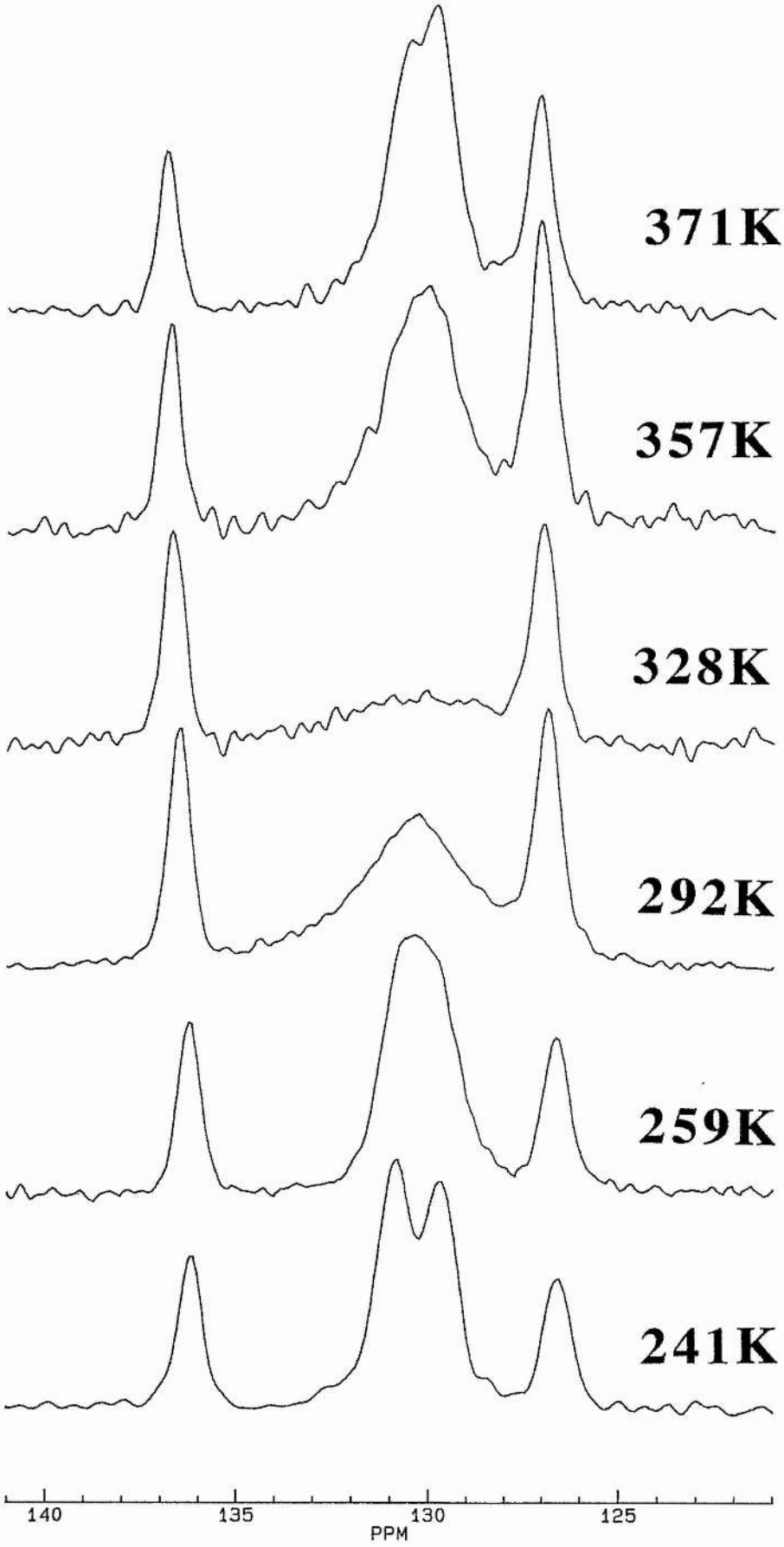

Figure 3.34: Variable Temperature ^{13}C CP/MAS Spectra of the Phenyl carbons of compound 11(c).

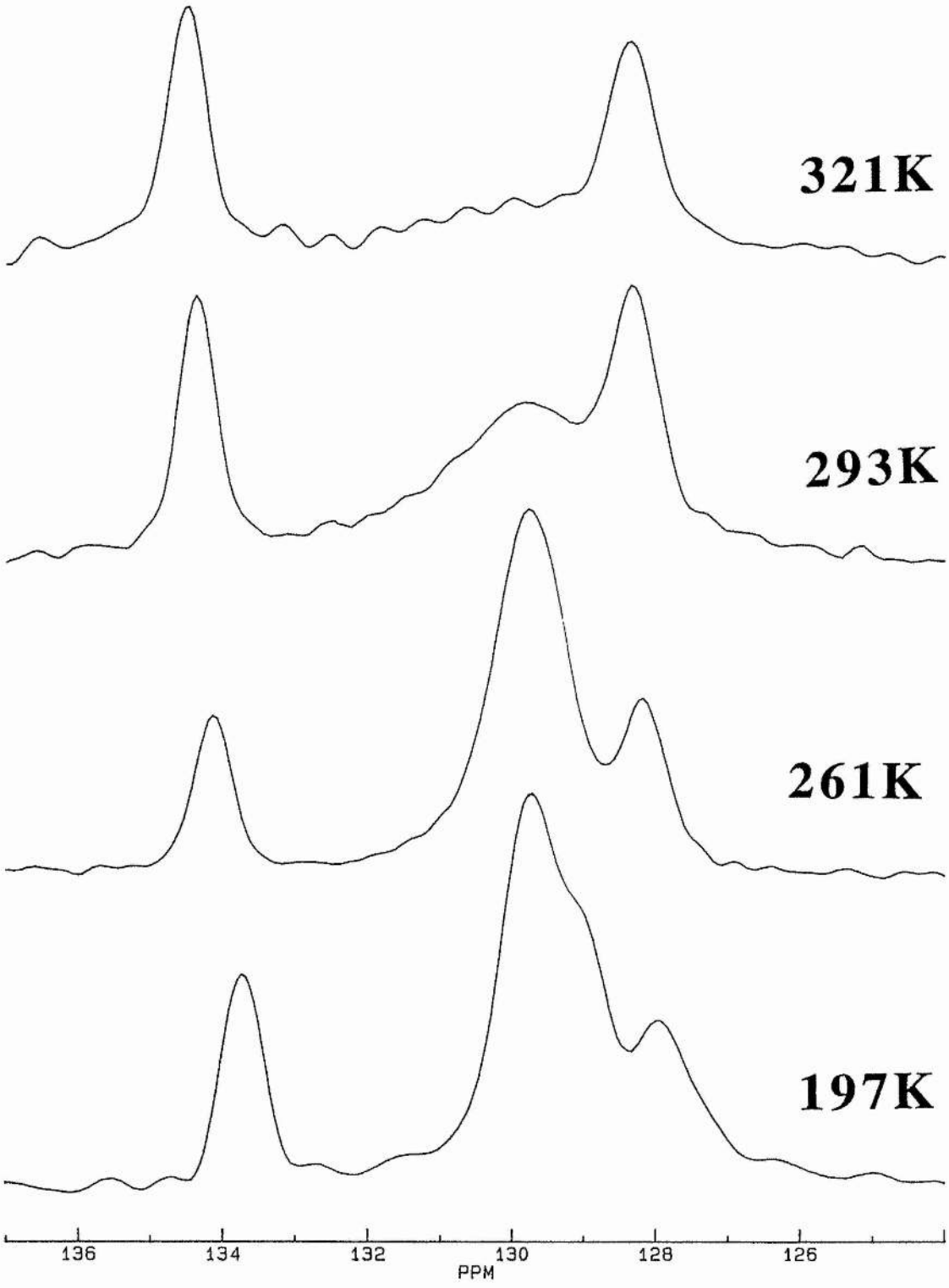

Figure 3.35: ^{13}C CP/MAS spectra of the two phases of Compound 11(c).

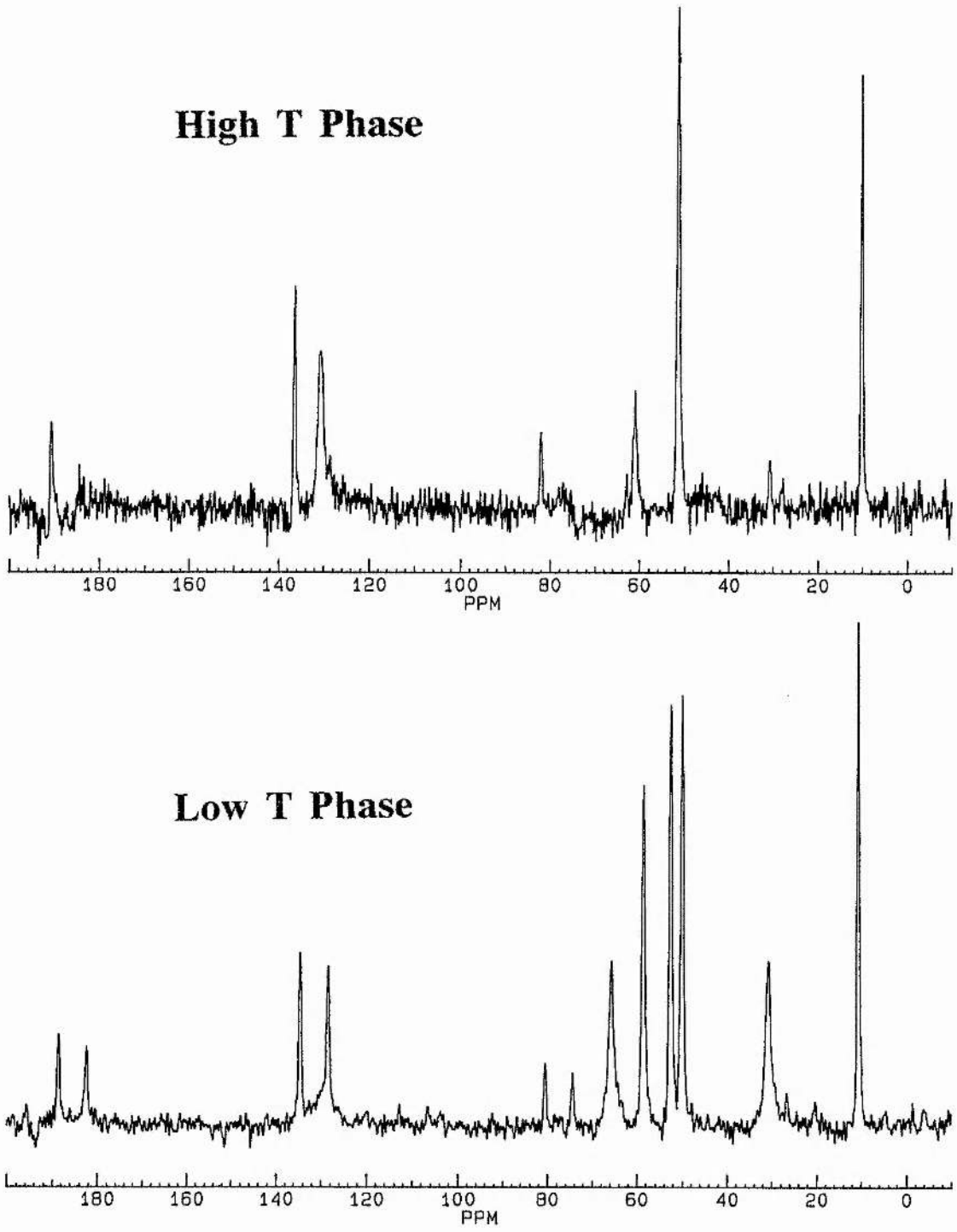

The room temperature spectra of compounds 11(a), (b) and (c) are shown in Figure 3.30.

The spectrum of compound 11(a) shows the N-methyls at 43 and 46 ppm. The benzylic CH_2 is at 32ppm with the N-CH_2 at 60 ppm. The ring carbons are located at 130 ppm while the quaternary aromatic carbon is at 137 ppm. There is no change in the relative intensity of the methyl peaks with temperature. However, at low temperature (263K) the aromatic ring carbons are represented by four peaks; Figure 3.31. As the temperature is increased the inner two peaks broaden (292K), coalesce (299K) and sharpen dramatically (364K) into one peak. This phenomenon is symptomatic of a rapidly rotating group. No $T_1\rho$ data was collected.

The spectrum of compound 11(b) shows the N–methyls at 53 ppm, the benzylic CH_2 at 32 ppm, the N–CH_2 at 66 ppm and the aromatic carbons ca. 130ppm. On cooling the intensity of the N-methyl signal decreases with temperature due to $T_1\rho$ relaxation until it is completely relaxed at 212K; Figure 3.32. The $T_1\rho$ data is shown in Table 3.16. The observed process is presumed to be a $-N^+Me_3$ rotation Since a minimum in the function could not be measured, and hence an experimental value of B^2 could not be derived. A plot of $\ln(T_1\rho)$ against 1/T was made which gives an activation energy, Ea, of 26.4±0.9 $kJmol^{-1}$.

At low temperatures the aromatic carbons are shown as four peaks at 123, 127, 128, and 133 ppm; Figure 3.33. On heating, the central two peaks coalesce (259K), broaden (292K), go through a $T_1\rho$ minimum (328K) and sharpen (371K). Again this is due to the rapid rotation of the phenyl ring. Only the two carbons on the axis of rotation are unaffected. In this case it was possible to measure the $T_1\rho$ relaxation of the coalesced peaks and the results enabled the activation parameters to be determined giving $\Delta H^{\ddagger}$ = 63.9±6.3 $kJmol^{-1}$ and $\Delta S^{\ddagger}$ = 75.1±20.6 $JK^{-1}mol^{-1}$.

Table 3.16: $T_1\rho$ (msec) and Rate (s^{-1}) Data for Compound 11(b); [ω_1 = 61 kHz]

	53ppm	130ppm	
T(K)	$T_1\rho$	$T_1\rho$	k
356		3.86	2.6×10^7
350		2.23	1.5×10^7
342		2.22	1.5×10^7
335		0.78	4.6×10^6
327		0.87	5.3×10^6
320		0.73	4.2×10^6
313		0.51	1.3×10^6
306		1.31	3.3×10^5
299		1.58	2.7×10^5
292		3.88	1.1×10^5
284	16.82	3.65	1.2×10^5
277	14.20	12.55	3.3×10^4
270	9.82	21.41	2.0×10^4
263	7.01	26.02	1.6×10^4
255	4.96		
248	3.54		
241	2.42		
233	1.49		

The spectrum of compound 11(c) shows the N–ethyl CH_2 and methyl at 58 and 11 ppm respectively with the N–methyls at 50 and 53 ppm. The benzylic CH_2 is at 66 ppm with the ring carbons at ca. 130 ppm.

On cooling the N–methyls and ethyl CH_2 change in relative intensity due to $T_1\rho$ relaxation. The data acquired is shown in Table 3.17. Since no minimum in the function can be measured a plot of $\ln(T_1\rho)$ against 1/T was performed instead. The

activation energy is derived from the average slope of three very similar lines and is found to be 20.9±1.7 kJmol^{-1}.

Table 3.17: $T_1\rho$ (msec) and Rate (s^{-1}) Data for Compound 11(c); [ω_1 = 60 kHz]

	50ppm	53ppm	58ppm	130ppm	
T(K)	$T_1\rho$	$T_1\rho$	$T_1\rho$	$T_1\rho$	k
342				8.40	6.3 x 10^6
335				6.71	4.9 x 10^6
328				4.48	3.0 x 10^6
313				2.30	1.1 x 10^6
306				3.53	6.4 x 10^5
299				6.71	2.7 x 10^5
292				7.69	2.3 x 10^5
283				13.70	1.3 x 10^5
277	17.56	32.26	26.95	23.26	7.4 x 10^4
269	13.40	26.36	25.41	40.65	4.2 x 10^4
262	10.75	25.73	17.64		
255	7.76	18.99	12.51	78.74	2.2 x 10^4
247	5.58	16.71	11.75		
240	3.91	11.82	10.56		
232	2.88	8.11	5.97		
225	1.57	6.08	4.33		
218		3.12	2.55		
211		2.26	2.32		

Similar to the previous two compounds, dynamic line shape changes show that this sample also exhibits a phenyl group rotation; Figure 3.34. At low temperatures the phenyl carbons are shown as three peaks at 133, 135 and 139 ppm. The central peak represents the average of four carbons rapidly exchanging position during the rotation. On heating, the relaxation becomes quicker and the minimum intensity occurs at 306K. The peak grows in intensity until at ca. 335K, a phase change occurs and all the peaks are replaced by others; Figure 3.35. Up to this point $T_1\rho$ measurements were taken and the result are expressed in Table 3.17. The activation parameters for the phenyl rotation were determined to be; $\Delta H^{\ddagger} = 48.0 \pm 4.6$ kJmol^{-1} and $\Delta S^{\ddagger} = 23.5 \pm 15.5$ JK^{-1}mol^{-1}.

Figure 3.36: Room Temperature ^{13}C CP/MAS Spectra of Compounds 12(a), (b) and (c)

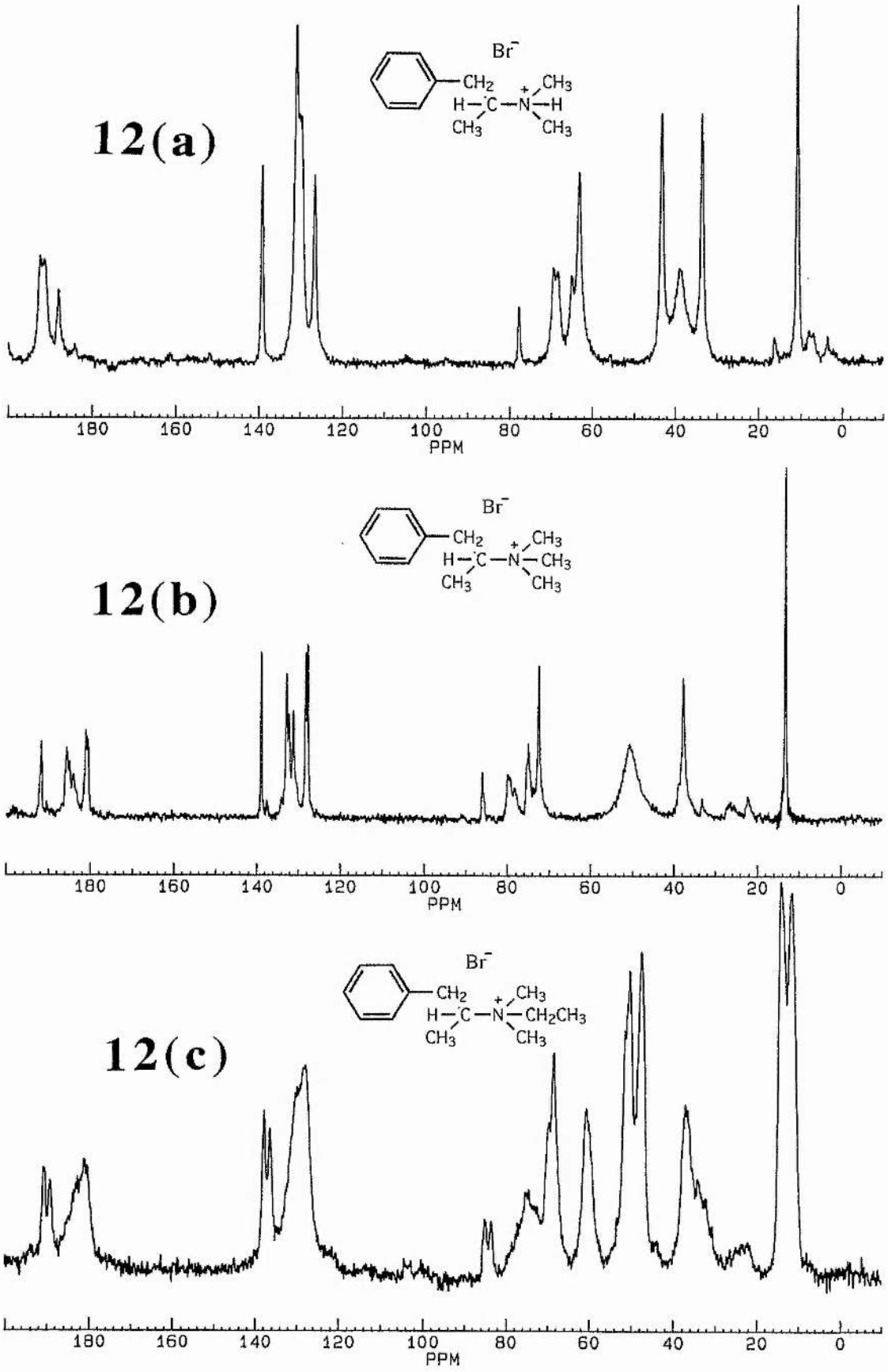

Figure 3.37: Variable Temperature ^{13}C CP/MAS Spectra of the N–Methyls of Compound 12(b)

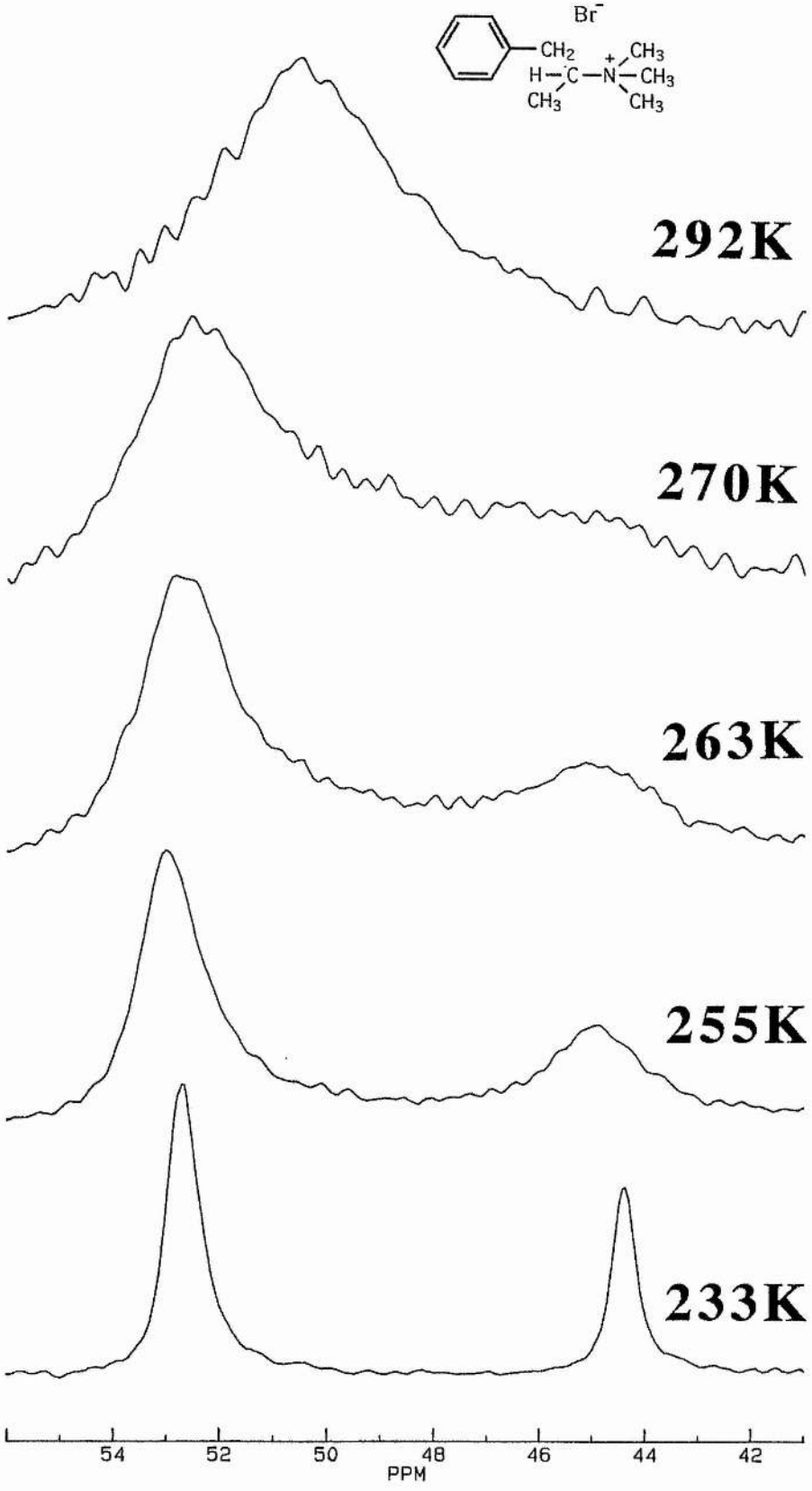

The room temperature spectra of compounds 12(a), (b) and (c) are shown in Figure 3.36.

The spectrum of compound 12(a) shows the N–methyls at 34 and 44 ppm, and the N–CH at 63 ppm. The remaining methyl and benzylic CH_2 are located at 11 and 39 ppm respectively. The aromatic carbons are at ca. 130 ppm. Variable temperature spectra show no significant change in the relative intensities of the peaks. No further data was collected on this compound.

The spectrum of compound 12(b) shows the N–methyls and N–CH at 50 and 72 ppm respectively. The remaining methyl and benzylic CH_2 are shown at 13 and 38 ppm respectively with the aromatic carbons at ca.130 ppm.

At room temperature the N–methyls are shown as one broadened peak. On cooling, the peak broadens and finally splits into a doublet (2:1); Figure 3.37. At higher temperatures the methyls undergo rapid $T_1\rho$ relaxation and the results are shown in Table 3.18. It was not possible to determine values above 335K as the signal/noise ratio decreased dramatically after this point due to the cross polarisation becoming very inefficient. This may have been due to a phase change. The activation parameters were determined and gave $\Delta H^{\ddagger} = 40.4 \pm 7.8$ kJmol^{-1} and $\Delta S^{\ddagger} = -8.0 \pm 26.7$ JK^{-1}mol^{-1}.

The spectrum of compound 12(c) shows the two N–methyls, N–CH_2 and N–CH at 48, 51, 61 and 69 ppm respectively. The remaining two methyls are at 12 and 14 ppm with the benzylic CH_2 at 37 ppm. The aromatics are ca. 130 ppm. The spectrum shows two lines for the aromatic quaternary carbon. This is due to two molecules in the asymmetric unit and is the reason why the other peaks are broadened. Variable temperature spectra show no significant change in the relative intensities of the peaks.

Table 3.18: $T_1\rho$ (msec) and Rate (s^{-1}) Data for Compound 12(b); [ω_1 = 60 kHz]

	37ppm	50ppm	
T(K)	$T_1\rho$	$T_1\rho$	k
335	15.86	1.49	3.2×10^6
328	15.77	0.96	1.0×10^6
320	20.86	1.63	4.5×10^5
313	25.70	1.42	3.7×10^5
306	27.65	2.97	1.9×10^5
299	46.29	4.02	1.4×10^5
292	71.58	5.43	1.0×10^5
Line Shape Data			
277			8.0×10^4
270			5.0×10^4
263			3.0×10^4
255			7.5×10^3

Figure 3.38: Room Temperature ^{13}C CP/MAS Spectra of Compounds 13(a), (b) and (c)

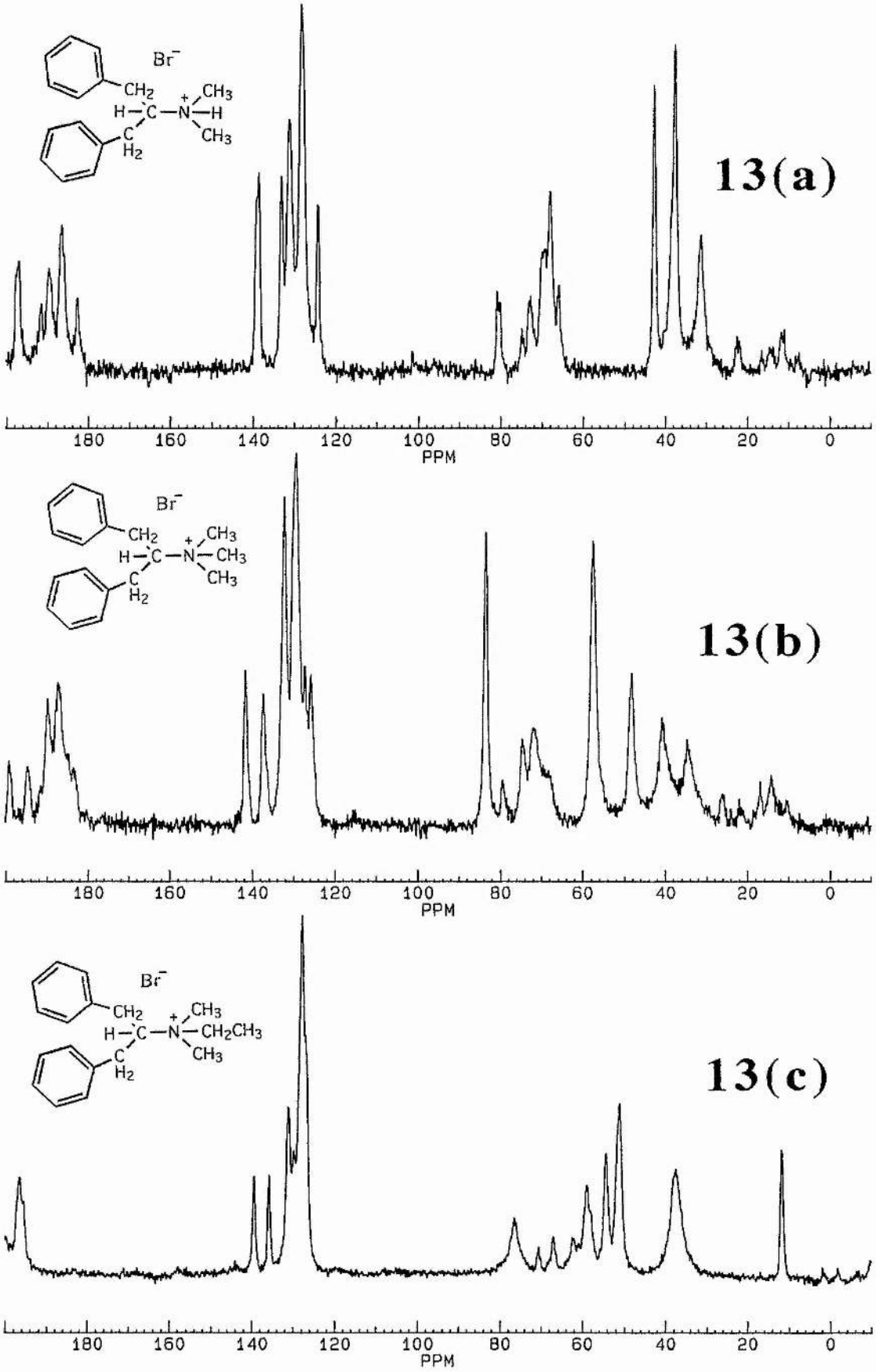

Figure 3.39: Variable Temperature ^{13}C CP/MAS Spectra of the N–Methyls of Compound 13(b)

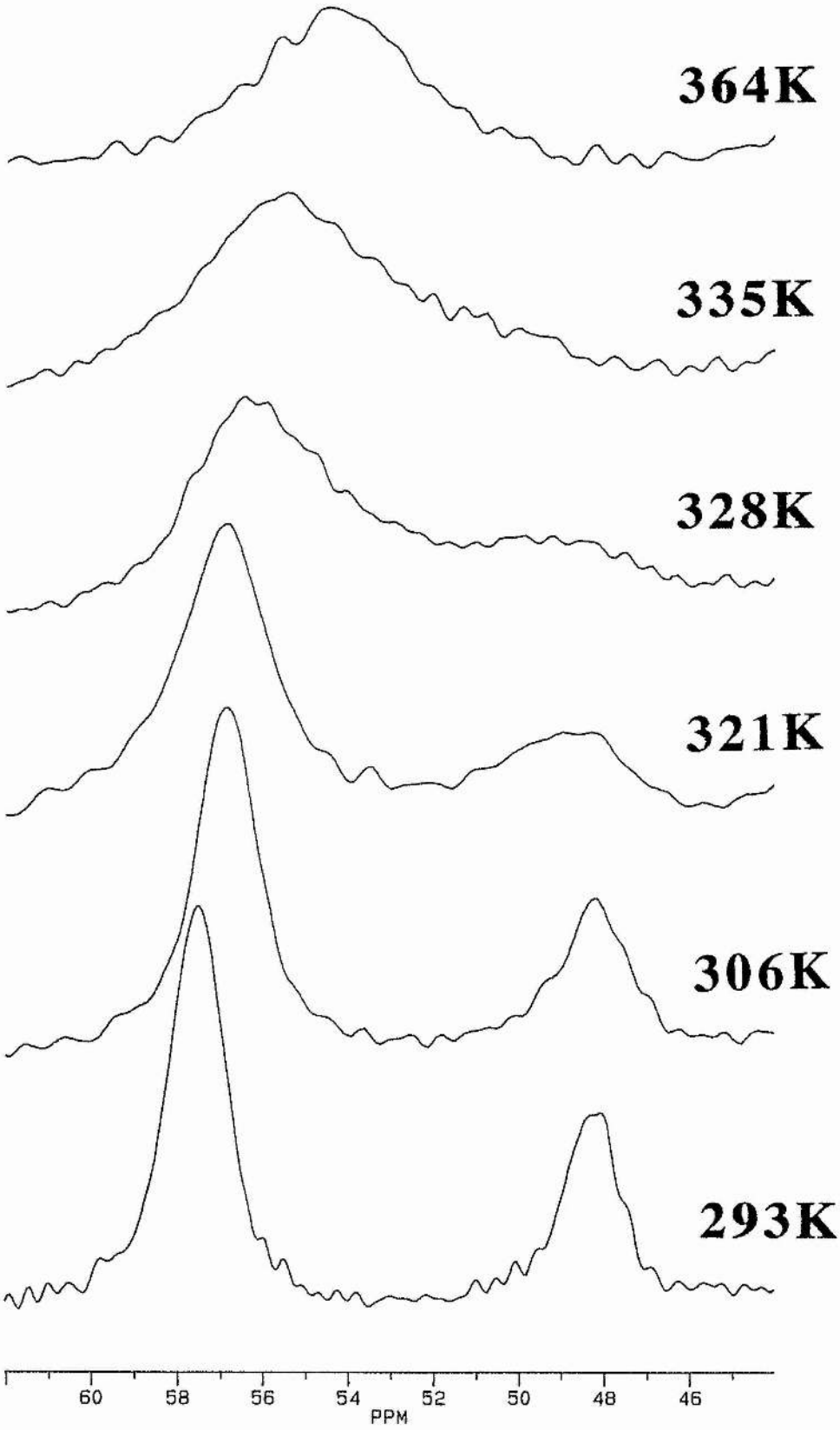

The room temperature spectra of compounds 13(a), (b) and (c) are shown in Figure 3.38.

The spectrum of compound 13(a) shows the two N–methyls and N–CH at 38, 43, and 68 ppm respectively. The benzylic CH_2s are located at 32 and 38 ppm with the aromatic carbons at ca. 130 ppm. This compound showed no change in the relative intensities of the peaks with temperature.

The spectrum of compound 13(b) shows the N–methyls frozen out in a doublet (Ratio 2:1) at 58 and 48 ppm. The N–CH is located at 83 ppm. The benzylic CH_2s are shown at 35 and 41 ppm with the aromatic carbons at ca. 130 ppm.

Variable temperature work done on this sample shows that on heating from RT to 364K the spectra undergo dynamic line shape changes. The two methyl peaks broaden and coalesce at 328K; Figure 3.39. Further heating sharpens this peak. No $T_1\rho$ data could be gathered as the upper temperature limit of the probe had been reached.

The spectrum of compound 13(c) shows the ethyl methyl and two overlapping N–methyls at 12 and 51 ppm respectively. The N–CH_2 and N–CH are located at 54 and 76 ppm respectively. The benzylic CH_2s are shown at 37 ppm with the aromatic carbons at ca. 130 ppm. Variable temperature studies showed no change in the relative intensities of the peaks.

Figure 3.40: Room Temperature ^{13}C CP/MAS Spectra of Compounds 14 and 15

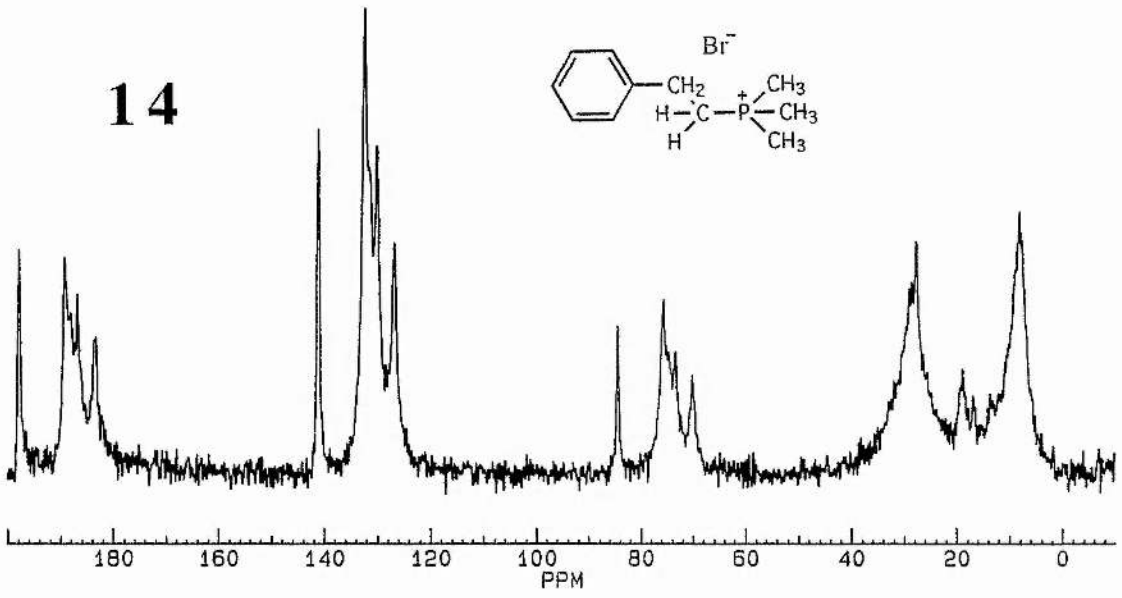

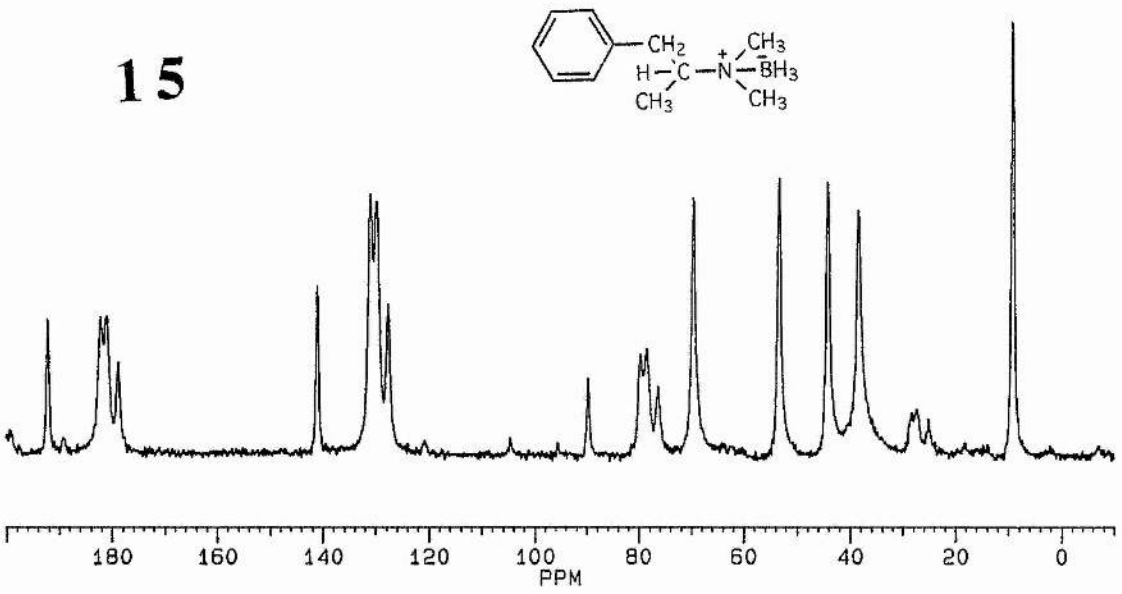

Figure 3.41: Variable Temperature ^{13}C CP/MAS Spectra of the P–Methyls of Compound 14

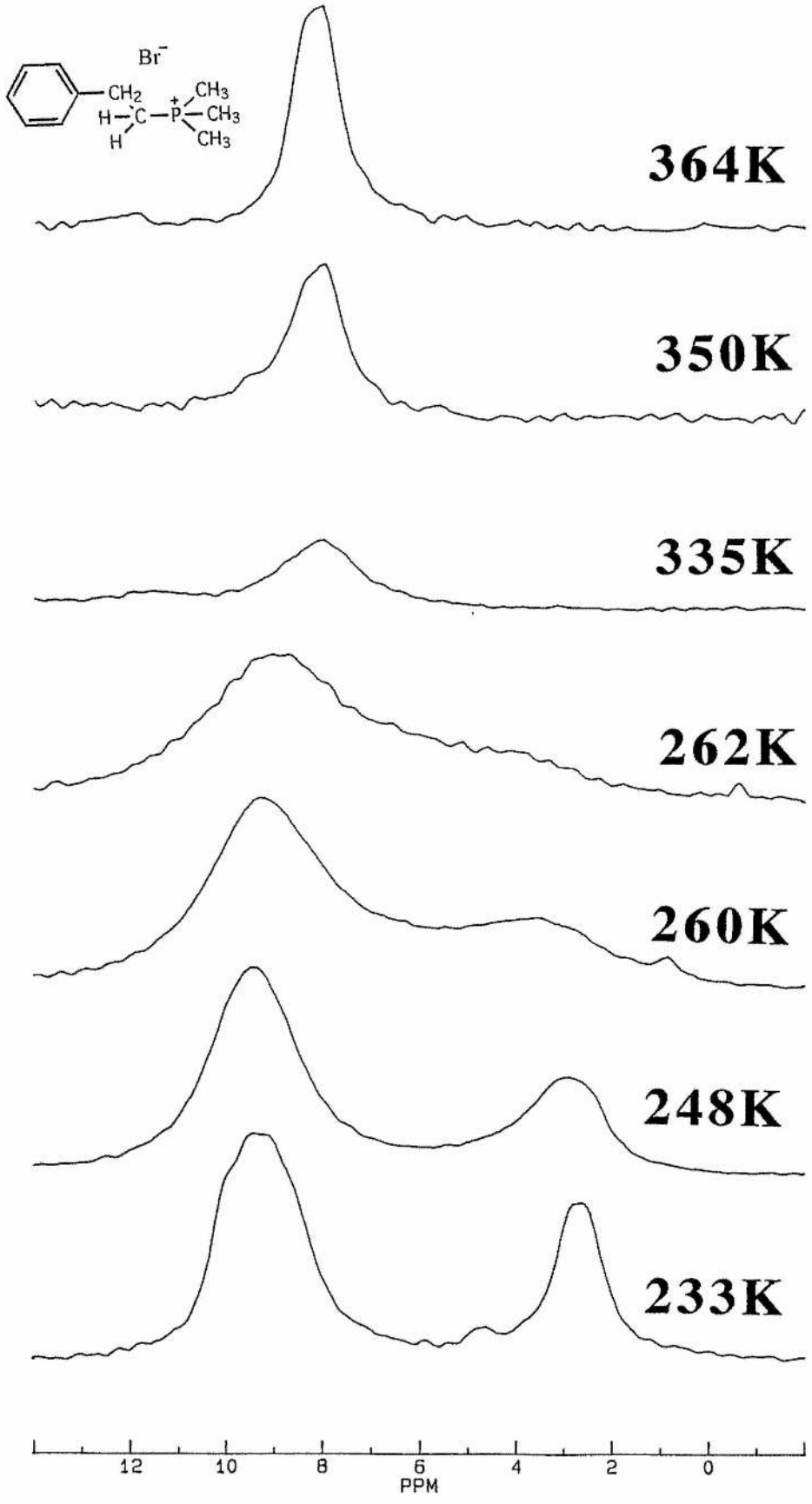

3.4 Group Rotations in Other Quaternary Salts

The above examples have shown a remarkable variety of dynamic processes in crystalline amines and ammonium salts. It was of interest to see if similar processes exist in related compounds such as phosphonium salts. How does the larger P^+Me_3 group behave? Does it, like all the CMe_3 and N^+Me_3 groups described above, show a measurable rate of rotation in the solid? Can ^{31}P measurements be made to provide rate data? Thus compound 14 was prepared for study.

The room temperature spectrum of compound 14 is shown in Figure 3.40. The $P^+(Me)_3$ group is rapidly rotating at this temperature and is represented as a single broad line at 8 ppm. Figure 3.41 shows the variable temperature spectra of the P^+Me_3 group of compound 14. At low temperatures the methyls are split into a doublet (2:1) at 10 and 3 ppm. Resolution enhancement shows a J coupling of ca. 50 Hz between ^{13}C and ^{31}P. On heating, the peaks coalesce (262K), sharpen, and proceed through a $T_1\rho$ minimum. Table 3.19 gives the $T_1\rho$ and line shape data derived from ^{13}C spectra. Additionally, it is possible to perform $T_1\rho$ measurements on the ^{31}P nucleus. The data collected from the two nuclei should be complementary and give identical rate data.

The data from three independent but complementary NMR methods is indeed consistent (Figure 3.42), adding further proof to the accuracy of the $T_1\rho$ method of determining the rate of motion of a group. The data gives $\Delta H^{\ddagger} = 49.4 \pm 2.8$ kJmol^{-1} and $\Delta S^{\ddagger} = 22.8 \pm 8.6$ JK^{-1}mol^{-1}.

Table 3.19: $T_1\rho$ (msec) and Rate (s^{-1}) Data for the P^+Me_3 group of Compound 14;

$[\omega_1 = 48$ kHz$]$

T(K)	^{13}C $T_1\rho$	k	^{31}P $T_1\rho$	k
364			11.57	9.4×10^6
357			7.77	6.2×10^6
349	4.84	5.8×10^6	5.63	4.4×10^6
342	4.30	5.1×10^6	4.30	3.3×10^6
335	2.01	2.0×10^6	3.26	2.3×10^6
328	1.52	7.8×10^5	2.60	1.6×10^6
324			2.51	1.5×10^6
320	1.57	6.7×10^5	2.22	7.7×10^5
317			2.23	7.7×10^5
313	1.81	4.9×10^5	2.31	6.6×10^5
306	1.87	4.6×10^5	2.74	4.5×10^5
299	2.20	3.6×10^5	3.48	3.2×10^5
294	4.72	1.5×10^5	4.47	2.4×10^5
Line Shape Data				
263		9.5×10^3		
260		8.0×10^3		
254		5.5×10^3		
250		3.5×10^3		
246		2.0×10^3		

Figure 3.42: Eyring Plot showing the Three Complementary Sets of Data for Compound 14.

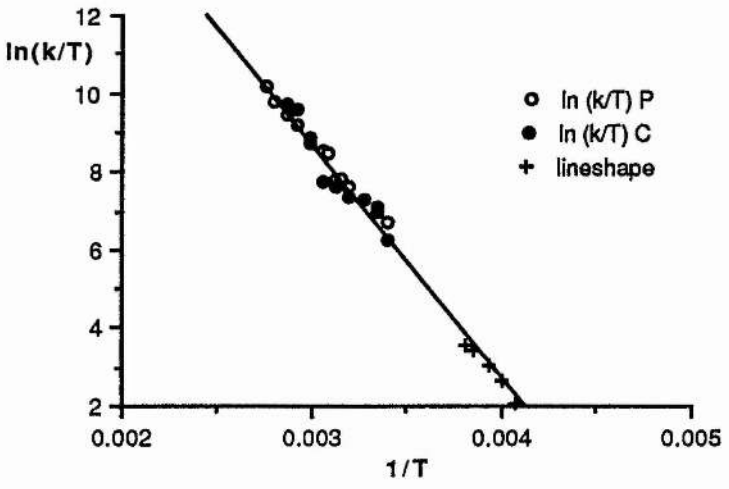

In order to prepare solid samples for study it was necessary in the above examples to use the quaternary salt of the amines as all but the dibenzyl amines were liquids. However, by using the BH_3 adduct of amines, a group of similar size to a CH_3 can be added without the need for a counter ion. The $N^+Me_2BH_3^-$ group is zwitterionic and the polarity of the N^+—B^- bond might affect the barrier to rotation of the group in the solid state. A comparison with the isostructural unit in 12(b) is of interest. Thus compound 15 was prepared for study.

The room temperature spectrum of compound 15 is shown in Figure 3.41. The N–methyls are located at 44 and 53 ppm. The remaining methyl and N–CH are at 9 and 70 ppm respectively. The benzylic CH_2 is shown at 38 ppm with the aromatic carbons at ca.130 ppm. Variable temperature studies on this compound show that, unlike the corresponding bromide quaternary salts, this compound shows no change in the relative intensities of the peaks with temperature. This lack of dynamic behaviour may be due to dipole dipole interaction between N^+—B^- dipoles in the solid raising the activation energy above that of compound 12(b).

3.5 Summary of Activation Parameters

Table 3.21: Activation Parameters for Group Rotations

Comp	Rot^{n} Type	E_a (kJmol^{-1})	$\Delta H^{\ddagger}$ (kJmol^{-1})	$\Delta S^{\ddagger}$ (JK^{-1}mol^{-1})	$\Delta G^{\ddagger}_{293K}$ (kJmol^{-1})
4	C-*t*-butyl	—	33.5±3.2	10.3±13.5	30.5±7.2
4	S-*t*-butyl	—	38.2±1.5	9.4±5.9	35.4±3.2
5	C-*t*-butyl	—	26.7±3.6	-11.3±13.9	30.0±7.7
5	S-*t*-butyl	—	32.2±2.2	-1.3±8.5	32.6±4.7
6(b)i	*t*-butyl	—	24.2±3.3	-57.3±9.9	41.0±6.2
6(b)ii	*t*-butyl	—	25.3±8.7	-11.7±38.3	28.7±19.9
7(b)	*t*-butyl	—	55.5±5.7	27.9±16.6	47.3±10.6
7(c)	*t*-amyl	—	54.9±7.8	17.8±22.9	49.7±14.5
8(a)	methyl	26.6±4.2	—	—	
8(b)	*t*-butyl	—	47.7±6.1	23.5±20.3	40.8±12.3
9(b)	*t*-butyl	—	33.3±3.1	13.32±12.1	29.4±6.6
10(b)	*t*-butyl	—	59.4±5.2	-33.9±16.4	69.3±10.0
11(b)	$N(Me)_3$	26.4±0.9	—	—	
11(b)	phenyl	—	63.9±6.3	75.1±20.6	41.9±12.3
11(c)	$N(Me)_2(Et)$	20.9±1.7	—	—	
11(c)	phenyl	—	48.0±4.6	23.5±15.5	41.1±9.2
12(b)	$N(Me)_3$	—	40.4±7.8	-8.0±26.7	42.7±15.7
14	$P(Me)_3$	—	49.4±2.8	22.8±8.6	42.7±5.3

3.6 Conclusions

There are many conclusions to be drawn from this extremely successful study into the occurrence of conformational motion in the solid state.

(1) This work has produced evidence of a remarkable variety of intramolecular motions in this series of crystalline solids, motions which consist of rotating *t*-butyl, *t*-amyl, methyl and phenyl groups.

(2) A comparison of these phenomena with the predictions made at the beginning of this section reveals many similarities.

(a) Every CMe_3 or N^+Me_3 group studied has an observable rotation in the solid. This is consistent with the idea that the conical symmetry of the group allows it to rotate more easily.

(b) Some, but not all, *t*-amyl and N^+Me_2Et groups show rotations in the solid state. It was predicted that these rotations would be of higher energy than the *t*-butyl group rotation and thus less common. This was due to the more bulky ethyl group which would have to rotate into the space normally occupied by a methyl. Only two *t*-amyl like group rotations were observed (7c and 11c) out of a total of eight possible compounds. However, the energy of activation for these compounds are comparable (7c) or less (11c) than the corresponding *t*-butyl (7b) or N^+Me_3 (11b) derivative.

(c) There were no *i*-propyl or N^+HMe_2 group rotations observed in these compounds. This was to be expected as the volume change required for a methyl group to rotate into the space normally occupied by a hydrogen atom should be too great. The energy required is not low enough for a rotation to be observable by these methods.

(d) Of the twenty six compounds studied, five contained observable, rapidly rotating phenyl groups (6a, 8a, 11a, b, and c). The rate of rotation of two of these compounds (11b and c) was measured and showed remarkably different activation

parameters for two closely related molecules. Phenyl rotations appear to be more common in *i*-propyl derivatives.

(e) Restricted rotation of methyl groups has been observed in three compounds (8a, b, and 9b). Compounds 8(b) and 9(b) show the slowing of a single methyl rotation in the *t*-butyl group such that it is $T_1\rho$ relaxed or broadened out. It is apparent that one of the methyl sites in the crystal lattice is much more hindered than the other two. Compound 8(a) shows the slowing of a N–methyl rotation due to the close proximity of the counter ion.

(3) The $T_1\rho$ method of determining rates of rotation is vindicated by this series of experiments. This is especially the case with the phosphonium salt where three independent but complementary methods have produced consistent results.

(4) X-ray diffraction studies would assist in the understanding of the nature of the processes involved in these motions.

(5) There is a fantastic range of activation parameters for rotations in the solid state. This is especially the case for $\Delta S^{\ddagger}$ which ranges from -57 $JK^{-1}mol^{-1}$ for a *t*-butyl rotation to +75 $JK^{-1}mol^{-1}$ for a phenyl group rotation.

It was never envisaged at the outset that so numerous and different motions could possibly occur in these restricting environments. This study is likely to be the tip of a considerably large iceberg of solid state intramolecular motions and chemists must now revise their widely held view that little conformational motion occurs in the solid state.

Chapter Four

Conformational Equilibria

4 Introduction

In any ring system there is bound to be some amount of strain caused by atoms or groups interacting with one another at close proximity. The particular conformation adopted would depend on the amount of ring strain caused by these interactions in each conformer. The relief of ring strain can best be brought about by bond angle deformation rather than changes in the bond length as discussed in section 1.6.

4.1 Cyclohexane

In 1890, Sachse[40] concluded that due to the relief of ring strain and the preference for carbon to have tetrahedral bond angles, cyclohexane doesn't exist in the planar form. Now it is known that there are four main conformations; figure 4.1.

Figure 4.1: The four conformations of cyclohexane

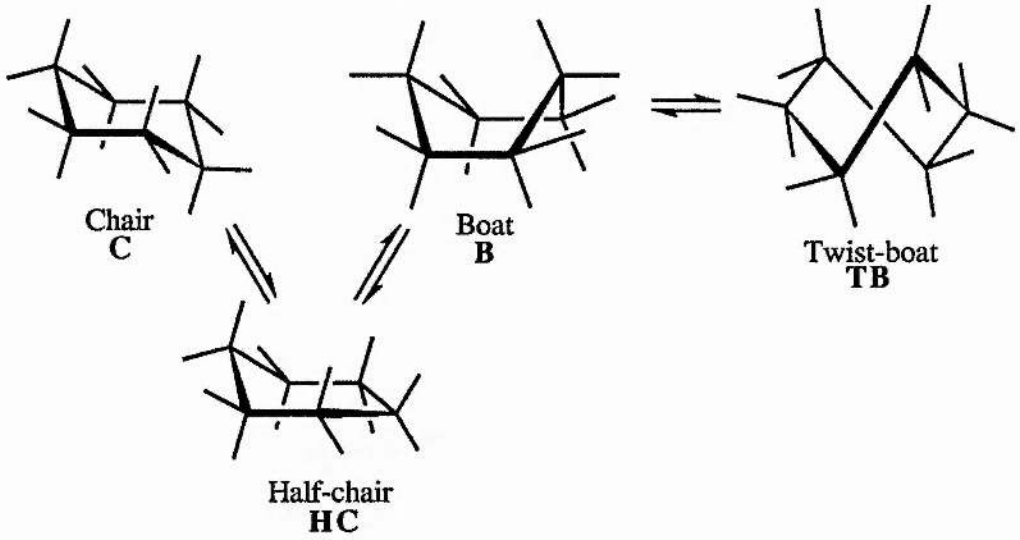

The lowest energy of these is the chair conformation in which all the bonds are staggered. This can interconvert between the boat and twist conformations by ring inversion. During the transformation, some angular distortion is required because several bonds have to be rotated at the same time. In the boat form there is no angle

strain, but there is bond opposition strain involving the four pairs of hydrogens eclipsing along the sides of the boat and also some strain due to the pair of hydrogens interacting at the top, known as the bowsprit interaction. As a result of these unfavourable interactions, the boat is considerably less stable than the chair. However, if the boat is distorted in such a way that it passes from one boat form to another, then an intermediate conformation is established in which the bowsprit interaction and eclipsing of adjacent hydrogens are alleviated somewhat. This is the twist boat form and it is 6.7 $kJmol^{-1}$ more stable than the boat. The potential energy of the system is shown in figure 4.2.

Figure 4.2: Potential Energy of Cyclohexane as a Function of Conformation

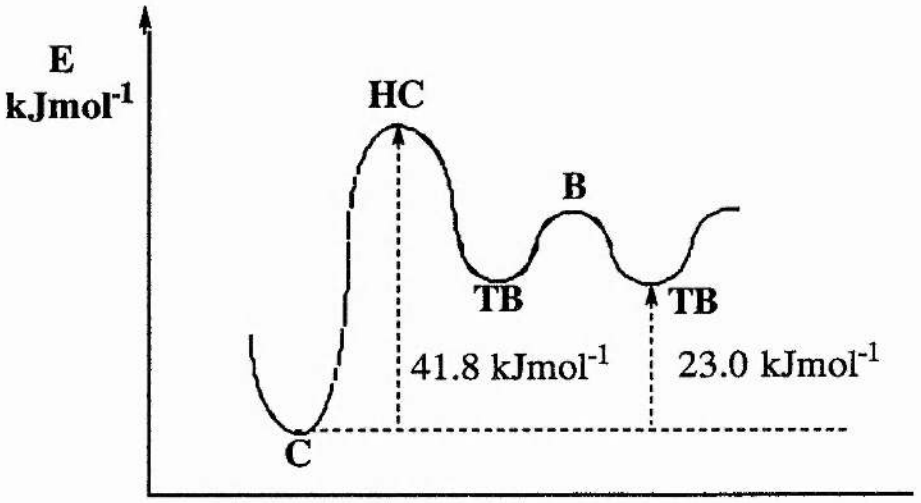

The energy difference of 23 $kJmol^{-1}$ between the chair and twist boat forms ensures that cyclohexane exists almost exclusively in the chair form at room temperature.

4.2 Related Ring Systems

Bicyclo[3.3.1]nonane and adamantane are interesting related molecules based on cyclohexane; figure 4.3. Bicyclo[3.3.1]nonane is related to adamantane in the removal of a CH_2 group between the two wings.

Figure 4.3: The Three Related Ring Structures.

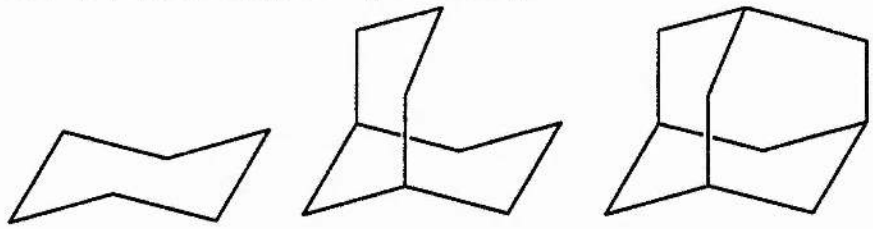

Cyclohexane **Bicyclo[3.3.1]nonane** **Adamantane**

The average C-C bond length in bicyclo[3.3.1]nonane (1.536Å) is closer to that in cyclohexane (1.534Å) than adamantane (1.54Å)[41]. Also, the average C-C-C bond angle of 111.5° in cyclohexane is much closer to that in bicyclo[3.3.1]nonane (111.4°) than adamantane (109.3°). As predicted before, this shows that the preferred method of ring strain relief in cyclohexane and bicyclo[3.3.1]nonane is by bond angle and torsional deformations, unlike adamantane where the strain is relieved through C-C bond lengthening. Thus bicyclo[3.3.1]nonane is more closely related to cyclohexane and is likely to adopt cyclohexane-like chair, boat and twist boat combinations of conformation.

4.3 Conformational Equilibria in Bicyclo[3.3.1]nonane derivatives

Bicyclo[3.3.1]nonane would seem to be an ideal model for the study of conformational equilibria and the possible conformations are described thus (Figure 4.4):

The *twin-chair* conformer: Strong interactions will be experienced between the endo hydrogens on C(3) and C(7) which are calculated as being 0.8A apart. However, the conformer can distort to accommodate this.

The *boat-chair* conformer: The interaction above is relieved in this conformation but additional interactions occur between the hydrogen below C(3) and the hydrogens below C(6) and C(8) which cancel any reduction in strain. There is also an interaction between the C(7) and C(9) hydrogens.

The *twin-boat.* conformer: Not only are there the C(3)-C(9) and C(7)-C(9) methylene interactions but there are also interactions between the 2,8- and 4,6-hydrogens.

The *twin-twist-boat* conformer: In this conformation there is a slight relief of the 3,9- and 7,9-hydrogen interactions but a large transverse 2,6 interaction below the ring is caused.

Figure 4.4: The four possible conformations of Bicyclo[3.3.1]nonane. Only those strongly interacting hydrogens are shown.

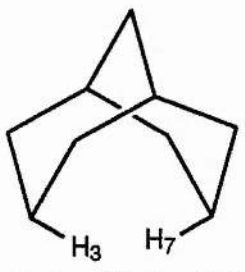

Twin Chair (CC)

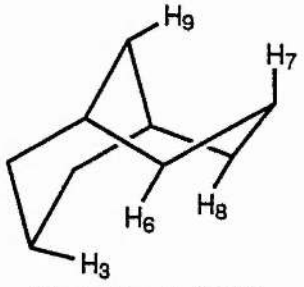

Chair-boat (CB)

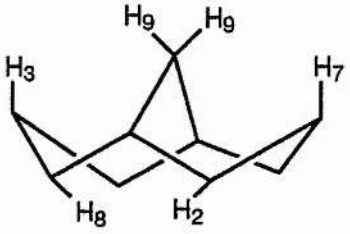

Twin Boat (BB)

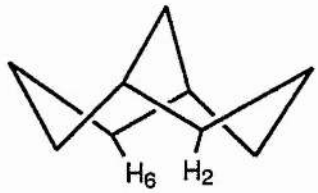

Twin Twist-Boat (TB)

It is clear that the most likely conformation adopted by bicyclo[3.3.1]nonane will be the twin chair where the only H-H interaction is between the 3,7-hydrogens. Indeed, electron diffraction studies performed in the gas phase show this to be the preferred conformation of the parent hydrocarbon[41], with the six membered rings slightly flattened to accommodate the 3,7-hydrogen interaction. Additionally, infra-red investigations on some simple derivatives in the solution and solid phases have been done and the results corroborate the gaseous observations[42].

Table 4.1: Conformations of some Bicyclo[3.3.1]nonan-9-one Derivatives.

Substituents	Conformation	Refs.
None	CC	47
3β-CO_2Me	CC	47
3β-CO_2Me, 7β-t-Bu	CC	47
3α-CO_2Me	CB	47
3α-CO_2H, 7α-CO_2H	CB	48
3α-t-butyl, 7β-CO_2Me	CB	47
3α-Me, 7α-t-Butyl	BB	44
3α-CMe_2OH, 7α-t-Butyl	BB	47
3α-CMe_2OH, 7α-CMe_2OH	BB	49

Much work has already been done in the study of conformational equilibria in bicyclo[3.3.1]nonane derivatives in solution. The two main areas of research are in twin chair/chair-boat[44,50] and chair-boat/twin boat[47-49] equilibria. However, these processes may very well be occurring in the solid-state. Bicyclo[3.3.1]nonane would seem to posses the properties required in the principle of least distress as there is only a small volume change required for transitions between the twin chair and chair-boat conformations.

As we have seen, for bicyclo[3.3.1]nonane in the solid-state, the twin chair conformation is much more stable than the chair-boat. The chair-boat is 10-13 kJ mol^{-1} higher in energy than the twin chair. Electron diffraction studies in the gas phase show that 5% of the molecules are in the chair-boat conformation at 338K increasing to 25% at 673K[51]. As predicted from these results, X-ray studies of bicyclo[3.3.1]nonane derivatives show no evidence of chair-boat/twin chair conformational disorder at room temperature.

However, the chair/boat energy difference for cyclohexanone is smaller than that for cyclohexane[52] by *ca* 6 $kJmol^{-1}$. Thus, the chair-boat/twin chair energy

difference for bicyclo[3.3.1]nonan-9-one should be less than that for bicyclo[3.3.1]nonane. NMR studies of bicyclo[3.3.1]nonan-9-one in solution have shown that 22% of the molecules are present in the chair-boat form at room temperature[53], which is consistent with a chair-boat /twin chair energy difference of *ca* 5 kJmol^{-1}. It was thought that derivatives of bicyclo[3.3.1]nonan-9-one might provide examples of a chair-boat/twin chair equilibrium in the solid-state. Several X-ray studies have been performed by Sim[54] on 9-substituted bicyclo[3.3.1]nonan-9-one compounds which have yielded examples of crystallographic disorder at room temperature. Of these, two seem to exhibit conformational processes in the solid-state. These are the p-toluenesulphonylhydrazone and p-methoxybenzenesulphonylhydrazone.

Sim claimed that at temperatures between 130K and 145K both compounds are fully ordered with the twin chair conformation. As the temperature is increased, the molecules become more disordered until at 293K, 31% of the molecules in the p-toluenesulphonyl derivative exist in the chair-boat form and similarly for 21% of the p-methoxybenzenesulphonyl derivative. The enthalpy for the chair-boat/twin chair equilibrium was calculated as being ca 6 kJmol^{-1} for the former and 12 kJmol^{-1} for the latter derivative.

A solid-state CP/MAS NMR investigation of these observations showed no evidence of a conformational equilibrium over the temperature range 173K to 293K[55]. It was concluded that should such an equilibrium exist then the rate of conformational exchange must be too fast to interact with the NMR processes.

Figure 4.5: Some Derivatives of Bicyclo[3.3.1]nonane

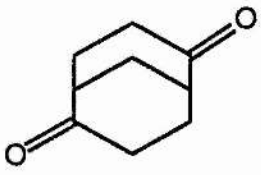

RB 1

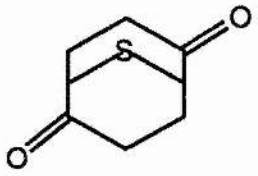

RB 2

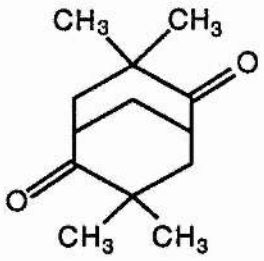

RB 3

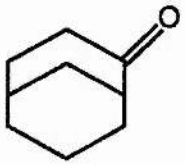

RB 4

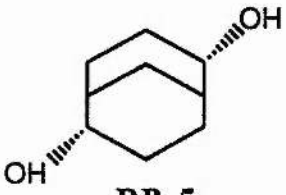

RB 5

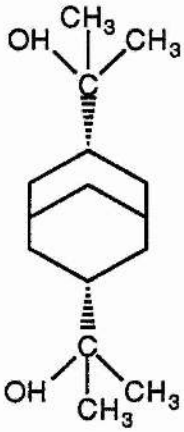

RB 6

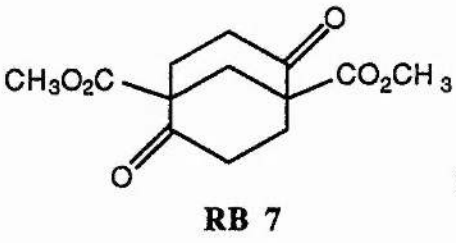

RB 7

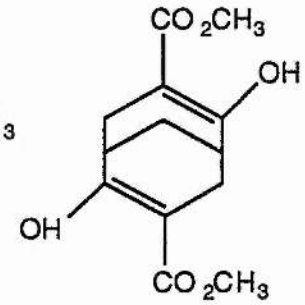

RB 8

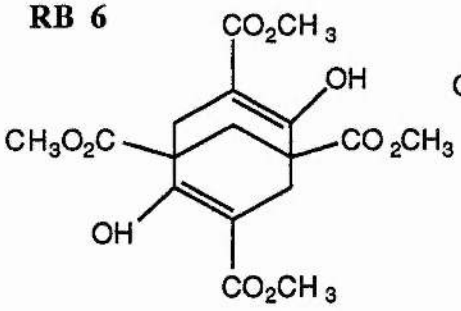

RB 9

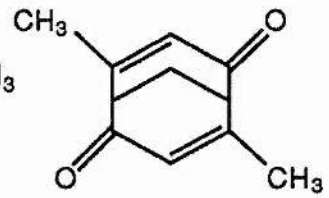

RB 10

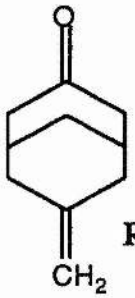

RB 11

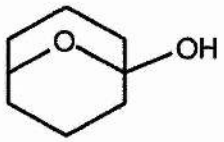

RB 12

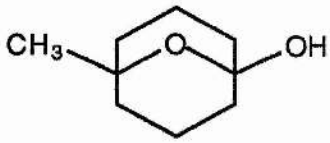

RB 13

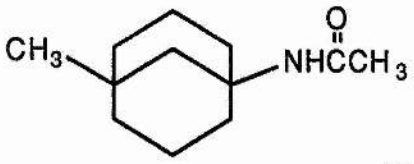

RB 14

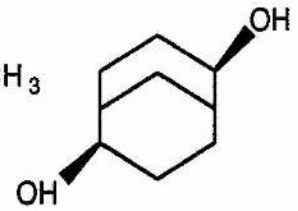

RB 15

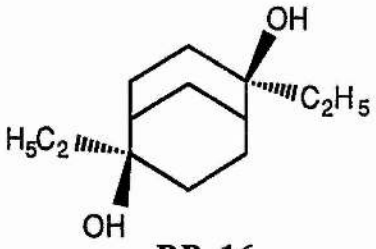

RB 16

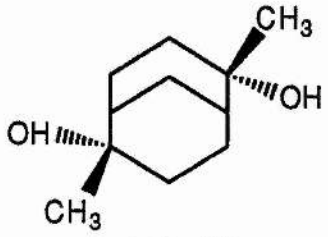

RB 17

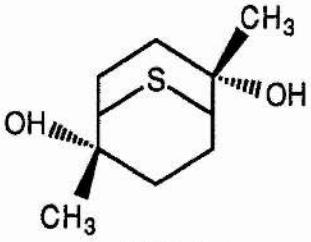

RB 18

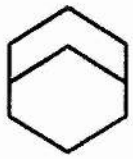

RB 19

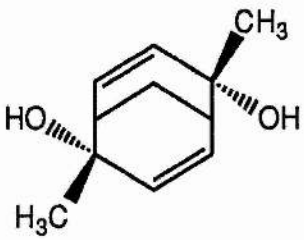

RB 20

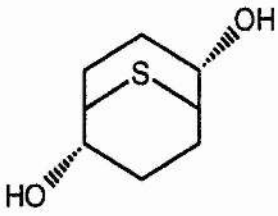

RB 22

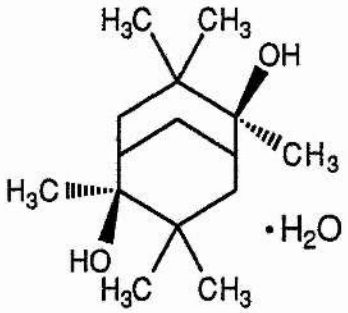

RB 23

4.4 Bicyclo[3.3.1]nonane Derivatives in the Solid State

Because of the possibility of conformational equilibria being present in suitable derivatives of bicyclo[3.3.1]nonane in the solid, it was decided to examine a wide range of bicyclo[3.3.1]nonane derivatives. The compounds used were kindly supplied and purified by Prof R. Bishop of the University of New South Wales, Australia.

Figure 4.5 shows the derivatives used for study. It was hoped that some of these compounds would exhibit conformational equilibria in the solid state. Each is described in turn. Where crystallographic data is known this has been included. Otherwise, the conformations have been estimated on the basis of the interactions detailed in the previous section.

The room temperature ^{13}C CP/MAS spectra of compounds RB 1, 2 and 3 are shown in figure 4.6.

The spectrum of **RB 1** shows 4 peaks between 30 and 48 ppm corresponding to the ring carbons with the carbonyls located at 216ppm. There seems to be only one conformation present and this is likely to be the twin chair as there are no bulky groups in the 3α or 7α position.

The spectrum of **RB 2** shows two peaks at 32 and 38 ppm corresponding to C(2) and (7) and (3) and (6). The third, at 45ppm shows the bridge head carbons, C(1) and (5), adjacent to the sulphur. The carbonyls, C(4) and (8), are situated at 207 ppm. This also is likely to be a twin chair. There is no NMR evidence for a second conformation.

The spectrum of **RB 3** shows ca.10 lines between 26 and 47 ppm. The methyl carbons are shown at 27, 28, 29 and 32 ppm with the quaternaries, C(3) and (7), at 43 and 46 ppm. The remaining ring carbons are located at 38, 42 and 47 ppm. The carbonyl peaks, C(4) and (8), are at 217 ppm. On cooling to 204K the spectrum shows no significant change in the relative intensities of the peaks. With two methyls in each of the 3 and 7 positions this compound may adopt the chair/boat conformation

to relieve the 3,7-α interaction. The asymmetric unit in the solid contains one molecule.

The room temperature ^{13}C CP/MAS spectra of compounds RB 4, 5 and 6 are shown in figure 4.7.

The spectrum of compound **RB 4** shows 9 exceptionally sharp lines corresponding to each carbon in the molecule. The carbonyl, C(4), is located at 214ppm. As the temperature is lowered to 204K there is no change in the relative intensities of the lines. This compound probably adopts the twin chair conformation but may be in equilibrium with the chair/boat. If so, this equilibrium is too fast to be measured by these techniques. Thus, no NMR evidence can be found for a second conformation. It may be that the sharpness of the lines is due to rapid molecular motion in a plastic crystal phase. However, there is no evidence to support this.

The spectrum of compound **RB 5** shows what appears to be five exceptionally broad lines. The existence of so few tends to suggest that there is a degree of symmetry in the crystal structure. The line at 73 ppm is due to C(4) and (8). The relative intensities of the lines remain the same on cooling to 204K. This compound is likely to assume the twin chair conformation as the chair/boat would have a significant 3,8–interaction. Again, there is no NMR evidence for a second conformation but the broadened lines may be due to some molecular motion. In contrast, the stereoisomer RB 15 gives much sharper lines in its spectrum. Interestingly, the substitution of the bridging carbon in RB 5 with a sulphur atom gives no significant change in the width of the lines in RB 22.

The spectrum of compound **RB 6** shows ca. 15 lines corresponding to each individual carbon in the molecule. The three peaks at 23, 29 and 34 ppm are due to the 4 methyls, two of them overlapping at 29 ppm. The doublet at 72ppm corresponds to C(3) and (7). This compound exists in the twin boat conformation due to a huge 3,7–interaction in the twin chair as well as 3,6– and 3,8–interactions in the chair/boat. This compound is unlikely to exist in equilibrium with another conformation, except in the

solution phase where it exists in equilibrium between the chair/boat and flexible twin boat conformation. Indeed, there is no NMR evidence to suggest otherwise.

The room temperature ^{13}C CP/MAS spectra of compounds RB 7, 8 and 9 are shown in figure 4.8.

The spectrum of compound **RB 7** shows 6 lines and is consistent with one molecule in the asymmetric unit. The peaks at 28 and 38 ppm are due to C(2), (3), (6), (7) and (9) with the quaternaries, C(1) and (5), and methyl peaks at 54 and 56ppm. The ring, C(4) and (8), and ester carbonyls are at 208 and 174 ppm respectively. There are, however, three methylene carbon environments yet only two peaks. The peak at 38 ppm is presumably composed of two overlapping lines which, because of the chemical shifts varying with temperature, can be observed individually at 204K. There is no NMR evidence of a second conformation at this temperature.

The spectrum of compound **RB 8** is consistent with one molecule in the asymmetric unit. The C(1), (2), (5), (6) and (9) signals are located at 29 and 32 ppm. The peak at 53ppm corresponds to the ester methyls and C(3) and (7) are shown at 96ppm. The signals at 173 and 175ppm correspond to the carbonyl and C(4) and (8) carbons. The 175 ppm peak is of lower intensity because of the chemical shift anisotropy as shown in the spinning side bands. By reference to RB9, this suggests that the peak at 175 ppm is due to C(4) and (8). A second conformation is not apparent.

The spectrum of compound **RB 9** shows C(2), (6) and (9) at 30 and 37 ppm with the methyls and bridge head C(1) and (5) at 49, 52 and 54 ppm. The C(4) and (8) quaternaries are shown at 97 ppm. The ester carbonyl and C(3) and (7) are located at 173 and 170 ppm respectively. The more intense peak at 173 ppm is of lower CSA and is almost certainly due to the ester carbonyl carbons. Thus the peak of lower intensity and greater CSA is due to C(4) and (8).

A solid state study of this compound, commonly known as Meerwein's ester, has shown that the compound exists exclusively in the dienol form rather than the diketo[56]. The absence of a ketone carbonyl in the ^{13}C CP/MAS spectrum confirms

this. An X–ray study concluded that there are four molecules in the asymmetric unit but this is not apparent from the spectrum...There is no conformational equilibrium in the solid state.

The room temperature ^{13}C CP/MAS spectra of compounds RB 10, 11 and 12 are shown in figure 4.9.

The spectrum of compound **RB 10** shows a doublet for each carbon environment. The methyls are at 23ppm with C(9) and bridge head C(1) and (5) at 35 and 50 ppm respectively. C(3) and (7) are shown at 121 and 124 ppm and the C(2) and (6) quaternaries and C(4) and (8) carbonyls are shown at 160–164 and 194–195 respectively.

The spectrum of compound **RB 11** shows the ring C(1), (2), (4), (5), (6), (8) and (9) at 31, 32, 41 and 46 ppm. The olefinic signals are at 114ppm for the CH_2 group and 144ppm for the C(7) quaternary. The carbonyl, C(3), is located at 211ppm. There is no NMR evidence for a second conformation.

The spectrum of compound **RB 12** shows two lines for every carbon. The peaks at 95ppm corresponds to the quaternary C(5) with C(1) at 73 and 74 ppm. The remaining signals show the ring carbons. The presence of two signals for each carbon may be indicative of another conformation or, more probably, a second molecule in the asymmetric unit. The lines in this spectrum are broader than for other compounds in this series. Variable temperature work may produce evidence for a conformational equilibrium.

There is the possibility of an equilibrium with 5-hydroxycyclooctanone, but no carbonyl peak is present in the spectrum.

The room temperature ^{13}C CP/MAS spectra of compounds RB 13, 14 and 15 are shown in figure 4.10.

The spectrum of compound **RB 13** shows two signals for each carbon. The methyl carbon, identified by a NQS sequence, is located at 32ppm with the C(1) quaternary carbon at 76ppm. The C(5) quaternary carbon is shown at 96ppm and the remaining ring carbons between 20 and 40 ppm.

Again, the possibility arises of a second conformation but no change in the relative intensities of the lines was observed on cooling the sample to 204K. The doubling of the lines is more probably due to more than one molecule in the asymmetric unit. There is no equilibrium with 5-hydroxy-5-methylcyclooctanone.

The spectrum of compound **RB 14** is consistent with one molecule in the asymmetric unit. The methyl is shown at 24 ppm with the C(1) quaternary at 34 ppm. The C(5) quaternary is located at 55 ppm and the amide methyl at 33 ppm. The carbonyl is at 171 ppm. The remaining signals are the other ring carbons. At 204K the ring methylenes have broadened markedly suggesting the slowing of a motional process.

The spectrum of compound **RB 15** shows the C(4) and (8) carbons at 70 and 71 ppm. There appears to be four lines for the two carbons. The remainder of the peaks are due to the ring methylenes. However, there is more than one line for each carbon. This is in complete contrast to the stereoisomer RB 5 whose spectrum is composed of only five broad lines. Substitution of the bridging C(9) in RB 15 with a sulphur atom gives similarly broad lines in RB 22.

An X–ray crystallographic study has shown that there are two molecules in the asymmetric unit, adopting the twin chair conformation[57]. Like RB 16, there is a great deal of H–bonding present in this compound. Here, the H-bonding network comprises of infinite ···OH···OH···OH··· connections which loosley approximate to a spiral. It would be more difficult in this case due to the addition of these H-bonds for an equilibrium to exist. There is certainly no NMR evidence in favour of a conformational equilibrium in this compound.

The room temperature ^{13}C CP/MAS spectra of compounds RB 16, 17 and 18 are shown in figure 4.11.

The spectrum of compound **RB 16** shows the C(4) and (8) quaternary carbons at 73 and 74 ppm. The methyls are located at 8ppm. The rest of the peaks are the ring methylenes and ethyl CH_2s.

X–ray crystallography shows that this compound contains only one molecule in the asymmetric unit which adopts the twin chair conformation[57]. The nmr is consistent with this in that there are two methyls and two C–OH lines in the spectrum. The crystal structure of this compound differs from RB 15 in that the H–bond connections occur in four membered cycles instead of infinite chains. The peaks in the region 20–40 ppm are broad, possibly indicative of molecular motion. A variable temperature study of this compound may produce some evidence for a second conformation.

The spectrum of compound **RB 17** shows four lines for the C(4) and (8) quaternary carbons at 72 and 73 ppm with the methyls at 30 and 33 ppm. The remainder of the lines correspond to the ring methylene carbons.

The spectrum of compound **RB 18** in contrast to RB 17, shows two lines for the C(4) and (8) quaternaries at 72 and 73 ppm with four methyl signals at 29, 30, 31 and 32 ppm. The remainder of the peaks are due to the ring methylene carbons. It may be that there are two molecules in the asymmetric unit and/or the molecule exists in the chair/boat conformation.

The room temperature ^{13}C CP/MAS spectra of compounds RB 19, 20 and 22 are shown in figure 4.12.

The spectrum of compound **RB 19** shows four peaks due to the ring methylenes. The peak at 22 ppm is due to the C(3) and (7) carbons with the bridging C(9) at 27 ppm. The large signal at 31 ppm corresponds to the four carbons (2), (4), (6) and (8). The bridge head carbons (1) and (5) are shown at 34 ppm. This molecule exists in the twin chair form in the solid state.

The spectrum of compound **RB 20** shows the C(2), (3), (6) and (7) carbons at 130 and 135 ppm. The C(4) and (8) quaternaries are located at 76 ppm with four methyl signals at 29, 30, 31 and 32 ppm. The remaining lines are due to the methylene carbons. The doubling of all the lines is indicative of two molecules in the asymmetric unit.

The spectrum of compound **RB 22** shows the C(4) and (8) carbons at 73 ppm. The bridge head C(1) and (5) are located at 38 ppm. The remainder of the lines are due

to the ring methylene carbons. The lines from this compound are very broad at room temperature. This is in contrast to RB 15 which has relatively sharp lines.

The room temperature ^{13}C CP/MAS spectrum of compound **RB 23** is shown in figure 4.13. The spectrum shows the C(4) and (8) quaternaries at 77 and 78 ppm with the C(3) and (7) quaternaries at 38 ppm. Both signals are split. The peaks at 27 and 33 ppm are probably due to the methyls of C(3) and (7) as these are more likely to be vastly different in a non twin chair conformation compared to the C(4) and (8) methyls. These are shown at 30 ppm.

X–ray crystallographic data shows that there are two molecules in the asymmetric unit[49]. This would account for the splitting of the lines in the ^{13}C spectrum. The molecule is known to exist in a flattened twin twist boat conformation in the solid state. There is no NMR evidence for a conformational equilibrium in the solid state.

4.5 Conclusions

Although this study has produced no evidence of conformational equilibria in solid bicyclo[3.3.1]nonane derivatives it has, however, produced some interesting results. Most of the spectra contained very sharp lines, indicating highly ordered crystal structures or possibly rapidly mobile groups. Where X-ray data exists, the nmr spectrum has concurred with the results.

Figure 4.6: Room Temperature ^{13}C CP/MAS Spectra of Compounds RB 1, 2 and 3.

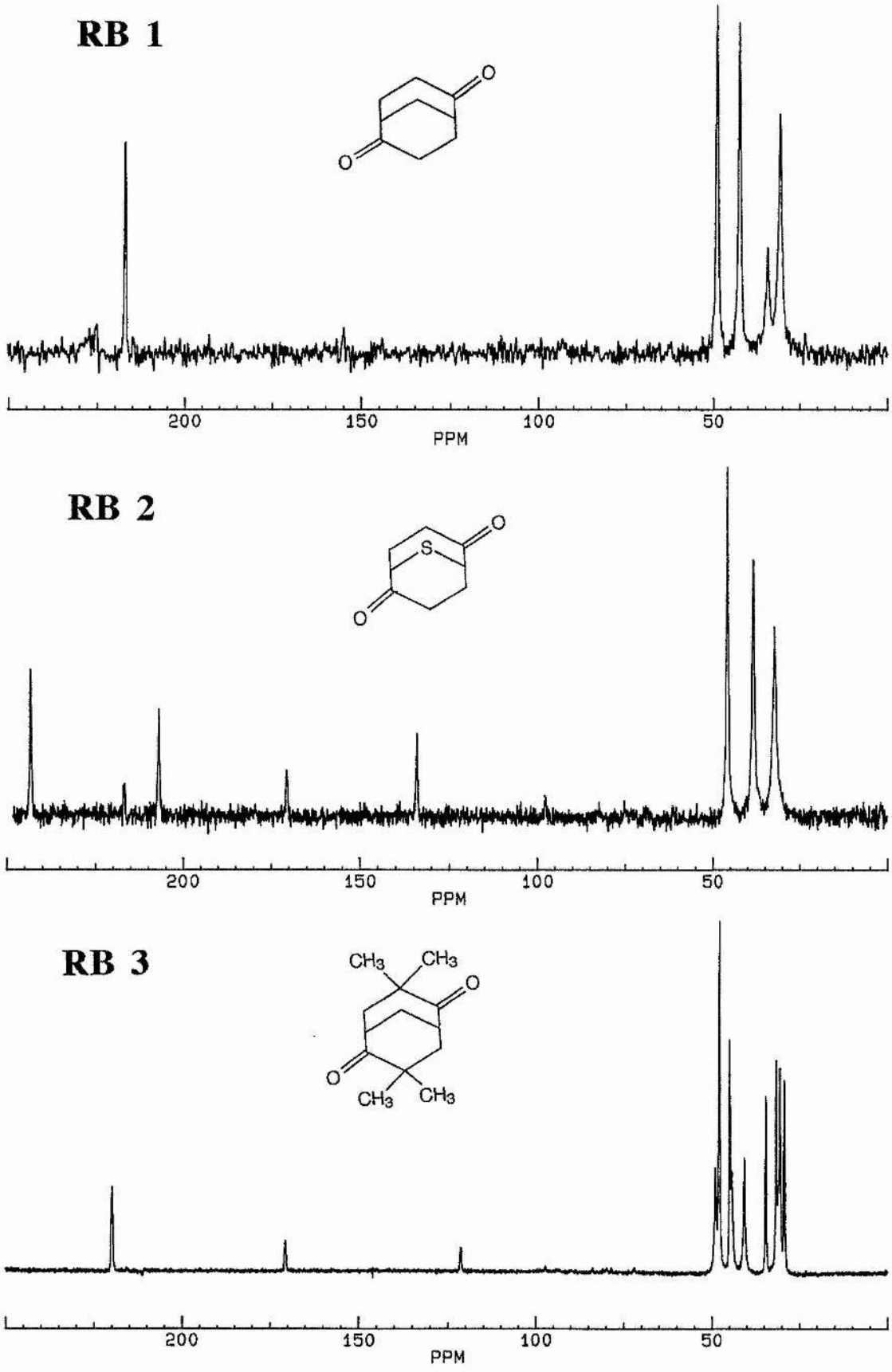

Figure 4.7: Room Temperature ^{13}C CP/MAS Spectra of Compounds RB 4, 5 and 6.

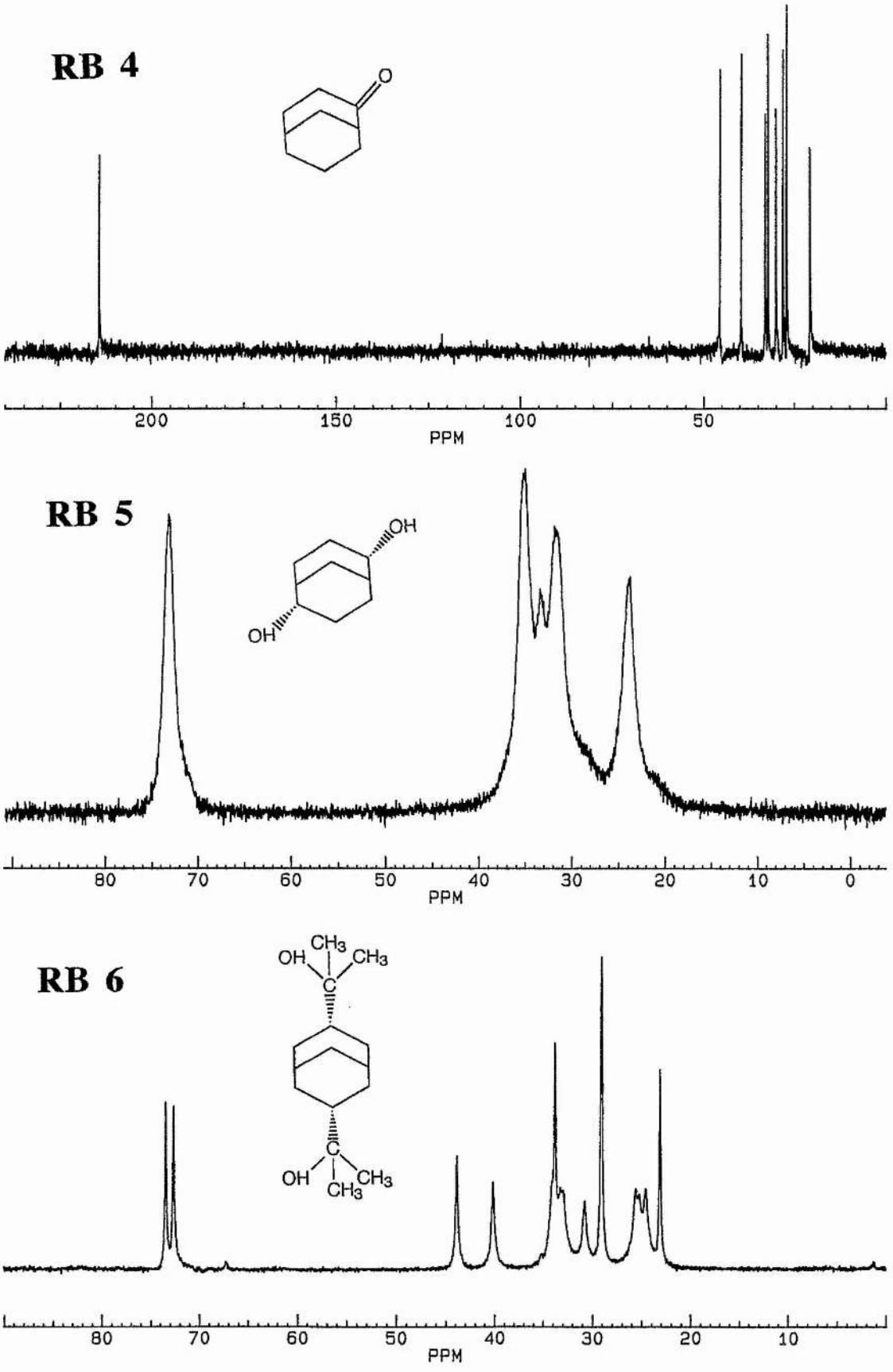

Figure 4.8: Room Temperature ^{13}C CP/MAS Spectra of Compounds RB 7, 8 and 9.

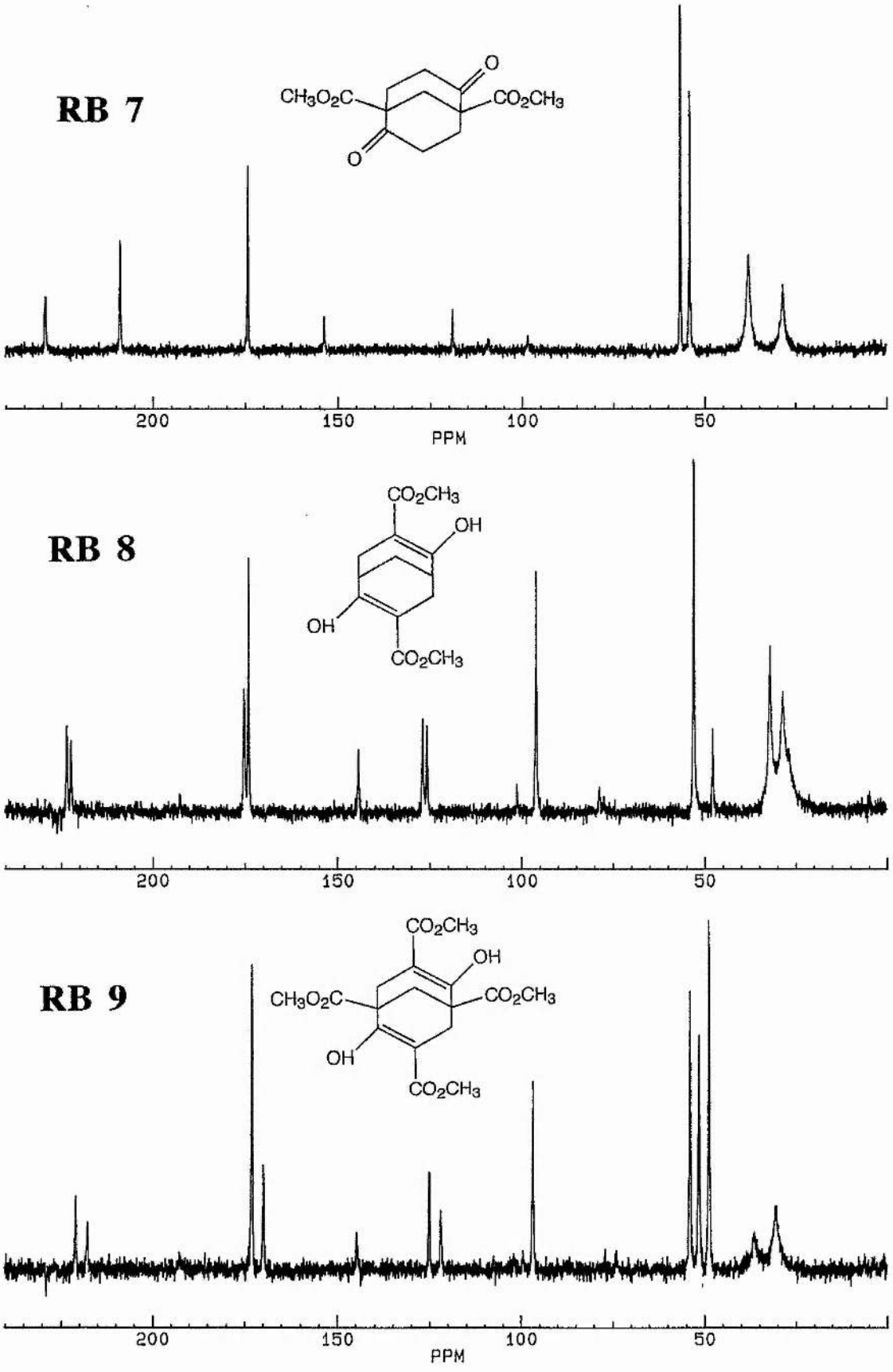

Figure 4.9: Room Temperature ^{13}C CP/MAS Spectra of Compounds RB 10, 11 and 12.

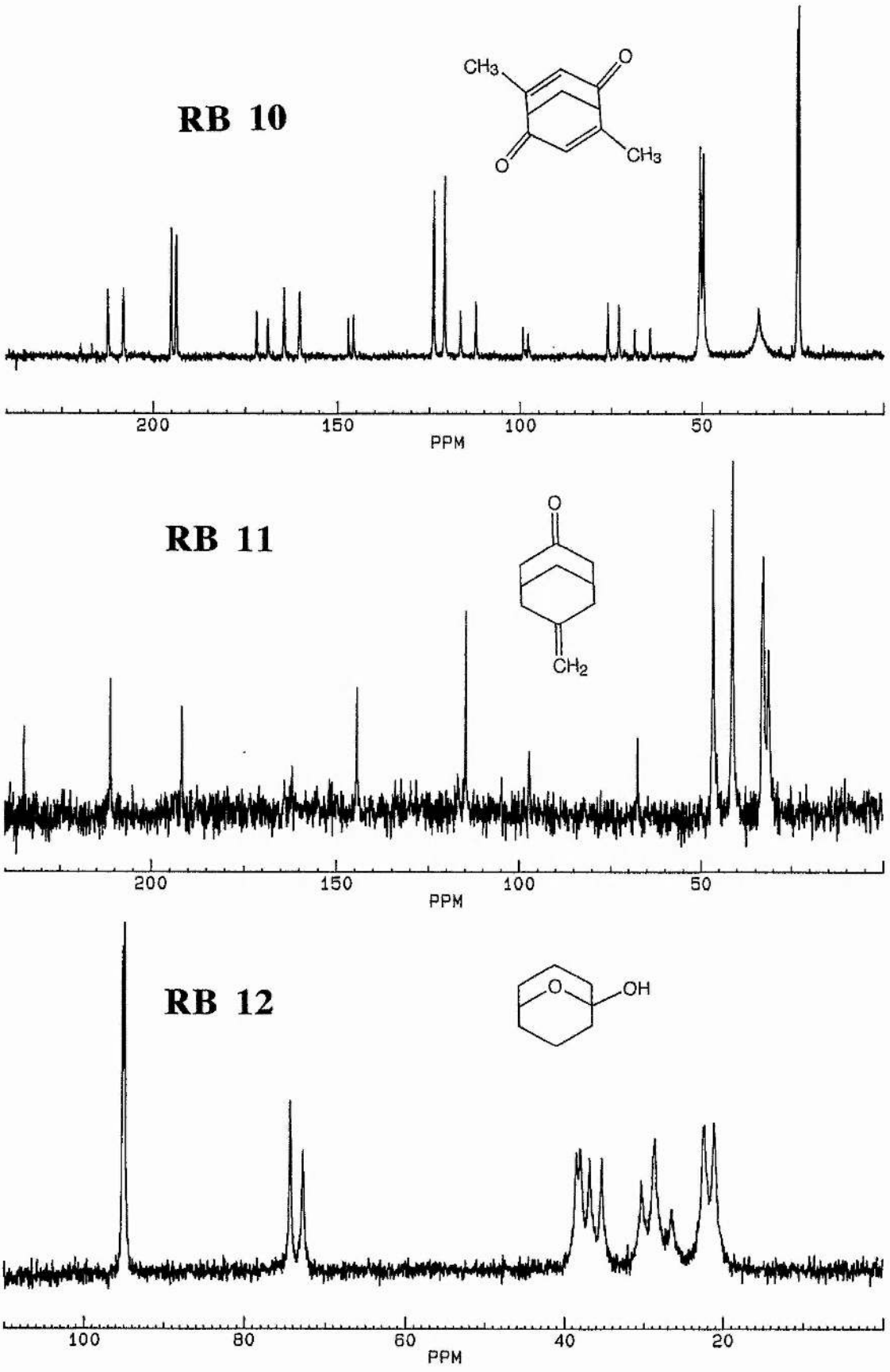

Figure 4.10: Room Temperature ^{13}C CP/MAS Spectra of Compounds RB 13, 14 and 15.

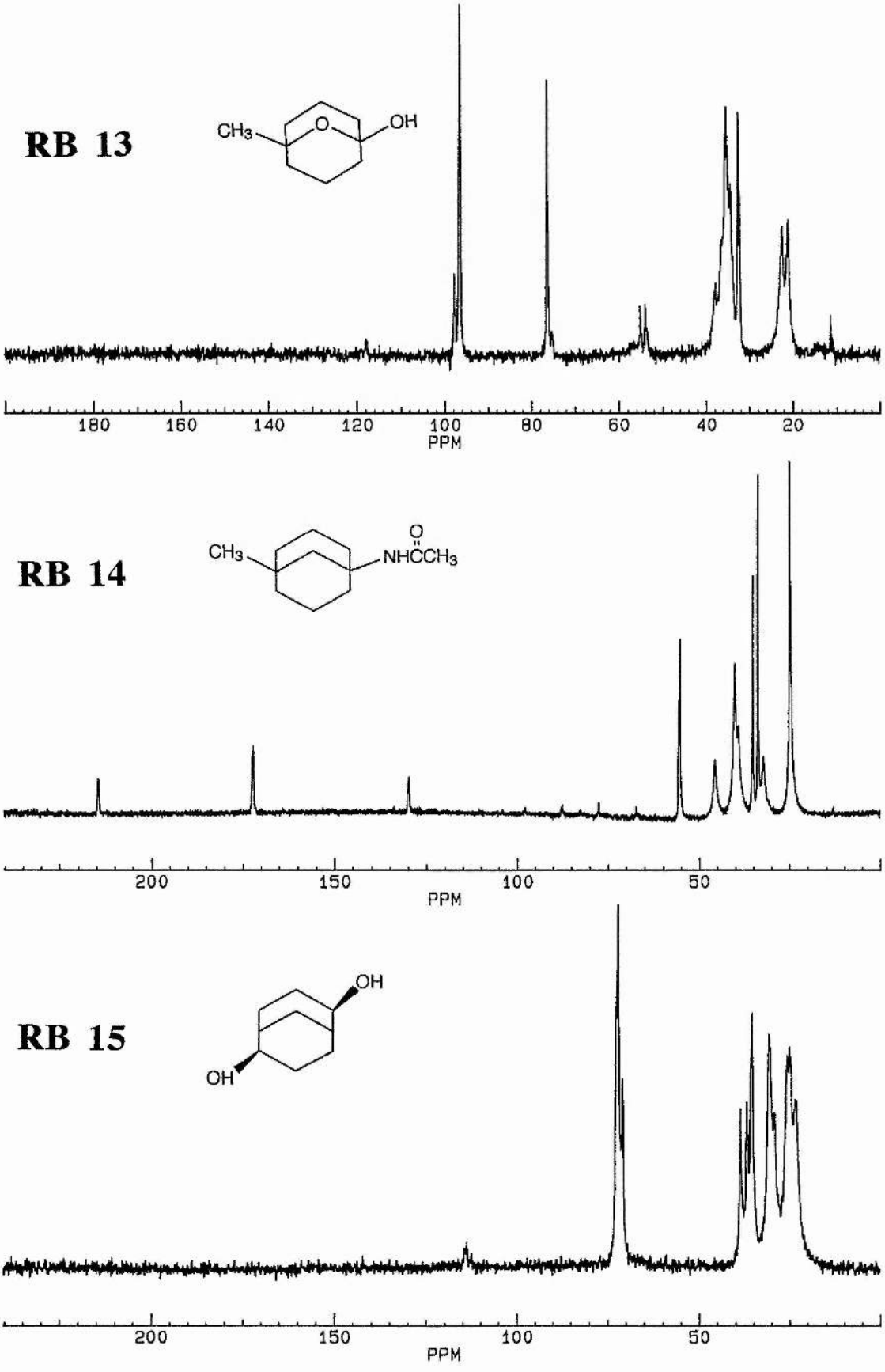

Figure 4.11: Room Temperature ^{13}C CP/MAS Spectra of Compounds RB 16, 17 and 18.

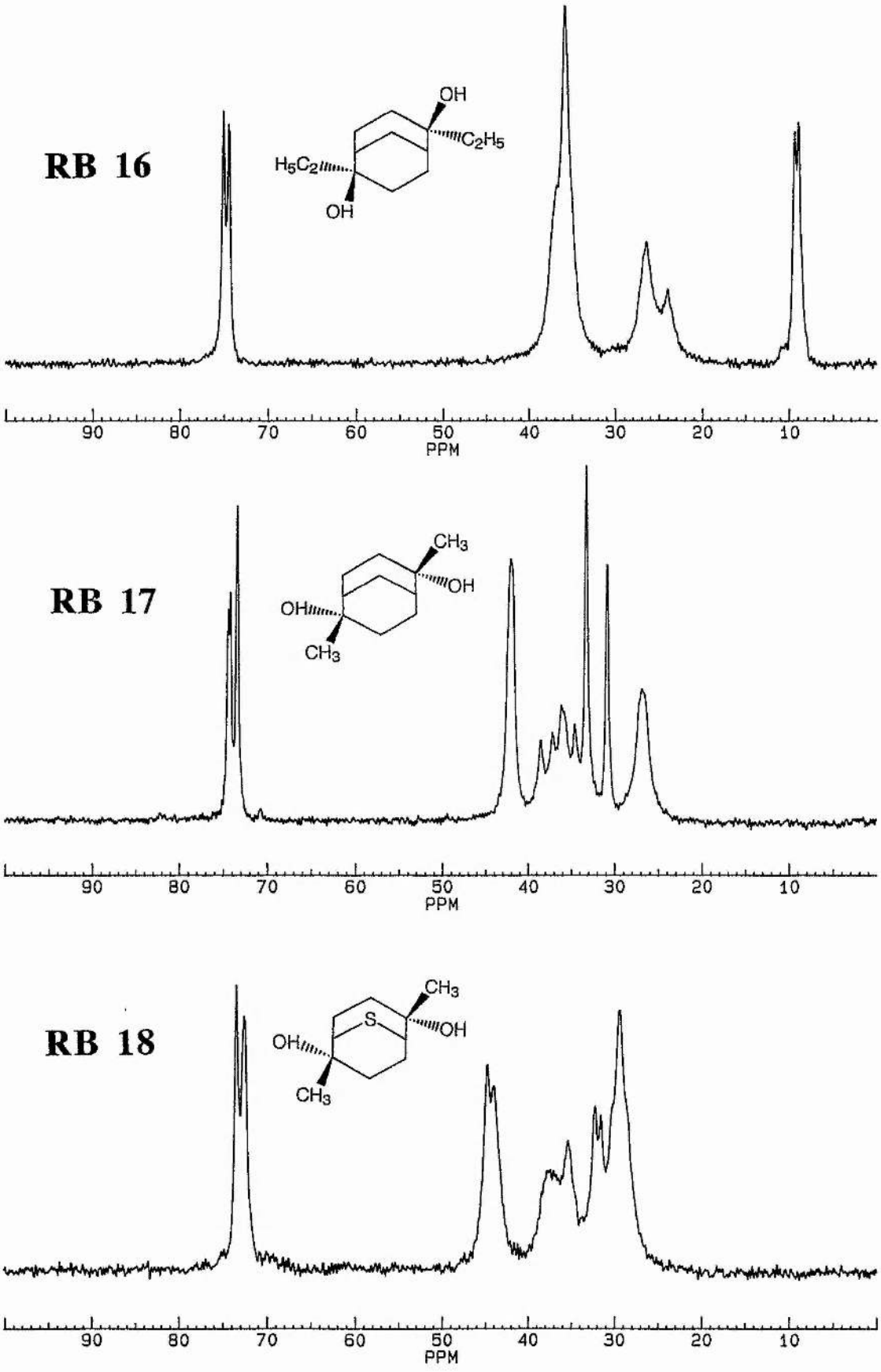

Figure 4.12: Room Temperature ^{13}C CP/MAS Spectra of Compounds RB 19, 20 and 22.

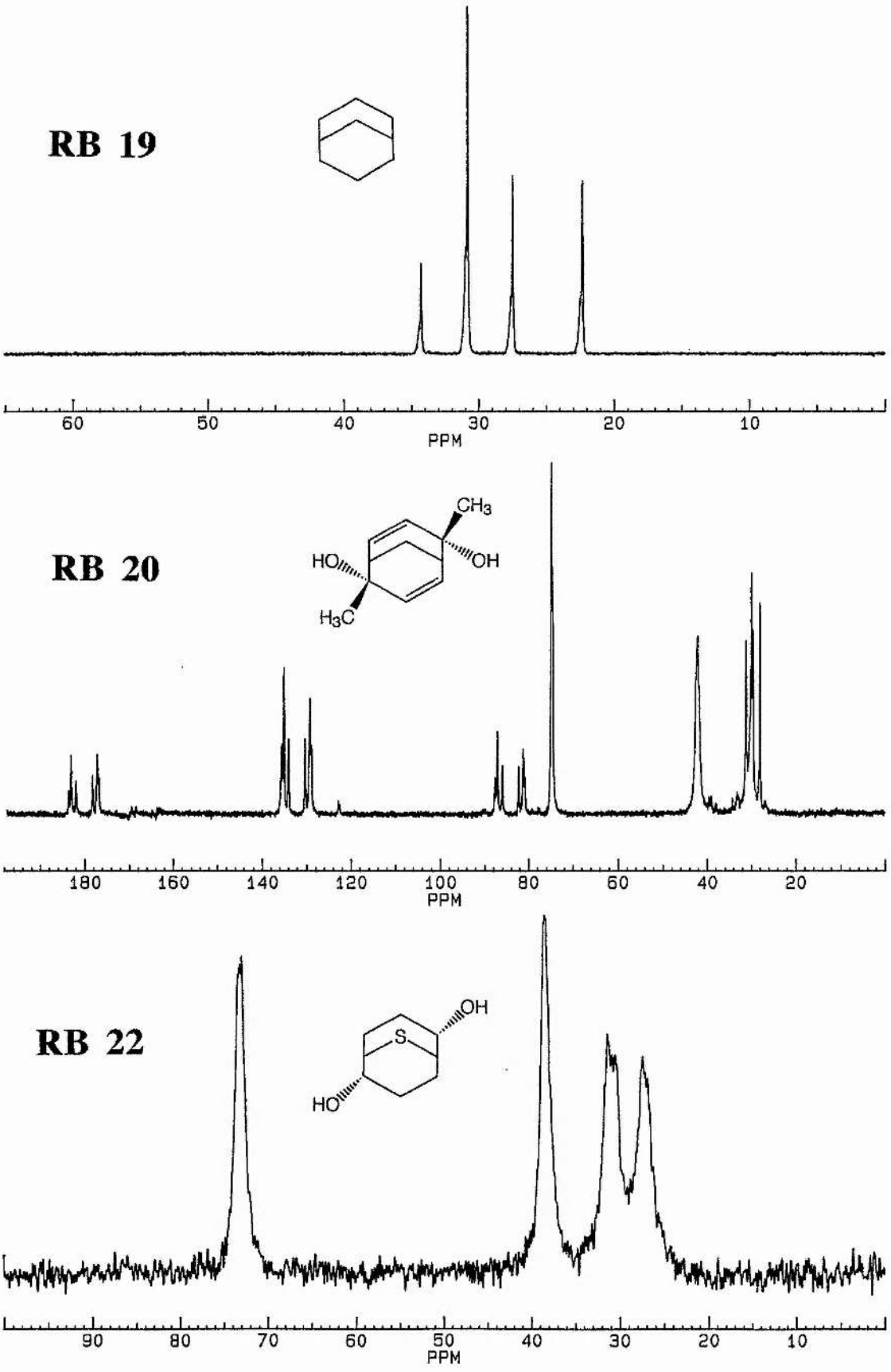

Figure 4.13: Room Temperature ^{13}C CP/MAS Spectra of Compound RB 23

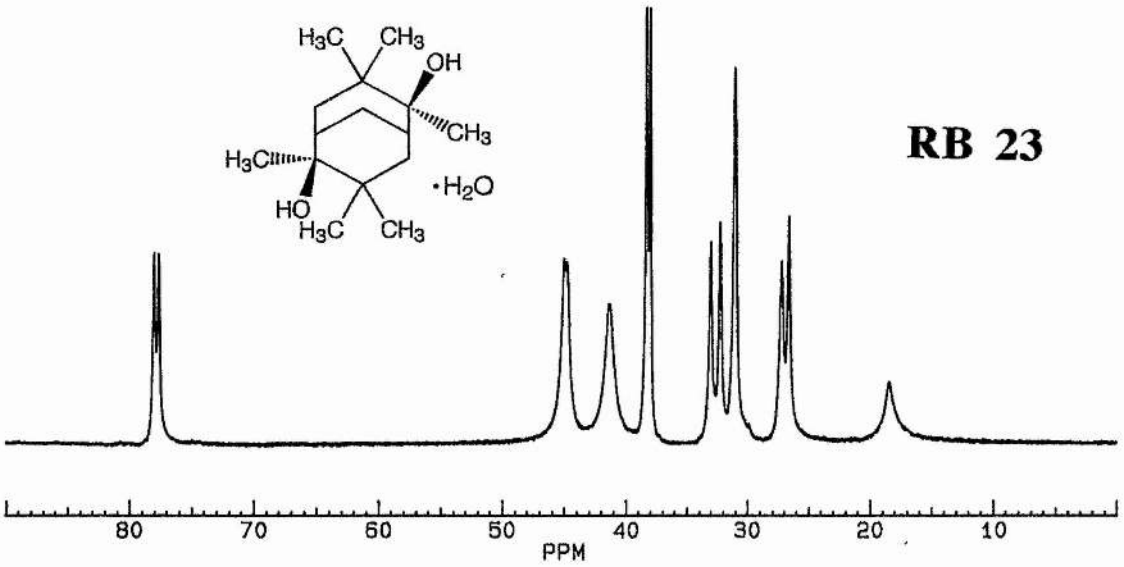

Chapter Five

Ring-Chain Tautomerism

5.1 Introduction

There are now many published examples of molecular transformations in the solid state[58, 59]. Many of these processes involve isomerism or rearrangements. It has been suggested that such transformations are initiated at defects in the crystal lattice and the transformation itself creates further defects and so on throughout the crystal[58, 60].

Examples of transformations include the rearrangement of dimethylamino–benzenesulphonic acid ester to its corresponding zwitterionic form[60] and acyl group migrations where the substrate is at temperatures close to melting[61, 62]. McNab *et al* have observed an interesting ambient temperature acyl migration in 3-amino-1-(chloroacetyl)pyrazole[63].

The ring–chain tautomerism in 1,3–*O*,*N*–heterocycles, such as tetrahydro-1,3-oxazines and oxazolidines has been intensively studied in recent years. These compounds exhibit ring–chain tautomerism in both solution[64-67] and gas phases[68,69]. The current work extends the field into the solid state by means of solid–state NMR spectroscopy.

In solution and gas phases equilibria between the ring and chain forms are observed. The solution and gas phase equilibria have been found to follow a Hammett σ–ρ relationship (i.e. linear free energy relationship). This would not be expected in the solid since the stronger crystal packing interactions should predominate over the smaller free energy differences in solution, forcing the equilibrium to one extreme or the other. Therefore, only one form should be seen. This is borne out in the limited number of cases where X–ray crystallography[70] has been applied and in a solid state NMR study[71].

The Ring-Chain Tautomerism of Compound RC1

Here, the product from the reaction of *cis*–2–aminomethylcyclohexanol with *p*–nitrobenzaldehyde in ethanol has been shown to initially form the chain tautomer (RC1)

which can be isolated in the solid. However, in the solid phase, this chain form is metastable and quickly cyclises to the ring; Figure 5.1. This compound also exists predominantly in the ring form in $CDCl_3$ solution.

Solid state NMR allows us to follow the kinetics of this cyclisation in the solid state since the spectra of the ring and chain forms of the molecule are readily distinguished.

The conversion of the chain form to the ring is shown in the ^{13}C CP/MAS spectra in figure 5.2. The chain tautomer is readily identified by the imine carbon resonance at 163 ppm. The chain isomerises in the solid state to the ring tautomer, readily identified by the C(2) ring carbon resonance at 86 ppm. The fully cyclised product was observed after heating the sample in the rotor for 2 hours at 30°C. The kinetics of the transformation appear to be first order. This is consistent with an intramolecular cyclisation. It was possible to calculate the rate of reaction of the molecule by measuring the height of the imine peak at 163 ppm as a function of time at various temperatures; table 5.1. The time required to obtain acceptable signal:noise ratios puts a limit on the upper rate range measurable. Also, time constraints on spectrometer use have a similar effect on the lower rate range.

Table 5.1: Rates of Reaction (cyclisation)

Temperature (K)	Rate k (sec^{-1})
297	4.46×10^{-4}
294	1.67×10^{-4}
290	1.03×10^{-4}
283	0.66×10^{-4}

From these results the activation energy for the cyclisation can be calculated and is found to be:

$$E_a = 85.0 \pm 14.7 \text{ kJmol}^{-1}$$

The approximate rate of the same reaction in $CDCl_3$ solution at 300K is ca. 5 x 10^{-4} sec^{-1}, very similar to the rate in the solid. The similar kinetics suggests that the OH is close to the C=N in the solid.

For this transformation to occur the molecule must undergo both ring closure and proton transfer. A proposed mechanism is shown in Figure 5.5(a). Here it is likely that the base, B, is the imine nitrogen from a neighbouring molecule and the H^+ the hydroxyl hydrogen in another neighbouring molecule. As the reaction follows first order kinetics the rate determining step will be either the proton transfer or the cyclisation step. Of the two it is more probable that the cyclisation step will be the slowest as proton transfer reactions are usually quite rapid. To corroborate this theory, it is highly unlikely that a hydrogen will migrate from a hydroxyl group to an imine nitrogen before cyclisation occurs. On cyclisation, this hydroxyl proton will become very acidic and will readily move from the O to the N. The proton transfer will then increase the electrophilicity of the imine carbon on the acceptor molecule facilitating cyclisation. It is now apparent that the rate determining step should be the cyclisation of the protonated imine; Figure 5.5(b).

The comparable rates of cyclisation in solid and solution phases suggests that little molecular movement is required in the solid state for this mechanism to occur. It may well be that the molecules are nicely aligned to facilitate proton transfer between neighbouring molecules.

5.3 The Ring-Chain Tautomerism of Compound RC2

The product from the reaction of 3-aminopropionamide oxime with p–nitrobenzaldehyde in ethanol, behaves similarly to that of RC1 in solution in that it readily forms the equilibrium shown in figure 5.3. However, in contrast to compound RC1, it appears to initially form the ring tautomer (RC2) when first crystallised from solution. Over a period of 35 minutes this metastable conformer ring opens to the chain

form and this progress can be followed in the solid state using ^{13}C CP/MAS NMR; Figure 5.4.

At zero minutes the C(2) ring carbon is clearly shown at 79 ppm. As the reaction progresses this line is seen to reduce in intensity with a simultaneous increase in the intensity of the imine peak at 161 ppm. An estimate of the free energy for the ring opening reaction gives a value of 17.9 $kJmol^{-1}$ at 293K

5.4 Conclusions

It was concluded that CP/MAS NMR can be used to study reactions in the solid state. However, the upper and lower rates of reactions are limited by accumulation time in both cases. Measurements of this kind are only possible when the kinetic product of condensation is not the thermodynamic product and exists in a metastable phase.

It would be of interest to get crystal structures of both form to see how far the atoms require to move in the solid to accomplish these reactions.

More work is required on compound RC2 before an activation energy can be determined.

Figure 5.2: Cyclisation of RC1 with Time (293K)

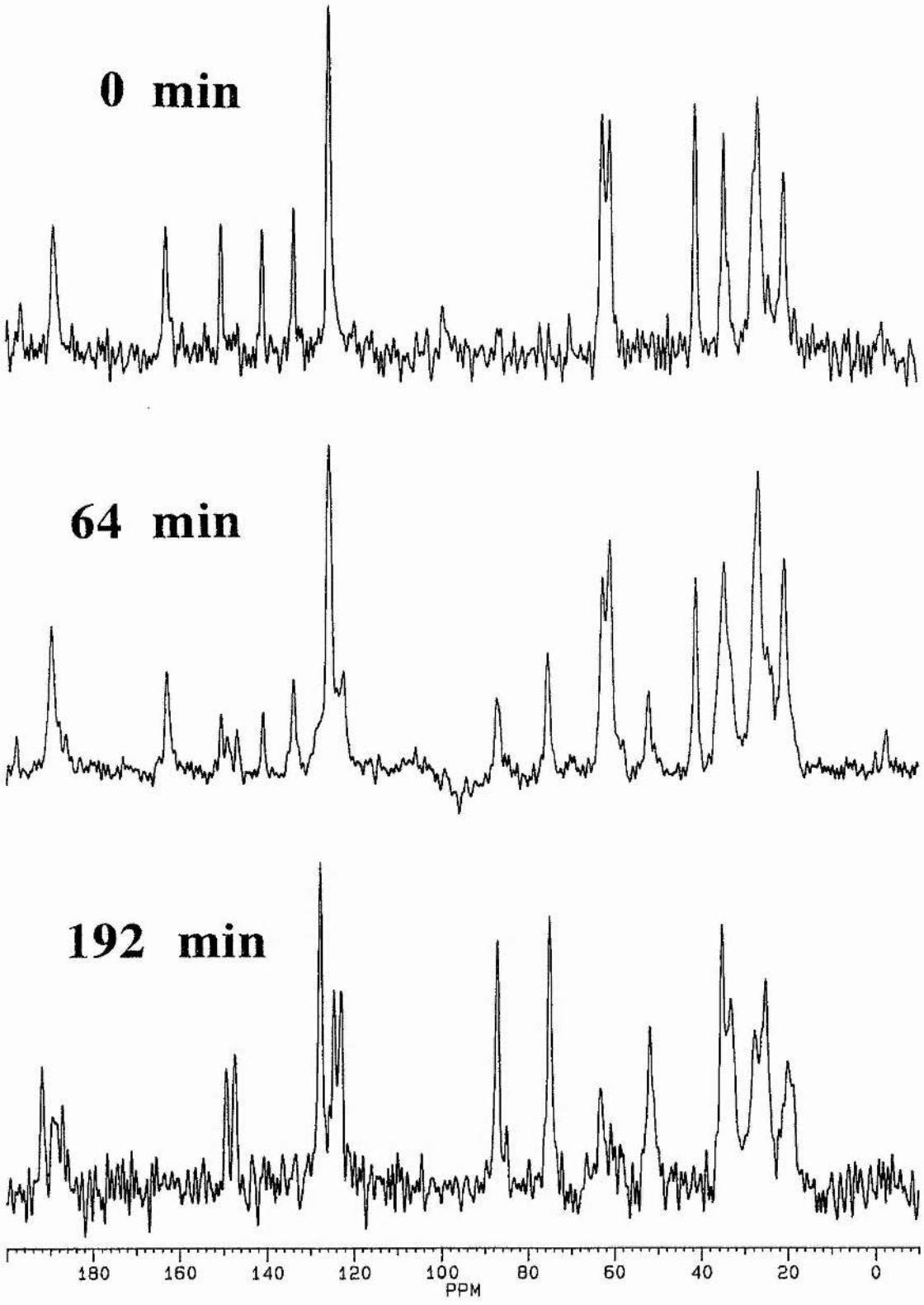

Figure 5.4: Ring Opening of RC2 with Time (293K)

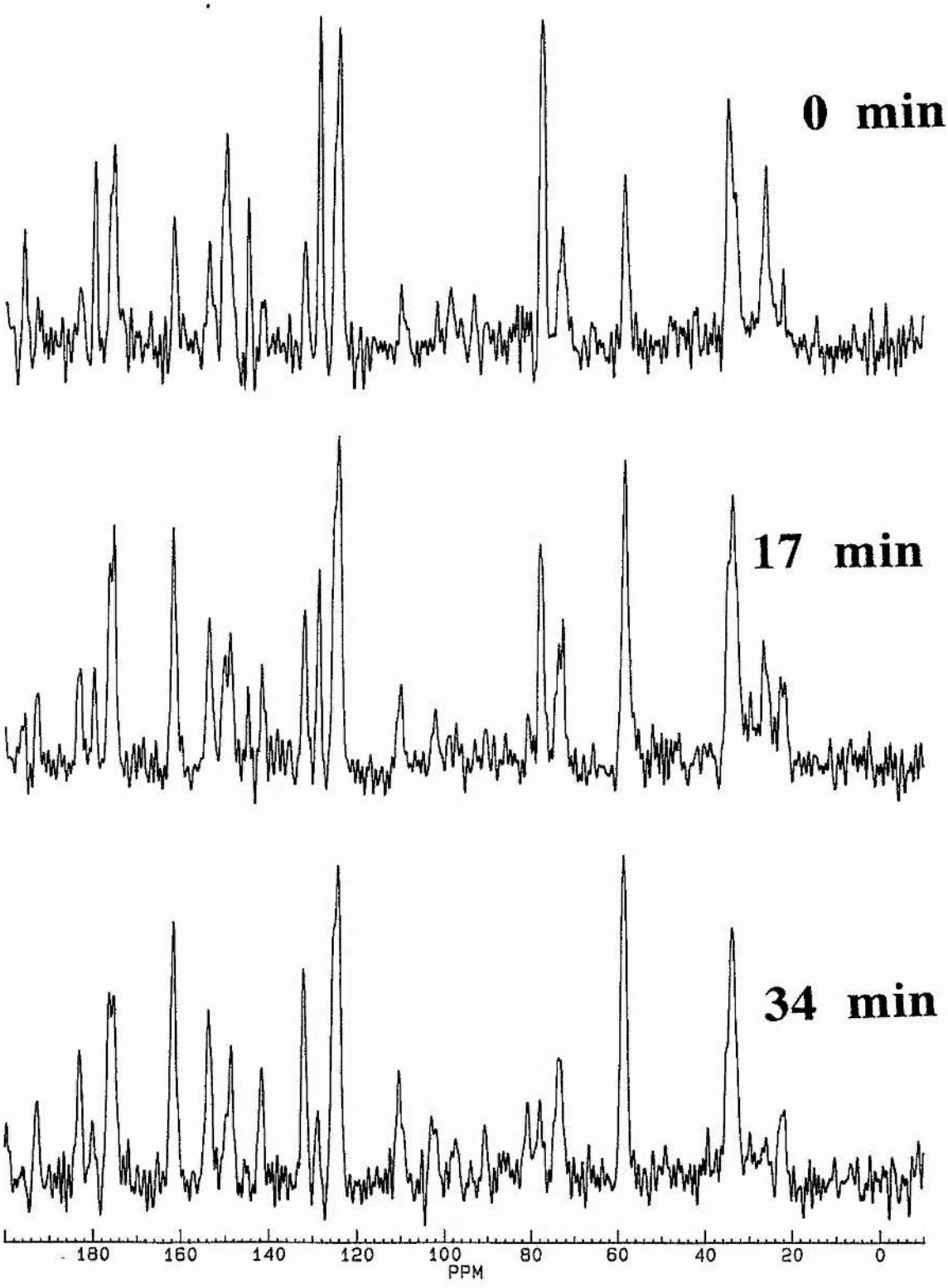

Figure 5.1: The Ring Chain Tautomerism of Compound RC1.

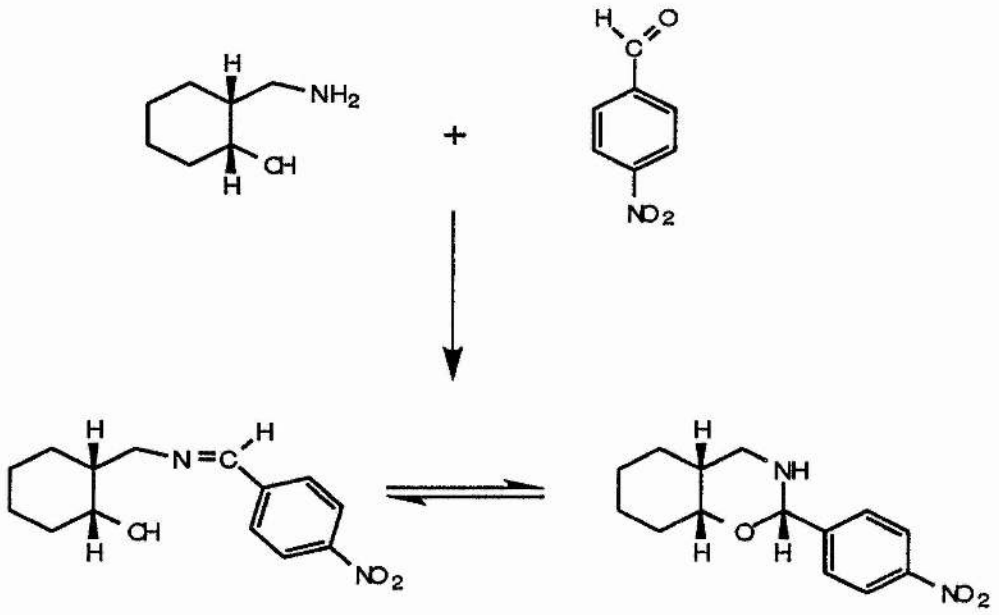

Figure 5.3: The Ring-Chain Tautomerism of Compound RC2

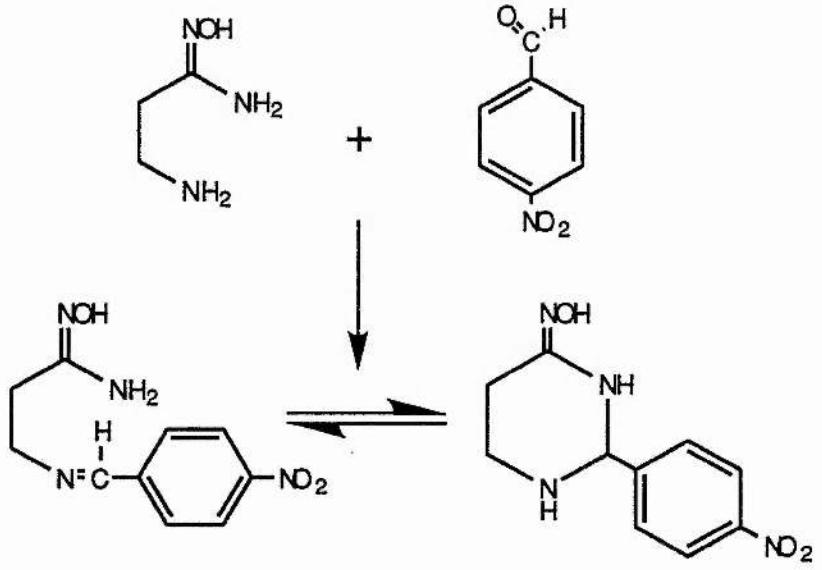

Figure 5.5: Proposed Mechanisms for the Ring Closure of RC1

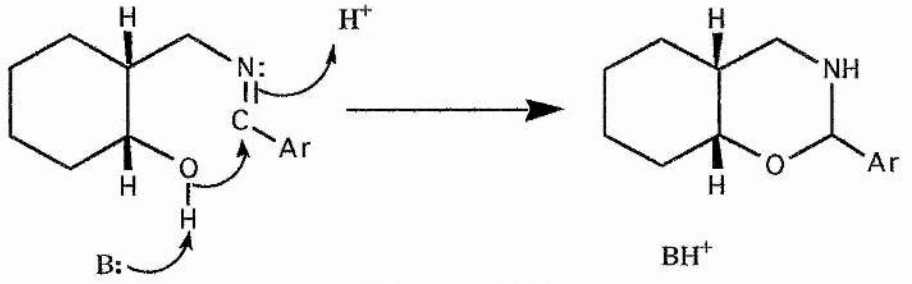

Figure 5.5(a)

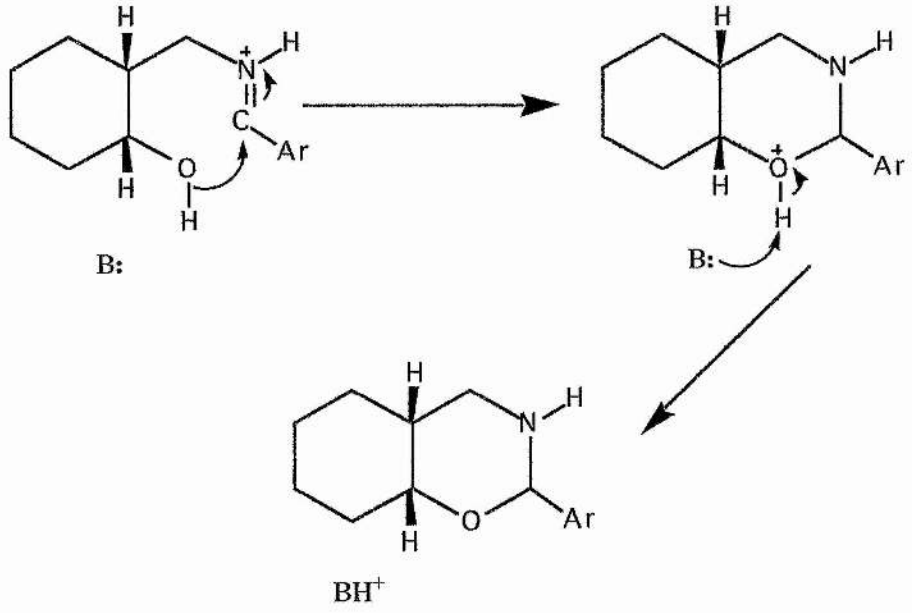

Figure 5.5(b)

References

References

[1] J. K. M. Sanders and B. K. Hunter, *Modern NMR Spectroscopy*; Oxford University Press: Oxford, 1993.

[2] D. H. Williams and I Fleming, *Spectroscopic Methods in Organic Chemistry*; MGraw-Hill Book Company (UK) Ltd.: Maidenhead, England, 1989.

[3] W. Kemp, *NMR in Chemistry*; Macmillan Education Ltd: London, 1986.

[4] C. A. Fyfe, *Solid State NMR for Chemists*; C.F.C. Press: Ontario, 1983.

[5] A. E. Derome, *Modern NMR Techniques for Chemistry Research*; Pergamon Press: Oxford, 1990.

[6] J Sandstrom, *Dynamic NMR Spectroscopy*; Academic Press: London, 1982, Page 96.

[6(a)] W. P. Rothwell and J. S. Waugh, *J Chem Phys*, **74**, 2721 (1981)

[7] H. Sachse, *Chem. Ber.*, **23**, 1363, (1890).

[8] J. D. Kemp and K. S. Pitzer, *J. Chem. Phys.*, **4**, 749 (1936).

[9] K. S. Pitzer, *J. Chem. Phys.*, **5**, 437-9 (1937).

[10] E. N. Lassettre and L. B. Dean, *J. Chem. Phys.*, **17**, 317 (1949).

[11] D. N. J. White and J. M. Bovill, *J. Chem. Soc.*, Perk. II, 1610 (1977).

[12] S. Weiss and G. E. Le Roi, *J. Chem. Phys.*, **29**, 340 (1958).

[13] J. B. Hendrickson, *J. Am. Chem. Soc.*, **83**, 4537 (1961).

[14] M. Bixon and S. Lifson, *Tetrahedron*, **23**, 769 (1967).

[15] C. P. Smyth and S. E. Kamerling, *J. Am. Chem. Soc.*, **53**, 2988 (1931).

[16] O. Hassel and H. Viervoll, *Arch. Math. Naturvidenskab*, B47, No. 13, **16** (1944).

[17] R. A. Bonham and L. S. Bartell, *J. Am. Chem. Soc.*, **81**, 3491 (1959).

[18] M. E. Milberg and W. N. Lipscomb, *Acta Cryst.*, **4**, 369 (1951).

[19] R. E. Kagarise, *J. Chem. Phys.*, **24**, 300 (1956).

[20] S. Mizushima, I. Nakagawa, I. Ichishima, and T. Miyazawa, *J. Chem. Phys.*, **22**, 1614 (1954).

[21] S. Mizushima, T. Shimanouchi, K. Kuratani, and T. Miyazawa, *J. Am. Chem. Soc.*, **74**, 1378 (1952)

[22] L. Pierce, *J. Chem. Phys.*, **34**, 498 (1961).

[23] F. G. Riddell, S. Arumugam and J. E. Anderson, *J. Chem. Soc., Chem. Commun.*, 1525-1527 (1991).

[23a] N. M. Bortnick, L. S. Luskin, M. D. hurwitz, W. E. Craig, L. J. Exner and J. Mirza, *J. Am. Chem. Soc.*, **78**, 4039-42 (1956)

[24] N. G. Parsonage and L. A. K. Stavely, *Disorder in Molecular Crystals*. Clarendon Press, Oxford, 1978.

[25] T. Bjorholm and H. J. Jakobsen, *J Magn.Reson.*, **84**, 204 (1989)

[25a] N. J. Leonard and E. W. Nommensen, *J. Am. Che. Soc.*, **71**, 2803-2813 (1949).

[26] P. J. Barrie and J. E. Anderson, *J. Chem. Soc. Perkin Trans. II*, 2031-2034 (1992).

[27] D. E. O'Reilly. E. M. Peterson, C. E. Scheie and E. J. Seyfarth, *J. Chem. Phys.*, **59**, 3576, (1973).

[28] T. Hasebe, *J. Chem. Soc., Faraday Trans. II*, **81**, 749-756 (1985).

[29] S. Mooibroek, R. E. Wasylishen, J. B. MacDonald, C. I. Ratcliffe and J. A. Ripmeester, *Can. J. Chem.*, **66**, 734-740 (1988).

[30] D. W. Aksnes and K. Ramstad, *Acta Chem. Scand.*, Ser. **A 41**: 1-7 (1987).

[31] T. Hasebe, N. Nakamura and H. Chihara, *Bull. Chem. Soc. Jpn.*, **57**, 179-183 (1984).

[32] T. Hasebe and J. H. Strange, *J. Chem. Soc.*, Faraday Trans. II, **81**, 735-747 (1985)

[33] J. C. Frost and A. J. Leadbetter, *J. Chem. Soc., Faraday Trans. II*, **78**, 2139-2154 (1982).

[34] J. M. Twyman and C. M. Dobson, *J. Chem. Soc., Chem. Commun.*, 786-788 (1988).

[35] J. B. Lambert, S. C. Johnson and L. Xue, *J. Am. Chem. Soc.*, **116**, 6167-6174 (1994).

[36] B. Gordillo, E. Juaristi, R. Martinez, R. A. Toscano, P. S. White and E. L. Eliel, *J Am. Chem. Soc.* 1992, **114**, 2157-2162.

[37] I. M. Hoodless, J. H. Strange and L. E. Wylde, *J Phys.* C 1971, **4**, 2742.

[38] A. Abragam. *Principles of Nuclear magnetism*; Oxford University Press; Oxford, 1961, Chapter 4.

[39] F. G. Riddell, S. Arumugam, K. D. M. Harris, M. Rogerson and J. H. Strange, *J. Am. Chem. Soc*, 1993, **115**, 1881-1885

[40] H. Sachse, *Chem. Ber.* 1890, 23, 1363

[41] E. L. Osina, V. S. Mastryukov, L. V. Vilkov and N. A. Belikova, *J. Chem. Soc., Chem. Commun.*, 12-13 (1976).

[42] G. Eglinton, J. Martin and W. Parker, *J. Chem. Soc.*,1243-1251 (1965).

[43] E. Osawa, K. Aigami and Y. Inamoto, *J Chem Soc., Perkin Trans. II*, 172-180.(1979).

[44] J. A. Peters, J. M. A. Baas, B. van de Graaf, J. M. van der Toorn and H. van Bekkum, *Tetrahedron*, **34**, 3313-3323.(1978).

[45] C. Y. Chen and R. J. W. Le Fevre, *Tetrahedron Letters*, **12**, 737 (1965).

[46] W. D. K. Macrosson, J. Martin and W. Parker, *Tetrahedron Letters*, **30**, 2589 (1965).

[47] J. A. Peters, J. M. van der Toorn and H. van Bekkum, *Tetrahedron*, **30**, 349-351 (1977).

[48] J. A. Peters, J. D. Remijnse, A. van der Wiele, and H. van Bekkum, *Tetrahedron Letters*, **32**, 3065-3068 (1971).

[49] R. Bishop, D. C. Craig and M. L. Scudder, *J. Chem. Soc., Perkin Trans. I*, 1473-1477 (1989).

[50] R. A. Appleton, S. C. Egan, J. M. Evans, S. H. Graham, *J. Chem. Soc.*, (C), 1110-1115 (1968).

[51] V. S. Mastryukov, M. V. Popik, O. V. Dorofeeva, A.V. Golubinskii, L. V. Vilkov, N. A. Belikova, and N. L. Allinger, *J. Am. Chem. Soc*, **103**, 1333-1337 (1981).

[52] N. L. Allinger, M. T. Tribble and M. A. Miller, *Tetrahedron*, **28**, 1173-1190 (1972).

[53] D. J. Raber, C. M. Janks, M. D. Johnston Jr and N. K. Raber, *Tetrahedron Letters*, **21**, 677-680 (1980).

[54] G. A. Sim, *Acta Crystallogr.*, Sect. **B 46**, 676 (1990).

[55] F. G. Riddell and M. Rogerson, *Magn. Reson. In Chem*, **30**, 1070-1074 (1992).

[56] M. D. Radcliffe, A. Gutierrez, J. F. Blount and K. Mislow, *J. Am. Chem. Soc.* 1984, 106, 682-687.

[57] R. Bishop, S. Choudhury and I. Dance, *J. Chem. Soc. Perkin Trans II*, 1982, 1159-1168.

[58] I. C. Paul and D. Y. Curtin, *Acc. Chem. Res.*, **6**, 217 (1973)

[59] A. Gavezzotti and M. Simonetta, *Chem. Rev.*, **82**, 1 (1982)

[60] C. N. Sukenik, J. A. Bonaface, N. S. Mandel, P. Y. Lau, G. Wood and R. G. Bergman, *J. Am. Chem. Soc.*, **99**, 851 (1977)

[61] R. Anschutz, H. Aschenberg, H. Kuckertz, F. Krone, K. Riepenkronger and C. Zerbe, *Liebigs Ann. Che.*, **442**, 18 (1925)

[62] A. J. Gordon, *Tetrahedron*, **23**, 863 (1967)

[63] D. Clarke, R. W. Mares, H. McNab and F. G. Riddell, *Magn. Res. Chem.*, **32**, 255 (1994)

[64] F. Fulop, K. Pihlaja, J. Mattinen and G. J. Bernath, *Org. Chem.* 1987, **52**, 3281.

[65] U. E. Alva Astudillo, N. C. J. Chokotho, T. C. Jarvis, D. J. Johnson, C. C. Lewis and P. D. McDonnell, *Tetrahedron.* 1985, **41**, 5919

[66] F. Fulop, G. Bernath, J. Mattinen and K. Pihlaja, *Tetrahedron.* 1989, **45**, 4317.

[67] F. Fulop, M. Dahlquist and K. Pihlaja, *Acta Chem. Scand.* 1991, **45**, 273.

[68] P. Vainiotalo, F. Fulop and K. Pihlaja, *Org. Mass. Spectr.* 1991, **26**, 438.

[69] P. Vainiotalo, S. Ronkanen, F. Fulop and K. Pihlaja, *Tetrahedron.* 1990, **46**, 3683.

[70] G. Argay, A. Kalman, F. Fulop and G. Bernath, *Acta Chim, Hung.* 1982, **109**, 39.

[71] F. G. Riddell, S. Arumugam, F. Fulop and G. Bernath, *Tetrahedron*. 1992, **23**, 4979-4984.

" This is the end, but the moment has been prepared for."

The Fourth Doctor
Logopolis (1981)